Development and Evaluation of Quinapyramine Sulphate Loaded Lipid-Based Nanocarriers for the Treatment of *Trypanosomiasis*

THESIS

Submitted in partial fulfilment

of the requirements for the degree of

DOCTOR OF PHILOSOPHY

by

Kedar Shridhar Prayag

2018PHXF0427P

Under the Supervision of

Prof. Anil B. Jindal

and

Co-supervision of

Prof. Atish T. Paul

BITS Pilani

Pilani | Dubai | Goa | Hyderabad

BIRLA INSTITUTE OF TECHNOLOGY AND SCIENCE, PILANI

Pilani Campus, Rajasthan, INDIA-333031

2023

BIRLA INSTITUTE OF TECHNOLOGY AND SCIENCE, PILANI

CERTIFICATE

This is to certify that the thesis entitled **"Development and Evaluation of Quinapyramine Sulphate Loaded Lipid-Based Nanocarriers for the Treatment of *Trypanosomiasis*"** submitted by **Kedar Shridhar Prayag**, ID. No. **2018PHXF0427P** for award of Ph.D. degree of the institute embodies original work done by him under my supervision.

Signature of the Supervisor
Prof. Anil B. Jindal
Associate Professor
Department of Pharmacy,
BITS-Pilani, Pilani Campus,
Rajasthan
Date:

Signature of the Co-supervisor
Prof. Atish T. Paul
Associate Professor
Department of Pharmacy,
BITS-Pilani, Pilani Campus,
Rajasthan
Date:

Acknowledgments

‘Acknowledging the good that you already have in your life is the foundation for all abundance’

- Eckhart Tolle

I am extremely grateful to the Department of Biotechnology, Govt. of India for providing us the financial assistance throughout my tenure. I am thankful to Prof. Souvik Bhattacharyya, Vice-Chancellor, BITS-Pilani, Prof. Sudhir Kumar Barai, Director, BITS Pilani, Pilani Campus, Col. Soumyabrata Chakraborty (Retd), Registrar, BITS Pilani, Pilani Campus, Prof. Ajit Pratap Singh, Associate Dean, AGSRD, BITS Pilani, Pilani Campus, for providing excellent work facilities and an absorbing research environment. I wish to express sincere thanks to Prof. Anil B. Gaikwad, Head, Department of Pharmacy, Prof. Hemant R. Jadhav & Prof. Atish T. Paul, former Head, for constant support in providing the resources required during my research work.

I would take the opportunity to express my feelings through humble prayer as a mark of respect for my research supervisor Prof. Anil B. Jindal, Associate Professor, Birla Institute of Technology Sciences - Pilani, Pilani Campus. I am thankful for his inspiration all the time throughout my dissertation work. He was kind, and cooperative, valuable help, guidance, and continuous encouragement during every phase of the dissertation. His way of sharing knowledge during the crucial times are memorable. His moral endorsement always propelled and lifted me to perform well. His innovative ideas helped me to productively complete work with spontaneity and passion.

I would also like to express my sincere feelings for my co-supervisor Prof. Atish T. Paul, Associate Professor, Birla Institute of Technology Sciences - Pilani, Pilani Campus for constant support and motivation throughout journey. His inspiration always kept me get going throughout my tenure.

I am also thankful to Dr. Samar Kumar Ghorui, Principal scientist, National Research Centre on Camels, Bikaner for constantly supporting me throughout my tenure in pre-clinical efficacy studies. I am thankful to him for providing me access to work at his institute and providing me valuable input in my work.

I am indebted to my Doctoral Advisory Committee (DAC) members, Prof. Anil B. Gaikwad and Prof. Aniruddha Roy, for reviewing my thesis and helping in constructive criticism of my work. I would express my sincere thanks to Prof. Anil B. Jindal, Convener, Departmental Research Committee, for valuable guidance while compiling this thesis.

I am thankful to all my faculty members of the Department of Pharmacy, Prof. R. Mahesh, Prof. S. Murugesan, Prof. Rajeev Taliyan, Prof. Deepak Chitkara, Prof. Anupama Mittal, Prof. Gautam Singhvi, Dr. Murali Manohar Pandey, Dr. Sandeep Sundriyal and Dr. Richa Shrivastava for their teachings. And I am thankful to Dr. Sushil Kumar Yadav for supporting in animal studies.

I would also like to extend my sincere thanks to my lab mates Mrs. Dhanashree, Ms. Ila Sarode and Mr. Sanat K. Dash for their immense support, giving their precious time, patience in always listening to me and motivation. Special mention of Mr. Athrava Bhide for constantly supporting and patient listening throughout the tenure.

All my seniors and colleagues Dr. Archana Khosa, Dr. Kowthavarapu Venkata Krishna, Dr. Saurabh Sharma, Dr. Kishan Italiya, Dr. Vajir Malek, Dr. Nisha Sharma, Mr. Ginson George, Dr. Pracheta Sengupta, Dr. Sudeep Pukale, Dr. Sarathlal K.C., Dr. Samrat Mazumdar, Dr. Paramita, Dr. Swetha, Dr. Violina, Ms. Swati Sharma, Ms. Karan Kumar, Mr. Rupesh Jain, Dr. Himanshu, Mr. Rajesh Pradhan, Mr. Amritansh Bhanot, Mr. Arihant Kumar Singh, Mr. Deepak Sahel, Mr. Imran Ansari, Ms. Moumita Basak, Ms. Nikita Hinge, Mr. Mahipal Donthi, Ms. Kavyashree, Ms. Manisha Choudhari, Mr. Ajinath Kale, Mr. Atharva Bhide, Mr. Prashant Auti, Ms. Karnam Sriravali, Ms. Nisha, Mr. Mukesh, Ms. Shreya, Mrs. Sharyu, Mr. Amit Sharma, Mr. Shubham Salunkhe, Mr. Sai Pradyuth, Mr. Vishwadeep Shelke, Mr. Shivanshu Bajaj, Mr. Jayant Singh, Ms. Shobha Kumari, Mr. Abhay Tharmatt, Mr. Shrikant Kirwale, Mr. Shailesh Tripathi, Ms. Shikha Thakur, Mr. Ala Chandu, Ms. Neha Dagar, Mr. Giriprasad, Ms. Sonia Guha, Ms. Sakshi Priya, Mr. Muzaffar, Ms. Yashika Tomar, Mr. Mukul Kore, Mr. Samarth Dwivedi, Mr. Vaghesh Verma, Mr. Utkarsh Jagtap, Ms. Shivangi Palival, Mr. Animesh Muzumdar, Ms. Pranali Kuthe, Ms. Shivangi Neema, Mr. Pratik Shinde, Ms. Lavanya, Ms. Aarti Sharma, Mr. Yash Patidar, Dr. Vivek and Dr. Yogeshvaran deserve special thanks for making the pleasant working environment in the lab, for all the fun and enjoyment, help and sarcasm.

I want to thank graduates and postgraduates with whom I worked closely for exploring things. I thank Mr. Mani Famta, Ms. Rucha Bhangale, Ms. Bhakti, Mr. Himanshu and Mr. G. Pramoda. I would also like to extend my sincere thanks to the entire non-teaching staff in the Department of pharmacy, Mr. Puran, Mr. Lakshman, Mr. Tarachand, Mr. Surendra, Mr. Naveen, Mr. Abhishek, Mr. Sandeep, Mr. Ram Suthar, Mr. Vishal, Mr. Mukesh, Mr. Shyam Sunder and Mr. Shiv Kumar for their kind support during this work.

With a deep sense of adoration and gratitude. I dedicate all my work to my parents, my wife Mrs. Vibhawari and my lovely daughter Miss. Kshiti who were the constant source of moral support in my life; without their encouragement and blessings, no achievement would have been possible. My life would be incomplete without them. It is to them and the almighty that I owe all.

Kedar Shridhar Prayag

Abstract

Trypanosomiasis is a parasitic infection caused by *Trypanosoma*. It is one of the major causes of deaths in underprivileged, rural areas of Africa, America and Asia. Depending on the parasite species responsible or the disease, it can take two forms namely African trypanosomiasis (sleeping sickness) and American trypanosomiasis (Chagas disease). The complete life-cycle stages of trypanosomes span between insect vectors (tsetse fly, triatomine bug) and mammalian hosts (humans, animals). Only few drugs have been approved for the treatment of trypanosomiasis. Moreover, current trypanocidal therapy has major limitations of poor efficacy, serious side effects and drug resistance. Due to the lack of economic gains from tropical parasitic infection, it has always been neglected by researchers and drug manufacturers. There is an immense need of more effective innovative strategies to decrease the deaths associated with these diseases. Nanotechnological approaches for the delivery of existing drugs have shown significant improvement in efficacy with the many-fold decrease in their dose.

In this dissertation, lipid based nanoformulations (solid lipid nanocarriers, and oily nanosuspensions) were explored for the enhanced therapeutic efficacy of quinapyramine sulphate (QS). The overall objective involved modification in physicochemical nature of hydrophilic QS in order to prolong the drug concentrations after administration. Protracted drug plasma concentrations of QS would enhance the efficacy of the therapy thereby reducing the side effects associated with the current anti-trypanosomal therapy.

A simple, accurate, robust isocratic ion-pair based HPLC method was developed to estimate QS in nanoformulations, *in-vitro* release, plasma samples of rat and camels. The developed HPLC method was validated according to ICH regulatory guidelines. The method was found to be linear in the range of 125 to 2500 ng/mL concentration ($R^2 \geq 0.999$) at 297 nm. The limit of detection and limit of quantification for quinapyramine sulphate was found to be 100 ng/mL and 180 ng/mL, respectively. The intraday and inter-day precision % relative standard deviation were less than 2%. The developed method was successfully evaluated for specificity and for its applicability for *in vivo* pharmacokinetic study in rats and camels.

QS-docusate sodium-loaded solid lipid nanoparticles (QS-DS-SLN) were prepared by solvent evaporation technique. QS was hydrophobic ionically complexed at a molar ratio of 1:2 of QS to DS, to prepare hydrophobic Quinapyramine Sulphate-Docusate sodium (QS-DS) ionic complex. Based on the difference in total solubility parameter and polarity of QS-DS complex and different lipids, precirol was selected as a lipid for the preparation

of lipidic nanoparticles. The particle size, zeta potential, and % entrapment efficiency (%EE) of QS-DS-SLN was found to be 250.10 ± 26.04 nm, -27.41 ± 4.18 mV and 81.26 ± 4.67% respectively. FTIR studies confirmed the formation of QS-DS ionic complex. DSC and XRD studies revealed the amorphous nature of QS in QS-DS-SLN. The spherical shape of nanoparticles was confirmed by scanning electron microscopy. QS-DS-SLN showed sustained release of QS for up to 60 h. Further, preclinical evaluation of QS-DS-SLN was done for the trypanocidal effect against *T. evansi* parasite. Nanoformulation showed low haemolysis (<10%) of rat erythrocytes and also to be safe (>60% cell viability) as compared to free QS in THP-1 cells. Confocal and flow cytometry analysis confirmed enhanced cellular uptake of Coumarin-6 (C6) solid lipid nanoparticles (C6 SLN) compared to free Coumarin 6. Cellular uptake studies showed C6 SLN could be internalized by THP-1 cell by different mechanisms including lipid-raft, clathrin- and caveolin-mediated pathways. *In vitro* trypanocidal studies against *T. evansi* showed that QS-DS-SLN exhibited low IC_{50} compared to free QS. A confocal microscopy study confirmed that both QS and QS-DS-SLN induced significant morphological changes in the *T. evansi* parasite after treatment. QS equivalent to 7.5 mg/kg in QS-DS-SLN treated *T. evansi* infected mice showed successful treatment without relapse of infection for 60-days, confirmed by the blood smear and DNA amplification by PCR assay. Moreover, scale up of QS-DS-SLN was studied for 20-times of lab scale batch which showed no significant difference in particle size, zeta potential, and % entrapment efficiency of pilot-scale batch prepared by utilizing geometrical similarity approach across scales for the preparation of QS-DS-SLN.

(QS) loaded long-acting oil-based nanosuspension was prepared by transforming QS to a hydrophobic ionic complex using anionic sodium cholate (Na.C). The complex was characterised by FTIR, DSC, and XRD. Oil-based nanosuspension was prepared by dispersing the QS-Na.C complex in thixotropically thickened olive oil. The nanoformulation was found to be cytocompatible [82.5 ± 5.87% cell viability at the minimum effective concentration (MEC)] in THP-1 cell lines and selectively trypanotoxic ($p<0.0001$). The pharmacokinetic studies of QS-Na.C complex loaded oily nanosuspension showed 13.54-folds, 7.09-folds, 1.78-folds, and 17.35-folds increase in $t_{1/2}$, $AUC_{0-\infty}$, Vz/F, and $MRT_{0-\infty}$, respectively as compared to free QS. Moreover, a 7.08-fold reduction in plasma clearance was observed after the treatment with the optimized formulation in Wistar rats. Furthermore, treatment with QS-Na.C complex loaded oily nanosuspension (7.5mg/kg) in *T. evansi*-infected mice model showed the absence of parasitaemia for more than 75 days after the treatment of during *in vivo* efficacy studies. The

efficacy of the treatment was assessed by observation of blood smear and PCR assay for DNA amplification.

To conclude, outcome of the present study emphasizes on solving basic difficulties existing in the treatment of veterinary infection i.e., *trypanosomiasis* by rational-based approach. The development of the nanoformulations of QS involved industrially viable option in delivering the highly hydrophilic drug. Our findings suggest that the efficient delivery of QS from the developed QS-DS-SLN and QS-Na.C complex-loaded oily nanosuspension could be a promising treatment option for veterinary infections against *trypanosomiasis*.

List of tables

List of Figures

List of abbreviations and symbols

ACN	Acetonitrile
ADMET	Absorption, distribution, metabolism, elimination and toxicology
API	Active pharmaceutical ingredient
AIC	Akaike Information Criteria
Al-MS	Aluminium monostearate
ANOVA	Analysis of variance
AUC	Area under curve
AUMC	Area under moment curve
BCS	Biological classification system
C_{max}	Maximum concentration
cm	Centimeter
°C	Degree Celsius
DAPI	4′,6-diamidino-2-phenylindole
DCM	Dichloromethane
DLS	Dynamic light scattering
%DL	% Drug loading
DS	Docusate sodium
DMSO	Dimethyl sulfoxide
%EE	% Entrapment efficiency
FDA	Federal drug administration
FESEM	Field Emission Scanning Electron Microscopy
FBS	Fetal bovine serum
GRAS	Generally regarded as safe

HIP	Hydrophobic ion pairing
HPLC	High-pressure liquid chromatography
ICH	The International Council for Harmonization of Technical Requirements for Pharmaceuticals for Human Use
IC_{50}	50% Inhibitory concentration
IM	Intramuscular
IVIVC	In vitro-in vivo correlation
LA	Long-acting
LOD	Limit of detection
LOQ	Limit of quantification
LLOQ	Lowest Limit of quantification
µg	Microgram
MTT	3-(4,5-dimethylthiazol-2-yl)-2,5-diphenyl tetrazolium bromide
mg	milligram
min	Minutes
mL	Milliliter
MRT	Mean residence time
ng	Nanogram
Na.C	Sodium cholate
PDI	Poly dispersibility index
SC	Subcutaneous
S/N	Signal to noise
K Da	Kilo Daltons
µL	Microliter
µM	Micromolar

λ_{max}	Lambda max
QS	Quinapyramine sulphate
RSD	Relative standard deviation
Vd	Volume of distribution
THP-1	human monocytic cell line derived from an acute monocytic leukemia
$t_{1/2}$	Half-life

Table of contents

Chapter 1: Introduction

1. Background

Trypanosomiasis is a neglected tropical disease that is mainly prevalent in low and middle-income countries, including regions of Africa, Asia, and America. Except for fexinidazole which was discovered in late 2018, no new drug has been discovered in the last 50 years for the treatment of *trypanosomiasis*. Furthermore, the emergence of drug resistance against FDA-approved antitrypanosomal drugs has also significantly affected the therapy. Current trypanocidal therapy has significant limitations; hence, there is an immense need for effective and innovative strategies to decrease the deaths associated with these diseases. Nanotechnological approaches for the delivery of existing drugs have shown significant improvement in efficacy with a many-fold decrease in their dose.

Various nano-carrier-based systems for anti-trypanosomal drugs have been discussed by researchers previously. Since risk: benefit ratio with the existing therapy is very low, modification of the pharmacokinetic profile of the drug through a nano-carrier system could find a rational for the treatment. Nanocarriers can alter the physicochemical and pharmacokinetic properties of the drugs to improve the concentration of the drugs in the microenvironment of the parasite and host. The impact of nanomedicine on overcoming drug resistance and improving efficacy is well established.

2. *Trypanosomiasis*

Trypanosomiasis is a vector-borne disease, caused by the parasite of the genus *Trypanosoma* (T.), which affects both animal and human populations. Depending on the protozoan species involved in the pathogenesis, it can take two forms 1) Human African *Trypanosomiasis* (HAT) or sleeping sickness and 2) American *Trypanosomiasis* (AT) or Chagas disease. Comparative features of both HAT and AT are presented in Table 1.1.

Geographically, both HAT and AT are endemic in low-income countries of Africa, Asia, and America where it is one of the major public health concerns. According to World Health Organization (WHO) report on human African trypanosomiasis, an estimated 55 million and 3 million people were at risk of infection with these 2 clinical variants named Trypanosoma brucei gambiense (98% of reported cases) and Trypanosoma brucei rhodesiense (2% of reported cases), respectively, during the period of 2012-2016 (WHO Report on trypansomiasis,

2001). However, due to the continuous effort to eliminate neglected tropical disease, in 2019 and 2020 there were 992 and 663 cases reported, respectively (WHO Trypansomiasis, n.d.).

On the other hand, there were around 28,000 cases of Chagas disease per year, which affects around 6 million people and results in nearly 12,000 fatalities with an estimate of around 65 million people are at risk of contracting the disease. Further, African Animal *Trypanosomiasis* (AAT) is also responsible for serious economic losses in wide range of livestock including camels, horses, buffaloes, sheep and goats(Pathak et al., 1993). *Trypanosoma evansi* is the causative agent for *trypanosomiasis* in various domestic animals. Whereas, *T. congolense, T. vivax, T.brucei* are other protozoan species of the parasite responsible for AAT (Chandrasekar, 2018; WHO Report on trypansomiasis, 2001).

Due to a lack of interest by the pharmaceutical industry and government most probably due to limited economic gains, except for fexinidazole which was introduced in late 2018, no new drug has been discovered in the last 50 years for the treatment of *trypanosomiasis* (Simarro et al., 2008). Therefore, in 1975, WHO classified *trypanosomiasis* as one of the neglected diseases to inspire the endemic states for development of more effective therapies. The emergence of drug resistance against available drugs has complicated the present situation. Above-described facts indicated an urgent need to identify new options to treat *trypanosomiasis*.

Table 1.1 Comparative features of African *Trypanosomiasis* and American *Trypanosomiasis*

	African *Trypanosomiasis* (Sleeping sickness)	**American *Trypanosomiasis* (Chagas disease)**	**Ref**
Protozoan parasites	*Trypanosoma brucei gambiense* (*T. b. gambiense*) and *Trypanosoma. brucei. Rhodesiense* (*T. b. rhodesiense*)	*Trypanosoma cruzi* (*T. cruzi)*	(WHO, n.d., n.d.)
Morphology and cell structure	Flagellated single-celled extracellular parasites with flagetted pockets and freely living in body fluids	Flagellated single-celled intracellular parasites with flagetted pocket	("Centers for Disease control and Prevention," n.d., "Chagas Disease," n.d.)
Vector	Tsetse flies	Triatomine bugs ("kissing bugs").	
Mode of transmission	Saliva of insect bite	Urine & feces of insect, congenital	(Barrett and Croft, 2012)
Host	Humans for *T. b. gambiense* Domestic cattle and wild animals for *T. b. rhodesiense*	Humans	
Nature of the illness	*T. b. gambiense* causes a chronic illness while *T. b. rhodesiense* causes a more acute illness	Acute illness in children followed by chronic manifestations later in life	(WHO Trypansomiasis, n.d.)
Incubation period	Weeks or months (*T. b. gambiense*), few days or weeks (*T. b. rhodesiense*)	-	
Host organs affected in advanced stage of infection	Central nervous systems	Cardiac and Gastrointestinal organs	(WHO Trypansomiasis, n.d.)

2.1 Life Cycle

The life cycle of trypanosome spans various stages in mammalian host and arthropod vector in which it regularly changes its phenotypic and replicative characteristics (fig. 1.1). Tsetse flies are responsible for African *trypanosomiasis* bite during daylight hours where, both male and female flies can equally transmit the infection whereas, triatomine bug is responsible for inoculation of *T. cruzi* causing American *trypanosomiasis* ("Centers for Disease control and Prevention," n.d., "Chagas Disease," n.d.). Trypanosome belongs to a class of hemo-flagellated protozoa which is responsible for *trypanosomiasis* in humans and animals. The parasite is characterized by the presence of typical eukaryotic flagellate, functional mitochondria and atypical nuclei. The complete life-cycle stages of trypanosomes are complex and spans between insect-vector (tsetse fly) and mammalian host (humans, animals). Fig.1.1 represents the complete life-cycle of trypanosomes (Lidani et al., 2017; Simarro, 2014). The parasite is transmitted from the insect-vector to the mammalian-host during the blood meal of fly. Moreover, the parasite undergoes various morphological and metabolic changes to adapt diverse environments experienced by it during entire life-cycle (Fig. 1.2) (Matthews, 2005). For instance, in mammals, it uses antigenic variations to escape from host immune system and undergoes metabolic changes to use available nutrients (glucose in blood and brain, lipids in adipose tissues). In case of insect vector, the parasite undergoes metabolic changes to survive in glucose-free and amino acid (proline) rich environment (Smith et al., 2017).

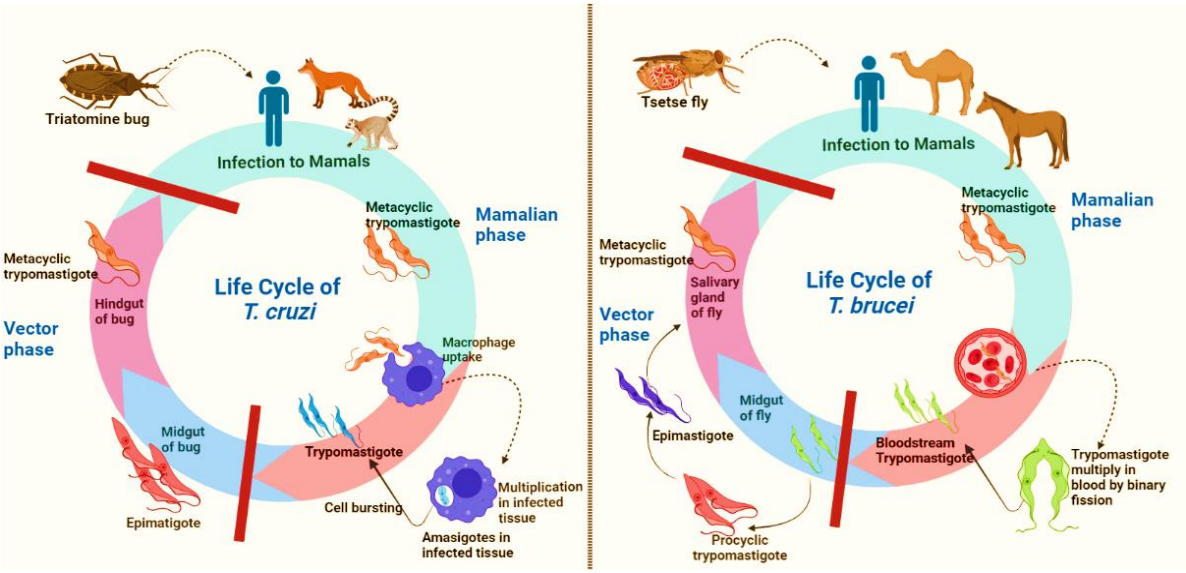

Fig. 1.1 Life cycle of trypanosome parasite, a) *T. cruzi* inoculated by triatomine bug responsible for American *trypanosomiasis*, b) *T. brucei* inoculated by tsetse fly responsible for African *trypanosomiasis*

Briefly, during a blood meal, tsetse fly passes short stumpy, metacyclic form of trypomastigotes inside mammalian host through saliva whereas, triatomine bugs pass these trypomastigotes through urine or faces near broken skin of bite or wound. In African *trypanosomiasis*, these trypomastigotes transverse freely in circulation from the skin to lymphatic, blood and spinal fluids but, they get accumulated inside the adjacent cells to multiply and differentiate to form amastigote form of trypomastigote in American *trypanosomiasis* (Landfear, 2011). Amastigote continues to divide by binary fission and after full maturation, cells burst to spread the bloodstream form of trypomastigote. There is a characteristic difference in American and African *trypanosomiasis* where the bloodstream trypomastigote is capable of replication later. After reaching a specific organ, replication gets seized to form a short stumpy form in African *trypanosome* where it continues to infect a new cell and multiply there in case of American *trypanosomiasis*. During the bloodstream form of trypomastigote, if a pathogen-free insect bites a mammal, it carries those trypomastigotes with them continuing the disease cycle. Through the saliva of insects, these trypomastigotes travel to the midgut where they replicate by binary fission to form procyclic trypomastigotes (absent in American *trypanosomiasis*). Ingested trypomastigotes convert to epimastigote in midgut in case of American trypanosome whereas, after leaving midgut procyclic form gets converted to epimastigote form. Further, short stumpy epimastigotes again multiply forming the most infective metacyclic form of trypomastigote in the hindgut. The metacyclic form is characterized by the presence of a highly mutagenic surface of a dense glycoprotein coat (about 15 nm thick), where dimerized glycoproteins (VSGs) provide protection. The VSG coat keeps antibodies and the complement system away from the parasite, and maintains key nutrient acquisition and communication within cell (De Koning, 2001; Glover et al., 2013; Mugnier et al., 2016; Nenarokova and Michels, 2017; Souza, 2002; Tiengwe et al., 2017).

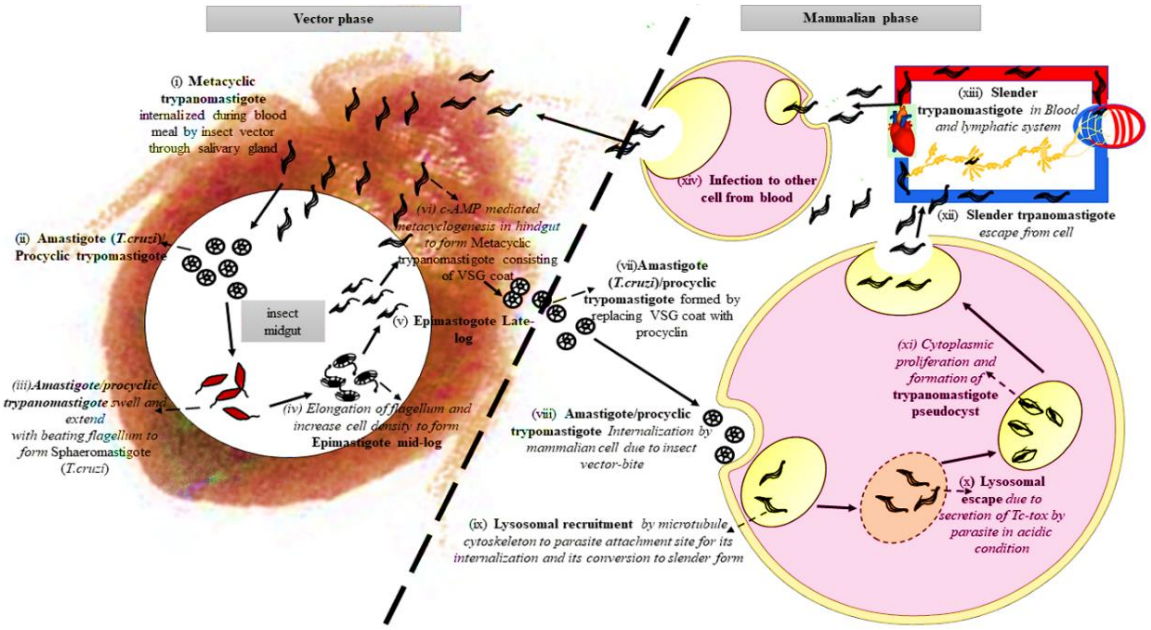

Fig. 1.2 Morphological and metabolic changes in the African and American trypanosome during its life cycle in vector and host

3. Current antitrypanosomal therapy and its challenges

3.1 Current antitrypanosomal therapy

African trypanosomes undergo continuous antigenic variations by producing the alterations in VSG surface coat during the mammalian infection cycle for successful immune evasion (Bangs, 2018; Borst et al., 2016; Mugnier et al., 2016). Therefore, the vaccine has not been developed for protection against trypanosome parasites. The treatment of *trypanosomiasis* completely depends upon chemotherapy. Only few drugs have been approved for the clinical use in trypanosome infection so far. Therapeutic agents used for the treatment of *trypanosomiasis* both in humans and animals are presented in Table 1.2.

Table 1.2 Therapeutic agents used for the treatment of *trypanosomiasis*

Drug	**Chemical Class**	**Cellular/molecular targets**	**Dosage form and route of administration**	**Clinical indication**	**Limitations**	**Ref.**
Suramin	Polysulfonated naphthyl amine	Non-specific, binds with L-α-glycerophosphate oxidase	Powder and ready to use solution administered by intramuscular (IM) route or intravenous (IV) route	Effective against *T. b. rhodesiense*	Toxicity, unable to cross blood brain barrier	(Babokhov et al., 2013a; Barrett et al., 2007; Fairlamb, 2003; Gutteridge, 1985)
Pentamidine, Diminazene	Diamidine	Binds to parasite DNA, inhibits type II topoisomerase and disrupts mitochondrial DNA	Colorless powder administered by IM route	Earlystage *T. b. gambiense* infection	Hypoglycemia, hypotension, drug resistance	(Baker et al., 2013; Barrett et al., 2007; Brun et al., 2010; Fairlamb, 2003)
Melarsoprol, Melarsomine	Melaminophenyl arsenical	Oxidative stress by inhibition of trypanothine reductase	Ready to use solution in propylene glycol, administered by IV route	Stage-2 *T.b gambiense* infection	Narrow therapeutic index, reactive encephalopathy	(Fairlamb, 2003; Giordani et al., 2017)
Homidium, Isometamidium	Phenanthridine	Inhibits topoisomerase II during DNA biosynthesis	Powder for reconstitution administered by IM route	Prophylaxis and treatment of *T.evansi, T.vivax, T.congolense* and *T.vivax*	Highly toxic, drug resistance	(Road, 1988; Thomas et al., 2018)
Quinapyramine	Aminoquinaldine	Trypanostatic, inhibits kinetoplastic DNA biosynthesis,	Powder for reconstitution	Effective against *T.congolense,*	Serious local reactions at site	(Biobaku, n.d.; Desquesnes et al., 2013)

		loss of ribosomal function	administered by IV or IM route	*T.vivax, T.brucei and T. evansi*	of action, drug resistance	
Eflornithine	Ornithine analogous	Inhibits ornithine de-carboxylase	Ready to use injection administered by IV route	Effective against *T. b. gambiense*	Large doses (400mg/kg) required,	(Barrett et al., 2007; Pink et al., 2005; Thomas et al., 2018)
Nifurtimox	Nitrofuran derivate	Generation of superoxide, $H_2O_2$and free radicals interacting with nitro-reductase disrupting cellular components DNA, membrane lipids and proteins	Oral tablets	Effective against *T.cruzi* and eflornithine, melarsoprol resistant treatment of Human African *trypanosomiasis*	Gastro-intestinal disturbances	(Romero and Morilla, 2010; Thomas et al., 2018)
Benznidazole	Nitroimidazole	DNA damage by nitroreductase present in *T.cruzi* parasite	Oral tablets	Effective against *T.cruzi*	Hypersensitivity, neurological disorder	(Urbina and Docampo, 2005)
Nifurtimox-eflornithine combination therapy	NECT	Synergistic effect of individual drugs	Nifurtimox by oral tablets orally and Eflornithine administered by IV route as infusion	Effective replacement of toxic melarsoprol in stage-2 *T.b gambiense* infection	Less effective against *T.b.rhodesiense*	(Samo and Jannin, 2012; Yun et al., 2010)

3.2 Major challenges with existing antitrypanosomal therapy

The problems including poor efficacy and high toxicity associated with the current therapy pose significant challenge in their clinical use. Moreover, development of resistance to existing drugs is another difficulty in treatment of this tropical parasitic infection.

Approved anti-trypanosomal drugs are either highly toxic (melarsoprol) or although are reasonably tolerable yet do not permeate through blood–brain barrier (suramin, pentamidine) restricting their use in treatment of first-stage of the disease only(Barrett, 2000; WHO Report on trypansomiasis, 2001). Moreover, except nifurtimox and benznidazole, all other drugs are administered by parenteral route, leading to poor patient compliance (Baker and Welburn, 2018).

Unfavourable physicochemical and pharmacokinetic properties of the available anti-trypanosomal drugs are other major limitations in their clinical use. For instance, most of the drugs are either highly polar (suramin, pentamidine, isometamidium and quinapyramine) or has short half-life (eflornithine, suramin). These drugs are available in the form of powder or ready-to-use solution for parenteral administration for the treatment of early stage of disease (Simarro et al., 2012). These drugs exhibit high serum protein binding, thereby resulting in poor brain permeability (Barrett et al., 2007). Melarsoprol, an arsenical water insoluble compound, is available in the form of ready to use solution in propylene glycol. It has potential to cross blood brain barrier and exhibits long half-life (35 h). Although, melasoprol is widely used in treatment of advanced *T. b.rhodesiense*, *T. b. gambiense* infections, the associated risks of drug resistance and encephalopathy are major drawbacks (Barrett et al., 2007). Pentamidine is a positively charged diamidine, another important drug to treat early stage of *T. gambiense* infection, which is given by intramuscular route (4mg/kg). Diminazene, another diamidine widely used to treat animal African *trypanosomiasis* also lacks poor brain permeation due to cationic polar nature (Olbrich et al., 2004). It is although well tolerated, requires repeated administration of 7-10 injections results in poor patient compliance(Babokhov et al., 2013a; Baker et al., 2013; Gutteridge, 1985; Olliaro et al., 2002). Another class of phenanthridine derivative includes isometamidium, widely used in treatment of animal *trypanosomiasis*. It is also a positively charged quaternary ammonium compound and is available as a mixture of four isomers wherein isomer-II exhibits higher trypanocidal activity than all the others three isomers(Road, 1988; Sahin et al., 2014; Schad et al., 2008).

Most of the existing drugs available in the market even don't satisfy the ideal conditions of drug like safety, efficacy and least toxicity. Marketed formulations mainly consist of powder

for reconstitution or ready to use solutions. Moreover, lack of introduction of new drug after 1970 clearly denotes the negligence of researchers towards anti-trypanosomal therapy. Various outbreaks of trypanosomal infection have been observed recently in the tropical regions of Africa. Inherent toxicity, lack of specificity and less potency are among prominent lacunas.

3.3 Drug resistance

Development of resistance of drugs against trypanosomes has been the most serious concern in the complete eradication of *trypanosomiasis*. Trypanosomes depend on their host for uptake of essential nutrients using specific transporters present on the surface of the parasite. Loss of function of these transporters has been identified as a major reason of development of drug resistance against trypanosomes(Barrett et al., 2007). Various drugs and their transporters have been listed in the Table 1.3.

Table 1.3 Anti-trypanosomal drugs and their transporters

Drug	**Transporter**	**Reference**
Eflornithine	Amino acid transporter AAT6	(Barrett et al., 2007)
Suramin	Endocytic pathway invariant surface glycoprotein ISG75	(Gutteridge, 1985)
Pentamidine	Aquaglyceroporin 2 (TbAQP2)	(Baker et al., 2012)
Melarsoprol	P2-purine transporter	(Baker et al., 2013)
Diminazene	TbAT1/P2	(Garcia-salcedo et al., 2014)
Nifurtimox	P2 aminopurine transporter	(Barrett et al., 2007)

Usually, in order to elicit its pharmacological effect, the drug must gain entry into the parasite which can occur through various transporters or through an active transfer with the help of a carrier. The specific transporters or receptors present on the surface of the trypanosome indicated in fig. 1.3 transport the drug/s across the parasite membrane. Besides practical challenges in the administration of antitrypanosomal agents, the protective coat of VSG over trypanosome surface, resistance caused by modifying or deleting one or more such transporters by mutations present limitations in therapy. Moreover, increased drug efflux or reduced drug absorption are other possible mechanisms of drug resistance exhibited by trypanosomes.

Although there are many limitations of existing therapy for treatment of *trypanosomiasis*, the propensity and severity of disease necessitates the use of these drugs for the treatment. Therefore, new drug discovery in the area of trypanocidal drugs is essential for reducing the disease and associated deaths. To conclude, the lack of safety and emergence of drug resistance to FDA-approved drugs demands technological interventions to improve trypanosomal therapy. In order to overcome above-described facts there is an urgent need to identify new options to treat *trypanosomiasis*. Nanomedicine-based drug delivery systems have shown significant potential in improving the efficacy of the antitrypanosomal drug (Babokhov et al., 2013b; WHO, n.d.).

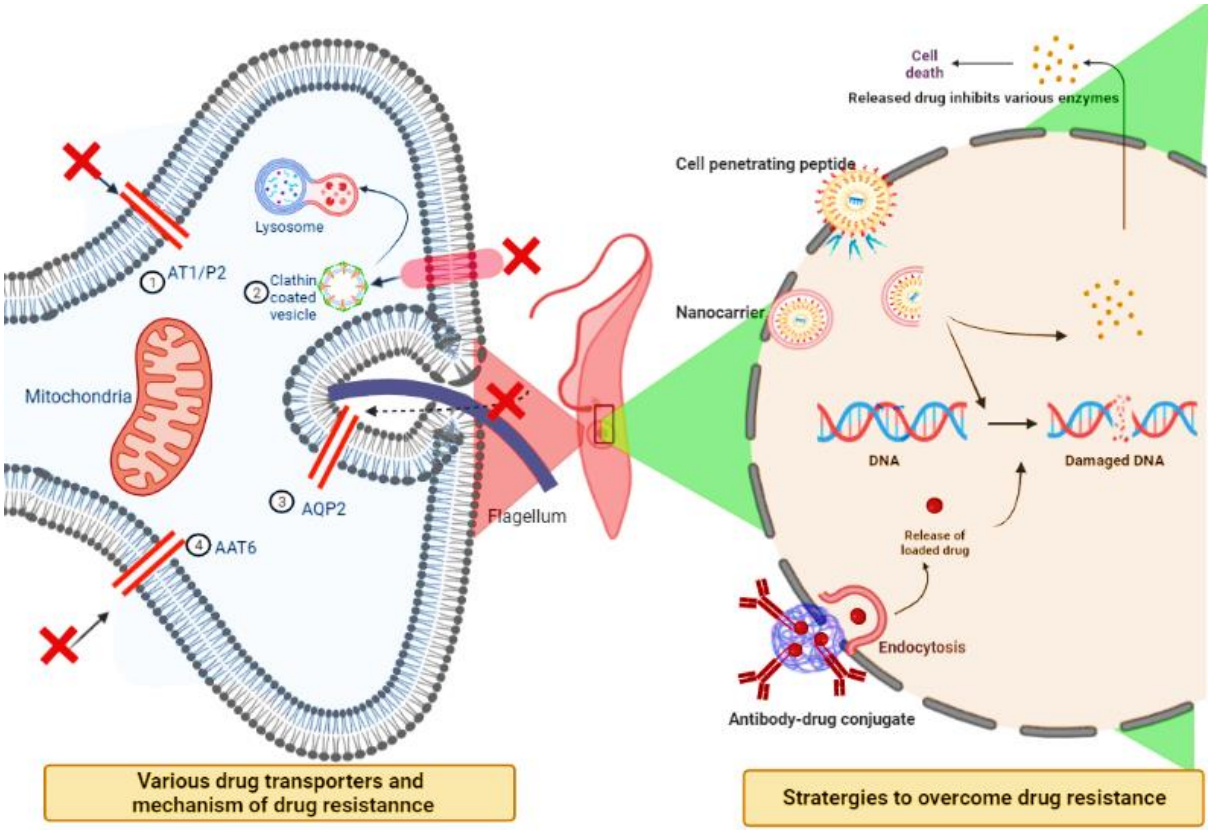

Fig. 1.3 Various drug transporters and drug resistance mechanism in *T. brucei*

4. Advances in conventional therapy and novel lead compounds

The recent advances in the treatment of *trypanosomiasis* involve the first clinical trial for an oral sleeping sickness drug pafuramidine and the introduction of eflornithine–nifurtimox (NECT) combination therapy to replace melarsoprol in an advanced stage of HAT (Samo and

Jannin, 2012; Yun et al., 2010). The development of new drugs which are safe, effective and affordable is a need of an hour to overcome many limitations of existing therapy.

However, the lack of safety and emergence of drug resistance to FDA-approved drugs demands technological interventions to improve trypanosomal therapy.

Development of new class of drugs (Barrett, 2010; Kaiser et al., 2011), novel lead compounds (Barrett et al., 2007; Cavalli et al., 2010) and combination of existing drugs (Priotto et al., 2007; Yun et al., 2010) have been attempted to increase the efficacy of therapy(Aksoy et al., 2017). For instance, Nirfurtimox-Eflornithine combination therapy (NECT) in 2009 was introduced in essential medicines list (Mordt, 2013) to focus treatment for cerebral stage of disease where, Melarsoprol was the only choice. Although, eflornithine alone can cross blood brain barrier (BBB) but it is accompanied with drawbacks including high dose (100mg/ kg) and short-half-life (3h). Randomized clinical trials showed combination of eflornithine with nifurtimox could elicit synergistic effect (Baker and Welburn, 2018; Samo and Jannin, 2012). Simplified regimen of NECT includes 7 days of eflornithine infusion twice a day and oral nifurtimox for 10 days(Bray and Pe, 2010) which led to reduced dosing frequency, decreased total cost of therapy and diminished dependency on melarsoprol which has potential of causing reactive encephalopathy.

Many new potential leads including 2-piperazine-1-yl-quinazoline-4-ylamine derivative and Lapachol (Croft, 2003), D0870 and triazoles (Urbina, 2015; Urbina et al., 2000), N-methyl-piperazien-urea-F-hF-vinyl-sulfonephenyl and semicarbazone scaffold (Cavalli et al., 2010), bisphosphonate (Montalvetti et al., 2001), allopurinol (Berens et al., 1982), miltefosine (Saraiva et al., 2002) and their corresponding targets namely; trypanothione, P-450-dependent C14α-dementhylase, squalene synthase (Shang et al., 2014), cruzipain inhibitor (Salas-sarduy et al., 2017), farnesyl pyrophosphate synthase (Montalvetti et al., 2003), purine salvage inhibitors (Berg et al., 2010) and prenyl and N-myristoyltransferase inhibitors (Frearson et al., 2010) respectively have been invented recently. However, thorough in-vitro and in-vivo efficacy studies and clinical studies are yet to be established for the same.

5. Nanotechnology based strategies for targeted delivery of anti-trypanosomal drugs

5.1 Passive targeting using conventional and PEGylated nanocarriers

Passive targeting of nanocarriers relies on the anatomy-physiology and patho-physiology coupled with physicochemical properties of the nanocarriers (Zhang et al., 2018). For instance, large nanoparticles (>200 nm) accumulate in the macrophages while nanoparticles of size <200

nm (He et al., 2010) or polyethylene glycol modified nanoparticles evade macrophages and show longer blood circulation (Kaul and Amiji, 2004) which could enable access and retention of nanocarriers in difficult-to-access locations including tumours (Press, 2012), inflammatory sites (Luo, 2018), spleen (Jindal, 2016), brain (Cole et al., 2011) leading to drug delivery in sub-cellular organelles (Suk et al., 2016). Therefore, selection of drug delivery strategy largely depends upon the target site in the body. In case of *trypanosomiasis*, location of parasite in the body depends upon type of causative agent. For instance, in case of American *trypanosomiasis* (chagas disease), parasite *T. cruzi* mainly resides within the cell cytoplasm while, in case of African *trypanosomiasis* (sleeping sickness), parasite resides in blood stream and lymph nodes in initial stages of infection and affects CNS in later stage. Similarly, *T. evansi*, responsible for *trypanosomiasis* in animals, resides in blood, tissues and body fluids. As the parasite resides either in blood stream or in remote locations in the body including lymph nodes or CNS, macrophages could be a major biological hurdle in drug accumulation in these organs. Passive targeting therefore could not be a viable option for targeted delivery of antitrypanosomal drugs to the site of infection thus making use of long circulating nanocarriers necessary (Bamrungsap et al., 2012). There are few reports present in literature demonstrating nanoparticle based passive targeting of antitrypanosomal drugs to improve efficacy in mouse model. Passive targeting strategy has been explored using liposomes and polymeric nanoparticles (Maniruzzaman et al., 2012). Details of these nanocarriers are presented in sections below.

5.2 Active targeting using ligand-anchored nanocarriers

Active targeting of cargo loaded-nanocarriers could be achieved by conjugating the infected-cell specific or parasite-specific ligand onto the surface of nanocarriers to enable enhanced accumulation of the drug in target site (Muro, 2012; Yamashita and Hashida, 2013). In case of active targeting, it is essential that receptors specific for ligands should be either solely expressed or over-expressed at the surface of infected cell or parasite. In case of African *trypanosomiasis*, lymph nodes and CNS are the main target sites. Surface modified-nanocarriers to enhance CNS delivery have been extensively exploited and reviewed elsewhere in detail (Molina-portela et al., 2008; Steverding, 2000). Ligand for receptors present on surface of *trypanosome* parasite has potential to modify the nanocarriers for active targeting (Bareford and Swaan, 2007; Jeevanandam et al., 2018). Few attempts using ligand based active targeting of antitrypanosomal drugs in experimental *trypanosomiasis* using liposomes and polymeric nanoparticles have been investigated like nanobody conjugation (Unciti-broceta et al., 2015),

conjugation with trypanolytic factor apolipoprotein L-I (Conrath et al., 2006a), transferrin surface conjugation for brain targeting (Chang et al., 2009) were studied for active targeting of drugs.

5.3 Impact of nanotechnology on trypanocidal therapy

Nano drug delivery systems have exerted profound impact on trypanocidal therapy by improving *in-vitro* and *in-vivo* efficacy, reducing toxicity, reducing dose and overcoming drug resistance. Furthermore, nanocarriers also improved accessibility of trypanocidal drugs to parasite reservoirs (brain) in African *trypanosomiasis*. Table 1.4 presents different nanocarriers used in the delivery of trypanocidal drugs. Impact of nanocarrier on trypanocidal therapy is also presented in Table 1.4.

5.3.1 Nanocarriers against Human African *Trypanosomiasis*

Encapsulation of anti-trypanosomal agents in nanocarriers exerted significant impact on in vitro and in vivo efficacy. Table 1.4 summaries different nanocarriers evaluated to study the anti-trypanosomal effect of the drugs. A brief highlight of each study is also indicated in the same table.

A. *In-vitro efficacy* studies in infected cell lines

Drug free-liposomes composed of specific lipids have shown promising trypanocidal effect against parasite infected cell lines. For example, stearylamine (SA) containing phosphatidylcholine (PC) liposomes were found to be effective against bloodstream form of *T.brucei gambiens*e. SA/PC-liposomes demonstrated more than 99% cell lysis within 30 min after treatment with 15 mol% liposomes. However, free-SA did not show any trypanocidal activity, suggesting the significance of liposome structure in efficacy of SA against parasite. Authors attributed that, this could be due to fusion of liposome with *T.brucei gambiens*e plasma membrane subsequently translocation of SA into plasma membrane which eventually causes cell death by interfering with shape-maintaining machinery (Tachibana et al., 1988). The study suggests that SA incorporated liposome could be used for the treatment of *T.brucei gambiens*e infection. In another study, Arsonolipids, lipid analogues of phospholipids, based liposome called Arsonoliposomes exhibited anti-leishmanial and trypanocidal effect. Arsonoliposomes showed minimum effective concentration from 0.20 to 0.87 µM when incubated with *T.b brucei* for 24h. Interestingly, arsonolipids were not active against trypanosomes, highlighting

the role of liposomal formulations in trypanocidal effect (Antimisiaris et al., 2003). Negative charge onto arsonoliposome surface (-42.0 to -69.5 mV) would have facilitated the entry of arsonoliposome within trypanosome, probably via ionic interaction. These studies suggest that both SA incorporated-liposome and arsonoliposome could be used for the treatment of trypanosome infection as viable alternative to existing trypanocidal therapy. However, an *in-vivo* proof of concept in infected animal models is yet to be established.

Trypanosome exhibits very high surface turnover rate. This enables the entry of active drug through specific region present in the flagellar pocket of parasite (Garcia-salcedo and Unciti-broceta, 2015). This phenomenon of trypanosome has been translated for delivery of drugs by using surface-modified nanoparticles. For instance, pentamidine loaded PLGA nanoparticles when surface modified with single domain antibody fragment (NbAn33) which is specific for cryptic epitope present on VSG surface coat of trypanosomes has shown significant dose reduction both *in-vitro* and *in-vivo*. (Arias et al., 2015). Anti-trypanosomal drugs effective against African trypanosomes enter into the parasite through cell-surface transporters. Functional loss of these transporters by mutation leads to impaired drug uptake by the trypanosomes, thereby results in development of drug resistance (Munday et al., 2015). For instance, loss-of-functions of aquaglyceroporins cell surface transporters are responsible for development of pentamidine resistance (Munday et al., 2014). Surface-modified nanoparticles enter into parasites by endocytosis, thus bypassing cell surface transporters and overcome drug resistance. For instance, pentamidine-loaded PEG-conjugated chitosan nanoparticles coated when modified with nanobodies (NBAn33) specific for cryptic epitopes on the trypanosome surface, showed anti-trypanosomal activity in pentamidine-resistant trypanosome cell-line (Unciti-broceta et al., 2015). Cellular uptake of nanobody conjugated PEGylated-chitosan nanoparticles occurred via endocytosis and was found to be accumulated in flagellar pocket of trypanosome. ApoL-I, a serum factor involved in natural defense mechanism against African trypanosome, was conjugated with nanobody (NbAn33) against ApoL-I resistant *T.b. rhodesiense. In-vitro* trypanolytic activity of these NbAn33–Tr-apoL-I specifically recognized the parasite cells of *T. brucei* with complete parasitaemia at the dose of 180 nM after 4 hrs of incubation (Conrath et al., 2006b; Molina-portela et al., 2008).

B. In-vivo efficacy

Arsonoliposomes:

Arosonoliposomes equivalent to 0.54 mg of arsonolipid when administered intraperitoneally in BALB/c mice revealed that 15% total dose accumulation in liver confirmed by X-ray fluorescent technique.(Antimisiaris et al., 2003).

Antibody conjugated pentamidine loaded polymeric nanoparticles were administered intraperitoneally in infected mice model with 100-fold reduced dose of Pentamidine. It was observed that the survival rate was 60% in antibody conjugated nanoparticle group while, no-survival was observed in mice with similar dose of free pentamidine. In case of *in-vivo* therapeutic efficacy of PEGylated-chitosan nanoparticles coated with NbAn33 it was observed that, 100% survival of mice infected with *T. brucei* at 0.025 mg/kg dose (100-fold less than clinically used dose) after 2nd dose while, the uncoated pentamidine loaded chitosan nanoparticles and free pentamidine failed to elicit their action even after 3rd dose, leading to 100% death rate at 22nd day when dosed intraperitoneally (Unciti-broceta et al., 2015). The *in-vivo* efficacy study of NbAn33–Tr-apoL-I in infected mouse reveled that one fourth of intravenous dose (5 µg) has same efficacy as that of intraperitoneal dose (20 µg) while, same study revealed equal effectiveness of administered dose in chronic *T. brucei* infection.

In summary, both conventional and surface-modified nanocarriers have shown significant improvement in trypanocidal efficacy with many-fold dose reduction. Cell specific delivery of anti-trypanosomal drugs using surface-modified nanoparticles has been used to overcome drug resistance, a major limitation associated with current treatment.

5.3.2 Nanocarriers against African Animal *Trypanosomiasis*

African *Trypanosomiasis* is considered as major cause of deteriorating socio-economic condition in sub-saharan countries. Very few anti-trypanosomal drugs have been approved for the treatment in animals. Clinical use of these drugs is limited due to poor efficacy, severe toxicity, drug resistance and reaction at injection site. Encapsulation of these trypanocidal agents in nanocarriers including lipid based and polymer-based nanoparticles has shown significant improvement in both *in-vitro* as well as *in-vivo* efficacy as described below.

A. In-vitro efficacy in infected cell lines

Majority of drugs available in market for treatment of African *trypanosomiasis* are hydrophilic making them ineffective for treatment against late stage of disease in central nervous system.

Lipid based nanocarriers encompass the ability to cross the hydrophobic blood-brain barrier and enhance the efficacy of treatment. For instance, stearic acid and oleic acid lipid-drug conjugate of Diminazene diaceturate were developed for late-stage African *trypanosomiasis*. 2D-PAGE demonstrated adsorption of ApoA-I and ApoA-IV which are vital proteins to cross blood brain barrier and lipid metabolism. Similarly, 2% of Diminazene loaded 1,2-dipalmitoyl-sn-glycero-3-phosphatidylglycerol nanoparticles depicted dose dependent enhanced activity against *T. brucei* cultures compared to free diminazene and free diminazene diaceturate. Enhanced interaction of cationic nanoparticles with negatively charged external surface of parasite could have led to enhanced parasite uptake and anti-trypanocidal activity compared to free drug (Kroubi et al., 2010).

Polymeric nanoparticles have also been explored as carriers for anti-trypanosomal drugs. For instance, sodium alginate based Quinapyramine sulphate nanoparticles were synthesized for animal *trypanosomiasis*. The nanoparticles showed significant reduction in cytotoxicity against vero cell lines when compared with free drug. *In vitro* anti-trypanosomal activity was also shown at significantly lower concentration (0.24 µg/ml) by QS-loaded sodium alginate nanoparticles in *T.evansi* culture. In another study, the same research group revealed that QS-loaded sodium alginate nanoparticles exhibited more cytotoxicity as compared to free-QS. However, hemolytic rate of QS-loaded sodium alginate nanoparticles was decreased as compared to free-QS when studied in equine erythrocyte. Interestingly, at higher dose (300 times higher than effective dose), QS-loaded sodium alginate nanoparticles showed more toxicity than free-QS. This observation necessitates the development of safe nanocarrier systems for the delivery of QS in animals. In an attempt of decrease toxic effect of QS, the same research group developed QS-loaded chitosan nanoparticles with enhanced trypanocidal activity. QS when loaded in chitosan nanoparticles were found to be safe against mammalian cells even at concentration significantly higher than the recommended dose. Nanospheres have also been explored to enhance the curative effect of Nerolidol (naturally derived from essential oil of many plants) against *Trypanosomiasis*. *In-vitro* efficacy studies depicted activity against *T. evansi* compared with free Diminazene after 9h of treatment (Baldissera et al., 2016a).

B. In vivo efficacy

Various nanoparticles described in earlier section depicted significant *in-vivo* efficacy. For instance, QS loaded sodium alginate nanoparticles (0.73 and 0.24 mg/kg) and free QS (5 mg/kg) showed similar effect in *T. evansi* infected mice when administered intraperitoneally.

QS loaded nanoparticles showed 100% and 85.71% survival rate when administered at dose of 0.73 mg QS/kg body weight and 0.24 mg QS/kg body weight respectively in *T. evansi* infected mouse model. Whereas, free QS showed same *in-vivo* efficacy at 5mg/kg dose (Manuja A, Kumar S, Dilbaghi N, Bhanjana G, Chopra M, Kaur H, Kumar R, Manuja B, Singh S, 2014). Further, *in vivo* efficacy was also carried for QS loaded chitosan nanoparticles with enhanced biocompatibility, RES evasion and circulation time. QS-chitosan nanoparticles when administered intraperitoneally in *T. evansi* infected mice depicted 100% survivability with significant reduction in parasitemia from day 3. Further, the dose of QS was reduced by 5.88 to 25-folds compared to free QS. Upon further administration of QS-chitosan nanoparticles after 45 days of *T. evansi* infection in rabbits, parasitemia was cleared from day 3 to 42 day. While, symptomatic relief was obtained from day 14. RT-PCR revealed presence to *T. evansi* DNA in positive control group, while the DNA was absent in animals treated with free QS and QS loaded chitosan nanoparticles. However, significant reduction in dose of QS-chitosan nanoparticles (5-folds) was obtained compared to free QS. *In-vivo* efficacy *of N*erolidol-loaded nanospheres (1.0 mL/kg/day) showed increase in survival time of mice infected with *T. evansi* after oral administration in10-days when compared with free-nerolidol and DMZ.

In summary, encapsulation of drugs effective against *trypanosomiasis* in animals was found to be safe and more effective with many-fold decrease in dose of the drugs. However, *in-vivo* efficacy along with thorough toxicological studies needs to be evaluated of before commercialization of developed nanoparticles.

5.3.3 Nanocarriers against Human American *Trypanosomiasis*

Only two drugs namely benznidazole and nifurtimox are approved for the treatment of American *trypanosomiasis*. Both drugs are available in the form of tablet dosage forms for oral administration which exhibit poor efficacy and serious side effects (Molina et al., 2015). Significant improvement in efficacy and safety profile of benznidazole and nifurtimox were observed after encapsulation in nanocarriers (Khalil et al., 2013).

A. *In-vitro* efficacy in infected cell lines

Nanocarriers has shown promising improvement in anti-trypanosomal activity when studied in trypanosome infected cell lines. Nirfurtimox-loaded polyethylcyanoacrylate (PECA) nanoparticles showed significantly improved trypanocidal activity against cultures of *T. cruzi* epimastigotes when compared with standard nirfurtimox solution. Nirfurtimox-loaded PECA

nanoparticles increased trypanocidal activity of 98.9% when compared to free drug that showed 40% of trypanocidal activity in *T. Cruzi* infected vero cell lines. The IC_{50} value of nifurtimox PECA nanoparticles was drastically reduced to 0.0015± 0.0006 µg/ml as compared to 0.683±0.269 µg/ml for free drug(Gonzalez-martin et al., 1998). Allopurinol conventionally used for treatment of gout, have been utilized to treat Human American *trypanosomiasis* (Berens et al., 1982) after incorporation into polyethylcyanoacrylate nanoparticles with anti-proliferative activity of 91.5% compared to 45.9% for free drug in vero cells infected with epimastigote form of *T. cruzi* (Gonza, 2000). Interestingly, these studies revealed that, unloaded PECA nanoparticles alone have greater trypanocidal activity than the free drug solutions of both nifurtimox and allopurinol highlighting potential usefulness of polyethylcyanoacrylate (PECA) as a carrier in the treatment of American *trypanosomiasis*.

Furthermore, BNZ encapsulated into nanocarriers has shown greater potential of selective targeting at various stages of parasite life cycle. For instance, nanoencapsulation of benznidazole in calcium carbonate led to trypanolytic activity against epimastigote and tryapnomastigote selectively in LLCM K2 cells. Time and dose dependent growth inhibition was observed in epimastigote while, IC_{50} of benznidazole nanoparticles was 37.79-fold higher compared to free benznidazole against trypanomastigote (Tessarolo et al., 2018). The selectivity ratio [ratio of cytotoxic (CC_{50}) and median lethal dose (LC_{50})] in LLC-MK2 cells was found to be 12-fold higher for encapsulated BNZ than free BNZ, highlighting selectivity of inorganic nanocarrier during targeting (Tessarolo et al., 2018).

Anti-trypanosomal therapy has also been explored with nanosuspension of benznidazole to treat acute stage of American *trypanosomiasis*. For instance, nanosuspension of BNZ has been studied for toxicity assays on vero cells as well as cardiac myocyte cultures cells, a primary tissue affected in *T. cruzi* infection. Study revealed that, with half the conventional dose of BZN, drug loaded nanoparticles had same inhibitory effect on the growth of *T. cruzi* amastigote form of parasite (Scalise et al., 2016). Moreover, benznidazole-loaded liposomes showed enhanced cellular uptake of benznidazole as compared to free benznidazole in J774 cells (Morilla et al., 2004, 2002). pH-sensitive liposomes (380 nm) composed of dioleoyl-phosphatidyl-ethanolamine: cholesteryl hemisuccinate were phagocytosed and subsequently deliver the drug in cytosol of both *T. cruzi*-infected and uninfected J774 macrophages. ETZ-loaded liposomes showed 72% of anti-amastigote activity in *T cruzi*-infected J774 macrophages, while no activity was observed in case of free ETZ at the same dose.

B. *In-vivo* efficacy studies

Nanoencapsulation of antitrypanosomal drugs effective against human American *trypanosomiasis* have also shown significant improvement in *in-vivo* efficacy of drugs in *trypanosomiasis* infected animal models.

Experimental molecule (D0870) (bis-triazole derivative) when encapsulated in PEGylated poly(lactic) acid nanoparticles (3 mg/kg/day) led to 60-90% cure rate in murine short-term Y-strain Chagas disease model (Molina et al., 2001).

Benznidazole nanosuspension when administered *in-vivo* intraperitoneally have shown effective inhibition of the parasite in C_3H/HeN mice with acute lethal infection leading to 100% survival even after 30 days when compared to treatment with free drug which elicited 70% survival after 15 days at 25 and 50 mg/kg/day dose (Scalise et al., 2016).

Biodistribution of BNZ encapsulated liposomes were studied after intramuscular (IM), intravenous (IV) and subcutaneous (SC). It was observed that, BNZ liposomes were accumulated in liver significantly higher concentrations after IV administration when compared to IM and SC route. 3-fold higher concentration of BNZ loaded liposomes was found to be in liver compared to blood when same formulation studied in *T. cruzi* infected BALB/C mice. However, the parasitemia was persistent until 2-days. In another study ETZ loaded pH sensitive liposomes (14µg/mouse dose) showed significant reduction in parasitaemia in *T. cruzi* infected mice model after IV administration. Whereas, even 180-fold higher dose of free ETZ failed to reduce the parasitaemia level in *T. cruzi* infected mice.

6. Enhanced antitrypanosomal effect of natural products

Traditional medical practices such as Ayurveda, Siddha, Unani and Chinese medicines are based on the use of naturally occurring plants and their derived products for the treatment of different diseases.

Table 1.4. Impact of nanocarriers on trypanocidal therapy

Sr. No.	Drug	Nanocarrier system	Composition	Particle size	Comments	Reference
Nanocarriers in African *trypanosomiasis*						
1.	None	Cationic liposome	Stearylamine and phosphatidylcholine	-	In-vitro lysis of bloodstream *T. b. gambiense* cells without any drug.	(Tachibana et al., 1988; Yoshihara and Nakac, 1986)
2.	None	Arsono-liposomes	arsonoliposomes with phosphatidyl-choline (PC)	72.6 nm to 110.8 nm	*In-vitro* trypanocidal activity against *T. b. brucei* cell line after 24 h of treatment	(Antimisiaris et al., 2003)
3.	Melarsoprol	Nano-suspension	Poloxamer 188, and poloxamer 407	324 nm to 663 nm	High solubility and bioavailability, brain targeting and reduced cytotoxicity in K562 cell line	(Zirar et al., 2008)
4.	Pentamidine	Polymeric Nanoparticles	Nanobody (NbAn33) fragment-conjugated PEGylated chitosan	~135 nm	Nanobody conjugated pentamidine specifically endocytosed by trypanosome, 100-fold dose reduction in *T. brucei* infected mice	(Unciti-broceta et al., 2015)
5.	Pentamidine	Polymeric Nanoparticles	NbAn33 conjugated PEGylated PLGA conjugated	~145 nm	7-fold decrease in IC_{50} value,100% surveillance rate of infected mice when treated with 10-fold reduced dose	(Arias et al., 2015)
6.	None	Polymeric Nanoparticles	Nanobody (NbAn33) conjugation with truncated ApoL-I	-	Effective against second stage of HAT by brain targeting.	(Conrath et al., 2006a)

7.	Diminazene	Cationic Nano-particles	Cationic lipidic core	74 nm	Improved DMZ stability and enhanced trypanocidal activity against infected cell lines	(Kroubi et al., 2010)
8.	Diminazene	Lipid-drug conjugate (LDC)	Stearic acid and oleic acid	442 nm	Reduced cytotoxicity against human granulocyte	(Olbrich et al., 2004)
9.	Nerolidol	Polymeric Nanospheres	Eudragit RS 100	149.5 nm	Improved efficacy against DMZ resistant *T. evansi* cell culture, no cytotoxicity.	(Baldissera et al., 2016a)
10.	Quinapyramine sulphate	Polymeric Nanoparticle	Sodium alginate	<60 nm	Many-fold dose reduction of QS when loaded in nanoparticles	(Manuja A, Kumar S, Dilbaghi N, Bhanjana G, Chopra M, Kaur H, Kumar R, Manuja B, Singh S, 2014)
11.	Quinapyramine sulphate	Polymeric Nanoparticle	Chitosan	161.4 nm	Significant improvement in safety of QS after encapsulating in nanoparticles	(Manuja A, et.al., 2018)
12.	Isometamidium chloride	Polymeric Nanoparticle	Sodium alginate	~190 nm	No cytotoxicity and hemolysis against equine PBMC	(Singh et.al., 2016)

	Nanocarriers in American *trypanosomiasis*					
13.	Nifurtimox	Polymeric Nanoparticle	Polyethylcyano-acrylate	<200 nm	Comparable trypanolytic activity with 0.1% Nifurtimox loaded nanoparticles and 100µg/ml Nifurtimox solution against epimastigote form *T. cruzi* infected vero cell line.	(Gonzalez-martin et al., 1998)
14.	Allopurinol	Polymeric Nanoparticle	Polyethyl-cyanoacrylate	187 nm	IC_{50} value of 0.5µg/ml, 54.7µg/ml and 37.3 µg/ml for allpurinol loaded NP, blank NP, and free drug respectively against *T. cruzi*(epimastigote form).	(Gonza, 2000)
15.	D0870 (Inhibitor of fungal cell wall synthesis)	Polymeric Nanosphere	PEG- polylactic acid	<200 nm	No acute toxicity with complete reduction in parasitaemia in *T. evansi* infected mice when given by oral or intravenous routes	(Molina et al., 2001)
16.	Benznidazole	Polymeric Nanoparticles	Pluronic F-68, $CaCo_3$	41.81 nm	Decrease in IC_{50} against various forms of *T.cruzi* like trypomastigote, epimastigote and amastigote in LLCMK2 cell lines.	(Tessarolo et al., 2018)
17.	Benznidazole	Polymeric Nanoparticles	Poloxamer 188	63.3 nm	Improved cytotoxicity, 100% survival rate in *T. cruzi* infected mice after treatment with drug loaded nanoparticles	(Esteva et al., 2017; Scalise et al., 2016)
18.	Etanidazole	pH sensitive liposome	Dioleoyl-phosphatidylethanolamine and cholesteryl hemisuccinate	380 nm	Cytosolic delivery of liposome, improvement in Anti-amastigote activity against murine macrophage-like cell line J774 infected with amastigote form of *T. cruzi*.	(Maria Jose et.al. 2005)

19.	(-)-α-Bisabolol	Solid lipid nanoparticles	Shea butter	191.8 nm	Improved In-vitro effectiveness against *T. evansi* infected cell line. Improved efficacy in *T. evansi* infected mice	(Baldissera et al., 2016b)
20.	Lychnopholide	Nanocapsule	PEGylated Polylactic acid	105.1 nm	Survival rate of 50% and none for free drug and drug loaded nanocapsules, respectively. No morphologic changes in myocytes with later group in *T. cruzi* infected C57BL/6 mice.	(Branquinho et al., 2017)
21.	Curcumin	Nanocapsule	Poly (ε-caprolactone)	198 nm	Effective against *T. evansi* infected cell lines decrease in liver and kidney related toxicities in *T. evansi*-infected adult male Wistar rats.	(Gressler et al., 2015)
22.	Achyroclinesatureioides essential oil	Nanocapsule	Poly (ε-caprolactone)	235.9	protective effects on various oxidative stress induced by *T. evansi* in Wistar female rat model.	(Souza et al., 2017)
23.	Transferrin	Gold nanoparticles	Transferrin, gold	15 nm	Gold nanoparticles when conjugated to transferrin. accumulated between the nucleus and the kinetoplast of *T. cruzi* epimastigotes	(Eger and José, 2012)
24.	5-hydroxy-3-methyl-5-phenyl-pyrazoline-1-(S-benzyl dithiocarbazate (H_2bdtc)	Solid lipid nanoparticles	Stearic acid, soya lecithin	127.4 nm	*Improved* IC_{50} against LLC-MK2 fibroblast cell line 100-fold dose reduction in infected female swiss mice with *T. cruzi*	(Carneiro et al., 2014)
25.	Tea tree oil	Solid lipid nanoparticles	Cetyl palmitate	287 nm	Time dependent trypanocidal activity of tea tree oil or tea tree oil-	(Matheus D

					loaded nanocarriers against trypomastigote Effective against *T. evansi* infected mice without any mortality when combined with diminazine aceturate (3.5). mg/kg	Baldissera et al., 2014)
26.	Ursolic acid	Polymeric Nanoparticles	Poly (ε-caprolactone)	173.2 nm	Ursolic acid-loaded polymeric nanoparticles showed comparative parasitaemia with less liver toxicity than benznidazole in male C57BL/6 mice	(Riul et al., 2017)

Moreover, the infectious diseases have been widely treated by the variety of plant extracts consisting of one or more active moieties including alkaloids (cinchona: antimalarial) (Andrade-Neto et al., 2003), flavonoids (quercetin: antibacterial)(Wu et al., 2008), terpenes (menthol: anti-inflammatory)(Del Prado-Audelo et al., 2021), and lactones (guaiantrienolides: antibiotic) (Cimmino et al., 2021). Hoet et.al. reported that various plant extracts rich in actives alkaloids, phenolic derivatives, quinones, terpenes and other metabolites exhibited antitrypanosomal effects against African *trypanosomiasis* (Hoet et al., 2004). The compounds isolated from naturally occurring medicinal plants such as phenylpropanoids obtained from rhizomes of *Alpinia Galanga*, flavonoids from roots of *Sophora flavescenes*, and terpenoids isolated from *Chenopodium ambrosioides* showed antitrypanosomal effect against *T. cruzi* responsible for Chaga's disease (Uchiyama, 2009).

Table. 1.5 List of natural compounds exhibiting antitrypanosomal activity

Compound	**Natural source**	**Effective against**	**IC_{50}**	**Ref.**
Quinoline alkaloid - waltheriones E−L, and antidesmone	Root extract of *Waltheria indica*	*T. cruzi*	0.02 – 3.1 µM	(Cretton et al., 2014)
Indolosesquiterpene alkaloid - polysin	Stem barks of *Polyalthia suaveolens*	*T. brucei*	~0.5 µM	(Ngantchou et al., 2010)
Almiramide C	Marine cyanobacteria: *Lyngbya majuscula*	*T. brucei*	3 µM	(Sanchez et al., 2013)
Flavonoid: quercetin 3-methyl ether,	*Lychnophora staavioides*	*T. cruzi*	-	(Takeara et al., 2003)
3-hydroxyacetylindole, N-acetyl-oxotryptamine, cyclo-(L-Phe-L-Pro), and 3-formylindole	Marine Bacterium *Bacillus pumilus*	*T. cruzi*	19.4-26.9 µM	(Martínez-Luis et al., 2012)

spoxazomicins A–C	Endophytic actinomycete, *Streptosporangium oxazolinicumK07-0460*	*T. b. brucei*	0.11 µg/mL	(Inahashi et al., 2011)
Neolignan dehydrodieugenol B	*Nectandra leucantha*	*T. cruzi*	4-63 µM	
Tetracyclic iridoids: molucidin, ML-2-3, and ML-F52	Leaves of *Morinda lucida* Benth.		Molucidin:1.27 µM, ML-2-3: 3.75 µM and ML-F52:0.43 µM,	(Kwofie et al., 2016)

It has been reported that advanced drug delivery systems could further enhance the antitrypanosomal effect of natural products. Furthermore, a combination of natural products with synthetic antitrypanosomal agents also showed an improved therapeutic effect in a mouse model. For instance, diminazene aceturate when combined with α-Bisabolol or tea tree oil and loaded in nanocarrier showed enhanced antitrypanosomal effect and mean survival rate of treated mice. α-Bisabolol is a sesquiterpene alcohol present in essential oils of several plants has shown an increase in trypanocidal activity against *T. evansi* parasite when loaded in solid lipid nanoparticles (SLNs) as compared to free α-Bisabolol (Baldissera et al., 2016b). Rani et.al. evaluated nanoencapsulation of piperine [an alkaloid presents in black pepper (Piper Nigrum)] against *T. evansi*. Nanoencapsulation of piperine enabled a 3-fold enhancement in inhibitory concentration along with the generation of intracellular reactive oxygen species which contributed to trypanocidal effect of drug (Rani et al., 2020). In order to find out prominent drug candidates of natural origin, Ibezim et.al. carried out molecular docking study against drug binding sites on *T. b. rhodensiense* and *T. b. gambiense* (Research et al., 2017). Clinically, *trypanosomiasis* infection is accompanied by hepatomegaly for which *Achyrocline satureioides* essential oil-loaded nanocapsules showed a marked reduction in liver toxicity in *T. evansi* infected rats (Ritter et al., 2017). In another study, the use of curcumin-loaded PLGA nanoparticles along with oral benznidazole was accessed for its cardioprotective role in American *trypanosomiasis*. *T. cruzi* usually affects the heart and gastrointestinal tract due to its intracellular multiplication and reviving nature. It potentiates myocardial injury by

cardiomyopathy and myocardial infarction. Curcumin derived from Curcuma *longa* consists of curcuminoids which exhibit known cardioprotective action, which on nanoencapsulation showed marked reduction in myocardial parasite load, cardiac hypertrophy, inflammation and fibrosis in *T. cruzi* infected mice. Despite the potential use of curcuminoids as a cardioprotective agent, low bioavailability, poor absorption and rapid metabolism are a few drawbacks associated with its use. Nanoencapsulated curcumin could have contributed to increased solubility, reduction in gastric degradation, and enhancement of bioavailability by facilitating permeation across the intestinal epithelium. Marked downregulation in various myocardial proinflammatory expression markers such as cytokines/ chemokines (IL-1β, TNF-α, IL-6, CCL5) was also observed after combination treatment with curcumin nanoparticles highlighting the role of nanocarriers in potentiating therapeutic benefits. Although many naturally occurring compounds exhibit antitrypanosomal activity *in vitro* as presented in table 1.6, there needs detailed evaluation for its *in vivo* efficacy. Natural products in combination with FDA-approved antitrypanosomal agents could be an important strategy to improve the current antitrypanosomal therapy.

Table. 1.6 Examples of natural compounds loaded in nanocarriers

Compound	**Nanocarrier**	**Remarks**	**Ref.**
(-) α-Bisabolol	Solid lipid nanoparticles using shea butter	Enhanced antitrypanosomal activity in *T. evansi* infected mice model when combined with commercially available diminazene aceturate	(Baldissera et al., 2016b)
Piperine	Polymeric nanocapsule	IC_{50} value of piperine and piperine nanocapsule was 14.45 μM and 5.039	(Rani et al., 2020)
Lychnopholide	PEGylated polymeric nanocapsule using polylactic acid	Improved cardioprotective activity and more than 50% survival in *T. cruzi* infected C57BL/6 mice in nanoencapsulated drug than free lychnopholide	(Branquinho et al., 2017)
Tea tree oil	Solid lipid nanoparticle	Enhanced survival in nanoencapsulated form than free tea tree oil	(Matheus D. Baldissera et al., 2014)

	using cetyl palmitate		
Ursolic acid	Poly(ε-caprolactone) polymeric nanoparticles	Comparative parasitaemia and reduced liver toxicity in *T. cruzi* infected mice as compared to free benznidazole	(Abriata et al., 2017)
Achyrocline satureioides	Polymeric nanocapsule	Hepatoprotective effect against the cytotoxic damage caused by *T. evansi* infection	(Ritter et al., 2017)

7. Vaccine delivery

Trypanosome after entering the host body, evades immune system because of the presence of specific molecular machinery on it (Tabel et al., 2013). Trypanosome have more than 1,000 VSG genes and pseudogenes in their genome, which on entry into mammalian host can undergo segmental gene recombination to encode more than 10,000 distinct VSG surface coats known as VSG switching. During course of infection trypanosome induces complex array of immune stimulation wherein, parasite derived components trigger B-cell activation and antitrypanosomal IgG production. Thereafter, activation of natural killer and T-cells occurs which results in production of interferon-γ, activation of macrophages and finally release of tumor necrosis factor responsible for parasite control (Stijlemans et al., 2017). Prominently, the destruction of B-lymphocyte memory cells at an early stage of infection, and variability of VSG and its components due to repeated mutations are responsible for the failure of development of an effective vaccine against African trypanosome. Although VSG has provided an immuno-protective role to the trypanosome, systematic genome-based sequencing in *T. vivax* has led to the discovery of possible vaccine candidates in near future. Vaccination with a single recombinant protein, consisting of the extracellular region of a conserved cell-surface protein located near the flagellum membrane of *T. vivax* showed long-lasting protection from the infection when studied in a mouse model of *T. vivax* infection for about 170 days after repeated challenge with the infection (fig. 1.4) (Autheman et al., 2021).

On the other hand, eradication of Chagas disease appears to be an impossible task due to the enormous number of mammalian reservoirs and triatomine vectors involved in the life cycle of *T. cruzi* (Bivona et al., 2020) although prophylactic and therapeutic vaccination trials have been carried out by several researchers. Cardiomyopathy induced by *T. cruzi* causes a major burden

on medical professionals. In order to reduce parasitaemia and induce cardioprotective action against *T. cruzi*, *the* therapeutic vaccine was developed using 2 plasmid DNA encoding trypomastigote surface antigens namely trypomastigote excretory-secretory protein (Tc24) and trypomastigote surface trans-sialidase (TSA-1). Antigens were selected from the library based on their ability to reduce parasitaemia and reduction in inflammation of cardiac cells from chronic degenerative changes induced by infection as evidenced in laboratory mice and dogs. The trypanolytic and cardioprotective role of Tc24 and TSA-1 was found to depend on CD8+ and the production of IFN-γ. Immunotherapy when given after 70 days post-infection showed improved survival of >70% with reduced cardiac tissue inflammation (Dumonteil et al., 2014, 2004). Although various attempts to design safe and effective therapeutic vaccines have been developed by researchers, the clinical use of these vaccines is questionable. Furthermore, prophylactic vaccine development is challenging and seems to present difficulties soon also due to the presence of antigenic variation furnished by the trypanosome.

Recently, synergistic utilization of nanoparticle-based technology with vaccine technology has provided significant improvements in the vaccination platform. For instance, antigens delivered by various polymeric, inorganic and liposomal based delivery system has shown, stable delivery of antigens, enhanced immunogenicity, high antigen loading and most importantly concentration of antigens in lymph node (Bhardwaj et al., 2020; Pati et al., 2018). Although many attempts have been done by researchers in this regard, only some FDA-approved products are available currently.

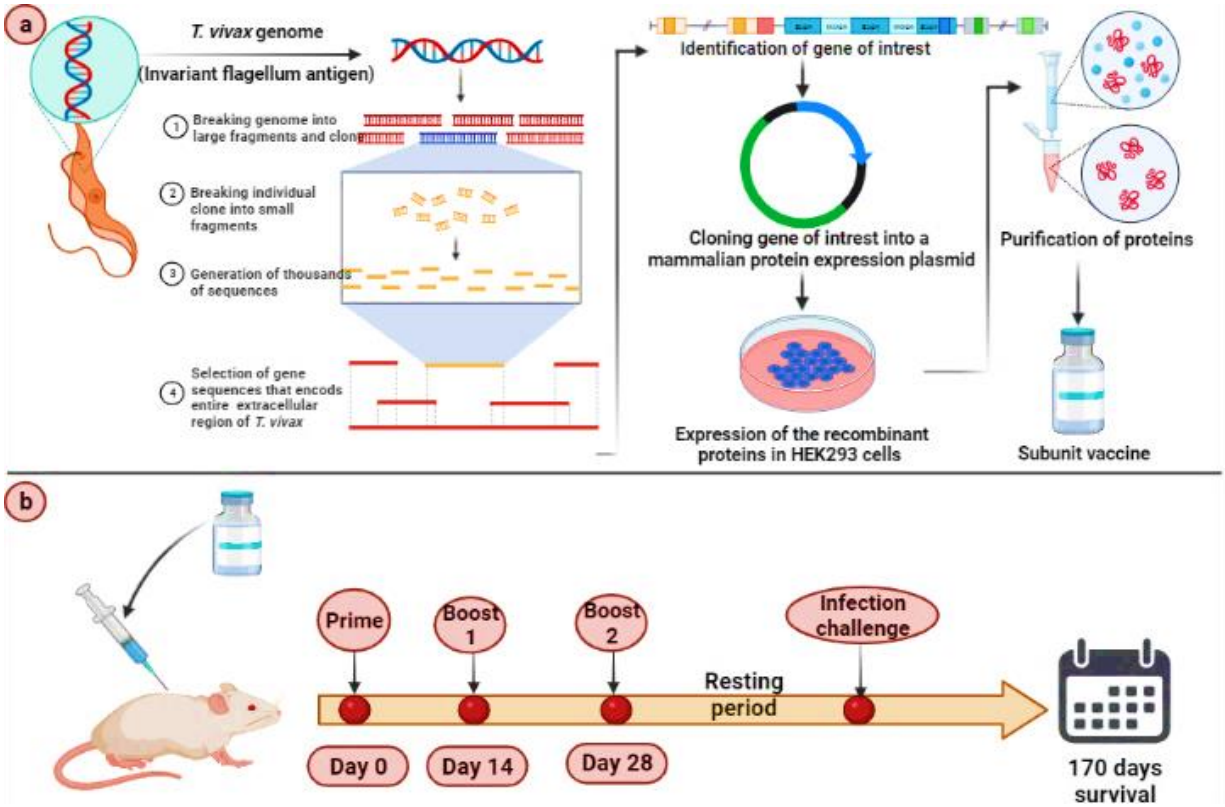

Fig. 1.4 Development of vaccine against *T. vivax* by recombinant DNA technology a) Production of single recombinant protein consisting of extracellular region of a conserved cell-surface protein of *T. vivax* located near flagellum membrane (invariant flagellum antigen) b) dosing regimen of subunit vaccine in mice.

8. Introduction to quinapyramine sulphate

Quinapyramine sulphate for curative purpose and quinapyramine chloride for prophylaxis of disease in endemic areas has been widely used in treatment of *trypanosomiasis* in camels. Repeated use of these drugs and under dosing has been the cause of developing drug resistance. There is immense need of more effective and innovative strategies to decrease the deaths associated with these diseases. With lack of introduction of new drug and very few marketed formulations available for treatment ranks the disease amongst most neglected tropical disease (WHO, n.d.). Besides activity against *T. evansi*, quinapyramine sulphate exhibits a wide spectrum of activity against trypanosomal strains causing animal *trypanosomiasis* in various domestic and wild animals such as *T.equinum, T.equiperdum, T.congolense, T.vivax, T.brucei*, and *T.simiae* [3]. Depending on the type of pathogen involved in the disease, its hosts, the reservoir of the parasite in vectors, their environment and interrelations usually determine the

epidemiology of the disease. The physicochemical properties of the drug have been described in table 1.7.

Table 1.7 Physicochemical properties of quinapyramine sulphate

Drug name	**Quinapyramine sulphate**
Structure	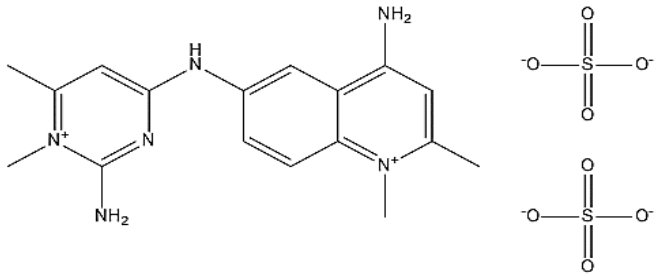
IUPAC name	4-Amino-6-[(2-Amino-1,6-Dimethylpyrimidin-1-Ium-4-Yl) Amino]-1,2-dimethylquinolinium
Chemical formula	$C_{17}H_{24}N_6O_8S_2$
Molecular wt.	504.533 g/mol
Class of drug	Anti-protozoal
Indication	Anti-trypanosomal agent for veterinary use
Mechanism of action	DNA synthesis inhibitor
pKa	14.05, 9.55 and 0.19
Log p	-2.80
Solubility	Highly water soluble, insoluble in organic solvents.

9. Rationale of the present work

Trypanosomiasis is a disease transmitted by vectors and caused by *Trypanosoma* parasites, which can infect both animals and humans, depending on the species of parasite involved. In animals, the most effective treatment for trypanosomiasis is usually administered parenterally to ensure a quick clinical response. This treatment involves daily injections, and the duration of treatment depends on the level of parasitaemia in the host. For drugs with short half-lives and narrow therapeutic indices, a slow infusion is necessary for their administration. However, many of the available drugs for veterinary trypanosomiasis, such as suramin, diminazen aceturate, isometamidium chloride, and quinapyramine sulphate, lack specificity, are highly toxic, and have poor efficacy due to high hydrophilicity, leading to rapid elimination.

In the late stage of the cerebrospinal phase of *trypanosomiasis*, drugs have limited access to the central nervous system (CNS) due to the structure of the capillaries and pericapillary glial cells that make up the blood-brain barrier. As a result, the available chemotherapy options are restricted to long courses of parenteral administration, which can have variable efficacy and multiple side effects. For example, quinapyramine sulphate (QS), which is used to treat trypanosomiasis in various domestic and wild animals, exhibits high hydrophilicity and dose-dependent side effects, including injection site reactions, tremors, salivation, and stiffening of limbs, which can lead to collapse in the treated animals. The marketed formulation of QS appears to have these side effects because the drug is directly administered in a free form that is reconstituted in water for injection. To address these problems, it is important to find alternative routes of administration for QS and other drugs.

Nanotechnology has been shown to be an effective tool for delivering existing drugs, improving their efficacy, and reducing their dose-dependent side effects. The presence of quaternary ammonium makes quinapyramine sulphate highly basic and increases its hydrophilicity, which poses challenges in loading the drug into lipid-based nanocarrier systems due to its multiple basic pKa values (14.05, 9.55) and a log P of -2.80. Researchers have attempted to use polymeric nanoparticles of quinapyramine sulphate utilizing chitosan and sodium alginate to increase its therapeutic efficacy in animal models infected with *T. evansi*. Although these nanoparticles have shown promising results, they have some drawbacks, such as low drug loading and the need for FDA approval of excipients used in their formulation. Given the limitations of current trypanocidal chemotherapies, novel drug delivery strategies are needed to optimize drug absorption, distribution, metabolism, and elimination.

10. The objective of the present work

The primary objective of the work involves the development of quinapyramine nanoformulations to enhance the antitrypanosomal efficacy against *T. evansi* parasite. The specific objective of the work includes.

i) Development and validation of HPLC-based analytical and bioanalytical method for quantification of quinapyramine sulphate
ii) Development and evaluation of quinapyramine sulphate loaded lipidic nanoparticles
iii) Development and Evaluation of Long-Acting Oil-Based Nanosuspension for Efficient Delivery of Quinapyramine Sulphate

iv) In vitro-in vivo correlation of Quinapyramine Sulphate-Loaded Oil-Based Nanosuspension

References:

Abriata, J.P., Eloy, J.O., Riul, T.B., Campos, P.M., Baruffi, M.D., Marchetti, J.M., 2017. Poly-epsilon-caprolactone nanoparticles enhance ursolic acid in vivo efficacy against Trypanosoma cruzi infection. Mater. Sci. Eng. C 77, 1196–1203. https://doi.org/10.1016/J.MSEC.2017.03.266

Aksoy, S., Buscher, P., Lehane, M., Solano, P., Abbeele, J. Van Den, 2017. Human African trypanosomiasis control : Achievements and challenges. PLoS Negl. Trop. Dis. 1–6. https://doi.org/10.1371/journal.pntd.0005454

Andrade-Neto, V.F., Brandão, M.G.L., Stehmann, J.R., Oliveira, L.A., Krettli, A.U., 2003. Antimalarial activity of Cinchona-like plants used to treat fever and malaria in Brazil. J. Ethnopharmacol. 87, 253–256. https://doi.org/10.1016/S0378-8741(03)00141-7

Antimisiaris, S.G., Ioannou, P. V, Loiseau, P.M., 2003. In-vitro antileishmanial and trypanocidal activities of arsonoliposomes and preliminary in-vivo distribution in BALB / c mice. J. Pharm. Pharmacol. 55, 647–652. https://doi.org/10.1211/002235702982

Arias, J.L., Unciti-broceta, J.D., Maceira, J., Hernández-quero, J., Magez, S., Soriano, M., García-salcedo, J.A., 2015. Nanobody conjugated PLGA nanoparticles for active targeting of African Trypanosomiasis. J. Control. Release 197, 190–198. https://doi.org/10.1016/j.jconrel.2014.11.002

Autheman, D., Crosnier, C., Clare, S., Goulding, D.A., Brandt, C., Harcourt, K., Tolley, C., Galaway, F., Khushu, M., Ong, H., Romero-Ramirez, A., Duffy, C.W., Jackson, A.P., Wright, G.J., 2021. An invariant Trypanosoma vivax vaccine antigen induces protective immunity. Nat. 2021 5957865 595, 96–100. https://doi.org/10.1038/s41586-021-03597-x

Babokhov, P., Sanyaolu, A.O., Oyibo, W.A., Fagbenro-beyioku, A.F., Iriemenam, N.C., 2013a. A current analysis of chemotherapy strategies for the treatment of human African trypanosomiasis. Pathog. Glob. Health 107, 242–252. https://doi.org/10.1179/2047773213Y.0000000105

Babokhov, P., Sanyaolu, A.O., Oyibo, W.A., Fagbenro-beyioku, A.F., Iriemenam, N.C., 2013b. A current analysis of chemotherapy strategies for the treatment of human African trypanosomiasis. Pathog. Glob. Health. https://doi.org/10.1179/2047773213Y.0000000105

Baker, C.H., Welburn, S.C., 2018. The Long Wait for a New Drug for Human African Trypanosomiasis. Trends Parasitol. 34, 818–827. https://doi.org/10.1016/j.pt.2018.08.006

Baker, N., Glover, L., Munday, J.C., Aguinaga, D., Barrett, M.P., Koning, H.P. De, Horn, D., 2012. Aquaglyceroporin 2 controls susceptibility to melarsoprol and pentamidine in African trypanosomes. PNAS 109, 1–6. https://doi.org/10.1073/pnas.1202885109

Baker, N., Koning, H.P. De, Ma, P., Horn, D., 2013. Drug resistance in African trypanosomiasis : the melarsoprol and pentamidine story. Trends Parasitol. 29, 110–118. https://doi.org/10.1016/j.pt.2012.12.005

Baldissera, Matheus D, Da, A.S., Oliveira, C.B., Santos, R.C. V, Vaucher, R.A., Raffin, R.P., Gomes, P., Dambros, M.G.C., Miletti, L.C., Boligon, A.A., Athayde, M.L., Monteiro, S.G., 2014. Experimental Parasitology Trypanocidal action of tea tree oil (Melaleuca alternifolia) against Trypanosoma evansi in vitro and in vivo used mice as experimental model. Exp. Parasitol. 141, 21–27. https://doi.org/10.1016/j.exppara.2014.03.007

Baldissera, Matheus D., Da Silva, A.S., Oliveira, C.B., Santos, R.C.V., Vaucher, R.A., Raffin, R.P., Gomes, P., Dambros, M.G.C., Miletti, L.C., Boligon, A.A., Athayde, M.L., Monteiro, S.G., 2014. Trypanocidal action of tea tree oil (Melaleuca alternifolia) against Trypanosoma evansi in vitro and in vivo used mice as experimental model. Exp. Parasitol. 141, 21–27. https://doi.org/10.1016/J.EXPPARA.2014.03.007

Baldissera, M.D., Grando, T.H., Souza, C.F., Cossetin, L.F., Ana, P.T., Dalla, D.F., Sagrillo, M.R., Da, A.S., Stefani, L.M., Monteiro, S.G., 2016a. Experimental Parasitology Nerolidol nanospheres increases its trypanocidal efficacy against Trypanosoma evansi : New approach against diminazene aceturate resistance and toxicity. Exp. Parasitol. 166, 144–149. https://doi.org/10.1016/j.exppara.2016.04.015

Baldissera, M.D., Grando, T.H., Souza, C.F. De, Cossetin, L.F., Silva, A.P.T., Giongo, J.L., Monteiro, S.G., 2016b. A nanotechnology based new approach for Trypanosoma evansi chemotherapy: In vitro and vivo trypanocidal effect of (-)-α-bisabolol. Exp. Parasitol. 170, 156–160. https://doi.org/10.1016/j.exppara.2016.09.018

Bamrungsap, S., Zhao, Z., Chen, T., Wang, L., Li, C., Fu, 2012. A Focus on Nanoparticles as a Drug Delivery System. Nanomedicine 7, 1253–1271.

Bangs, J.D., 2018. Evolution of Antigenic Variation in African Trypanosomes : Variant Surface Glycoprotein Expression , Structure , and Function. BioEssays 1800181, 1–8. https://doi.org/10.1002/bies.201800181

Bareford, L.M., Swaan, P.W., 2007. Endocytic mechanisms for targeted drug delivery. Adv. Drug Deliv. Rev. 59, 748–758. https://doi.org/10.1016/j.addr.2007.06.008

Barrett, M.P., 2010. Potential new drugs for human African trypanosomiasis : some progress at last Michael P. Curr. Opin. Infect. Dis. 23, 603–308. https://doi.org/10.1097/QCO.0b013e32833f9fd0

Barrett, M.P., 2000. Problems for the chemotherapy of human African trypanosomiasis. Curr. Opin. Infect. Dis. 647–651.

Barrett, M.P., Boykin, D.W., Brun, R., Tidwell, R.R., 2007. Review : Frontiers in Pharmacology. Human African trypanosomiasis : pharmacological re-engagement with a neglected disease. Br. J. Pharmacol. 2005, 1155–1171. https://doi.org/10.1038/sj.bjp.0707354

Barrett, M.P., Croft, S.L., 2012. Management of trypanosomiasis and leishmaniasis 175–196. https://doi.org/10.1093/bmb/lds031

Berens, R.L., Marr, J.J., Steele, F., Cruz, D.A., Donald, J., 1982. Effect of Allopurinol on Trypanosoma cruzi : Metabolism and Biological Activity in Intracellular and Bloodstream Forms. Antimicrob. Agents Chemother. 22, 657–661.

Berg, M., Veken, P. Van Der, Goeminne, A., Haemers, A., Augustyns, K., 2010. Inhibitors of the Purine Salvage Pathway : A Valuable Approach for Antiprotozoal Chemotherapy ? Curr. Med. Chem. 17, 2456–2481.

Bhardwaj, P., Bhatia, E., Sharma, S., Ahamad, N., Banerjee, R., 2020. Advancements in prophylactic and therapeutic nanovaccines. Acta Biomater. 108, 1. https://doi.org/10.1016/J.ACTBIO.2020.03.020

Biobaku, B.Y., n.d. Antiprotozoan drugs at a glance.

Bivona, A.E., Alberti, A.S., Cerny, N., Trinitario, S.N., Malchiodi, E.L., 2020. Chagas disease vaccine design: the search for an efficient Trypanosoma cruzi immune-mediated control. Biochim. Biophys. acta. Mol. basis Dis. 1866. https://doi.org/10.1016/J.BBADIS.2019.165658

Borst, P., Rudenko, G., Borst, P., 2016. Antigenic Variation in African Trypanosomes Published by : American Association for the Advancement of Science Antigenic Variation in African Trypanosomes. Am. Assoc. Adv. Sci. 264, 1872–1873.

Branquinho, R.T., Roy, J., Farah, C., Garcia, G.M., Aimond, F., Guennec, J. Le, Saude-guimarães, D.A., Grabe-, A., 2017. Biodegradable Polymeric Nanocapsules Prevent Cardiotoxicity of Anti- Trypanosomal Lychnopholide. Sci. Reports-Nature 1–13. https://doi.org/10.1038/srep44998

Bray, M.A., Pe, B., 2010. Fexinidazole – A New Oral Nitroimidazole Drug Candidate Entering Clinical Development for the Treatment of Sleeping Sickness. PLoS Negl. Trop. Dis. 4, 1–15. https://doi.org/10.1371/journal.pntd.0000923

Brun, R., Blum, J., Chappuis, F., Burri, C., 2010. Human African trypanosomiasis. Lancet 375, 148–159. https://doi.org/10.1016/S0140-6736(09)60829-1

Carneiro, Z.A., Maia, P.I.S., Sesti-costa, R., Lopes, C.D., Pereira, T.A., Silva, S., Milanezi, C.M., Pereira, M.A., Lopez, R.F. V, Deflon, V.M., 2014. In Vitro and In Vivo Trypanocidal Activity of H 2 bdtc-Loaded Solid Lipid Nanoparticles. PLoS Negl. Trop. Dis. 8. https://doi.org/10.1371/journal.pntd.0002847

Cavalli, A., Lizzi, F., Bongarzone, S., Belluti, F., Piazzi, L., Maria, C., Bolognesi, L., 2010. Complementary medicinal chemistry-driven strategies toward new antitrypanosomal and antileishmanial lead drug candidates. Immunol. Med. Microbiol. 58, 51–60. https://doi.org/10.1111/j.1574-695X.2009.00615.x

Centers for Disease control and Prevention [WWW Document], n.d. . African Trypanos. URL https://www.cdc.gov/parasites/sleepingsickness/index.html (accessed 1.18.20).

Chagas Disease [WWW Document], n.d. . Centers Dis. Control Prev. URL https://www.cdc.gov/parasites/chagas/index.html (accessed 1.18.20).

Chandrasekar, P.H., 2018. African Trypanosomiasis [WWW Document]. Medscape Rev.

Chang, J., Jallouli, Y., Kroubi, M., Yuan, X., Feng, W., Kang, C., 2009. Characterization of endocytosis of transferrin-coated PLGA nanoparticles by the blood – brain barrier. Int. Jpurnal Pharm. 379, 285–292. https://doi.org/10.1016/j.ijpharm.2009.04.035

Cimmino, A., Roscetto, E., Masi, M., Tuzi, A., Radjai, I., Gahdab, C., Paolillo, R., Guarino, A., Catania, M.R., Evidente, A., 2021. Sesquiterpene Lactones from Cotula cinerea with Antibiotic Activity against Clinical Isolates of Enterococcus faecalis. Antibiot. 2021, Vol. 10, Page 819 10, 819. https://doi.org/10.3390/ANTIBIOTICS10070819

Cole, A.J., David, A.E., Wang, J., Galbán, C.J., Yang, V.C., 2011. Biomaterials Magnetic brain tumor targeting and biodistribution of long-circulating PEG-modified , cross-linked

starch-coated iron oxide nanoparticles. Biomaterials 32, 6291–6301. https://doi.org/10.1016/j.biomaterials.2011.05.024

Conrath, K., Vanhollebeke, B., Pays, E., Baral, T.N., Magez, S., Muyldermans, S., Baetselier, P. De, 2006a. Experimental therapy of African trypanosomiasis with a nanobody-conjugated human trypanolytic factor 12, 580–584. https://doi.org/10.1038/nm1395

Conrath, K., Vanhollebeke, B., Pays, E., Baral, T.N., Magez, S., Muyldermans, S., Baetselier, P. De, 2006b. Experimental therapy of African trypanosomiasis with a nanobody-conjugated human trypanolytic factor. Nat. Med. 12, 580–584. https://doi.org/10.1038/nm1395

Cretton, S., Breant, L., Pourrez, L., Ambuehl, C., Marcourt, L., Ebrahimi, S.N., Hamburger, M., Perozzo, R., Karimou, S., Kaiser, M., Cuendet, M., Christen, P., 2014. Antitrypanosomal quinoline alkaloids from the roots of waltheria indica. J. Nat. Prod. 77, 2304–2311. https://doi.org/10.1021/NP5006554

Croft, O.K., 2003. Natural products as antiparasitic drugs. Parasitol. Res. 55–62. https://doi.org/10.1007/s00436-002-0768-3

De Koning, H.P., 2001. Transporters in African trypanosomes: Role in drug action and resistance. Int. J. Parasitol. 31, 512–522. https://doi.org/10.1016/S0020-7519(01)00167-9

Del Prado-Audelo, M.L., Cortés, H., Caballero-Florán, I.H., González-Torres, M., Escutia-Guadarrama, L., Bernal-Chávez, S.A., Giraldo-Gomez, D.M., Magaña, J.J., Leyva-Gómez, G., 2021. Therapeutic Applications of Terpenes on Inflammatory Diseases. Front. Pharmacol. 12, 2114. https://doi.org/10.3389/FPHAR.2021.704197/BIBTEX

Desquesnes, M., Dargantes, A., Lai, D., Lun, Z., Holzmuller, P., Jittapalapong, S., 2013. Trypanosoma evansi and Surra : A Review and Perspectives on Transmission , Epidemiology and Control , Impact and Zoonotic Aspects. Biomed Res. Int. 1–20.

Dumonteil, E., Bottazzi, M.E., Zhan, B., Heffernan, M.J., Jones, K., Valenzuela, J.G., Kamhawi, S., Ortega, J., Ponce, S., Rosales, L., Lee, B.Y., Bacon, K.M., Fleischer, B., Slingsby, B.T., Cravioto, M.B., Tapia-Conyer, R., Hotez, P.J., 2014. Accelerating the development of a therapeutic vaccine for human Chagas disease: rationale and prospects. Expert Rev. Vaccines. https://doi.org/10.1586/erv.12.85

Dumonteil, E., Escobedo-Ortegon, J., Reyes-Rodriguez, N., Arjona-Torres, A., Ramirez-Sierra, M.J., 2004. Immunotherapy of Trypanosoma cruzi Infection with DNA Vaccines in Mice. Infect. Immun. 72, 46–53. https://doi.org/10.1128/IAI.72.1.46-53.2004

Eger, I., José, M., 2012. Endocytosis in Trypanosoma cruzi (Euglenozoa : Kinetoplastea) epimastigotes : Visualization of ingested transferrin – gold nanoparticle complexes by confocal laser microscopy. J. Microbiol. Methods 91, 101–105. https://doi.org/10.1016/j.mimet.2012.07.013

Esteva, I., Scalise, L., Arru, E.C., Rial, M.S., Salomon, J., Fichera, L.E., 2017. Elucidating the impact of low doses of nano- formulated benznidazole in acute experimental Chagas disease. PLoS Negl. Trop. Dis. 1–16.

Fairlamb, A.H., 2003. Chemotherapy of human African trypanosomiasis : current and future prospects. Trends Parasitol. 19, 488–494. https://doi.org/10.1016/j.pt.2003.09.002

Frearson, J.A., Brand, S., Mcelroy, S.P., Cleghorn, L.A.T., Smid, O., Stojanovski, L., Price,

H.P., Guther, M.L.S., Torrie, L.S., Robinson, D.A., Hallyburton, I., Mpamhanga, C.P., Brannigan, J.A., Wilkinson, A.J., Hodgkinson, M., Hui, R., Qiu, W., Raimi, O.G., Aalten, D.M.F. Van, Brenk, R., Gilbert, I.H., Read, K.D., Fairlamb, A.H., Ferguson, M.A.J., Smith, D.F., Wyatt, P.G., 2010. N -myristoyltransferase inhibitors as new leads to treat sleeping sickness. Nature 464, 728–732. https://doi.org/10.1038/nature08893

Garcia-salcedo, J.A., Munday, J.C., Unciti-broceta, J.D., Koning, H.P. De, 2014. Progress Towards New Treatments for Human African Trypanosomiasis, in: Trypanosomes and Trypanosomiasis. pp. 217–238. https://doi.org/10.1007/978-3-7091-1556-5

Garcia-salcedo, J.A., Unciti-broceta, J.D., 2015. Could specific cell targeting overcome resistance associated with current treatments for African trypanosomiasis ? Nanomedicine 10, 3515–3517.

Giordani, F., Morrison, L.J., Rowan, T.I.M.G., Koning, H.P.D.E., Barrett, M.P., 2017. The animal trypanosomiases and their chemotherapy : a review. Parasitology 1862–1889. https://doi.org/10.1017/S0031182016001268

Glover, L., Hutchinson, S., Alsford, S., Mcculloch, R., Field, M.C., Horn, D., 2013. Antigenic variation in African trypanosomes : the importance of chromosomal and nuclear context in VSG expression control. Cell. Microbiol. 15, 1984–1993. https://doi.org/10.1111/cmi.12215

Gonza, G., 2000. Allopurinol encapsulated in polycyanoacrylate nanoparticles as potential lysosomatropic carrier : preparation and trypanocidal activity. Eur. J. Pharm. Biopharm. 49, 137–142.

Gonzalez-martin, G., Mkrino, I., Rodriguez-cabezas, 1998. Characterization and Trypanocidal Activity of Nifurtimox-containing and Empty Nanoparticles of Polyethylcyanoacrylates. J. Pharm. Pharmacol. 50, 29–35.

Gressler, L.T., Oliveira, C.B., Coradini, K., Rosa, L.D., 2015. Trypanocidal activity of free and nanoencapsulated curcumin on Trypanosoma evansi. Parasitology 142, 439–448. https://doi.org/10.1017/S0031182014001292

Gutteridge, W.E., 1985. Existing Chemotherapy and its limitations. Br. Med. Bull. 41, 162–168.

He, C., Hu, Y., Yin, L., Tang, C., Yin, C., 2010. Biomaterials Effects of particle size and surface charge on cellular uptake and biodistribution of polymeric nanoparticles. Biomaterials 31, 3657–3666. https://doi.org/10.1016/j.biomaterials.2010.01.065

Hoet, S., Opperdoes, Frederik, Brun, R., Quetin-Leclercq, J., Opperdoes, Fred, 2004. Natural products active against African trypanosomes: a step towards new drugs. https://doi.org/10.1039/b311021b

Inahashi, Y., Iwatsuki, M., Ishiyama, A., Namatame, M., Nishihara-Tsukashima, A., Matsumoto, A., Hirose, T., Sunazuka, T., Yamada, H., Otoguro, K., ¯ko Takahashi, Y., Mura, S.O.¯, Shiomi, K., 2011. Spoxazomicins A-C, novel antitrypanosomal alkaloids produced by an endophytic actinomycete, Streptosporangium oxazolinicum K07-0460T. J. Antibiot. (Tokyo). 64, 303–307. https://doi.org/10.1038/ja.2011.16

Jeevanandam, J., Barhoum, A., Chan, Y.S., Dufresne, A., Danquah, M.K., 2018. Review on nanoparticles and nanostructured materials : history , sources , toxicity and regulations. Beilstein J. Nanotechnol. 9, 1050–1074. https://doi.org/10.3762/bjnano.9.98

Jindal, A.B., 2016. Nanocarriers for spleen targeting: anatomo-physiological considerations, formulation strategies and therapeutic potential. Drug Deliv. Transl. Res. 6, 473–485. https://doi.org/10.1007/s13346-016-0304-0

Kaiser, M., Bray, M.A., Cal, M., Trunz, B.B., Torreele, E., Brun, R., 2011. Antitrypanosomal Activity of Fexinidazole , a New Oral Nitroimidazole Drug Candidate for Treatment of Sleeping Sickness. Antimicrob. Agents Chemother. 55, 5602–5608. https://doi.org/10.1128/AAC.00246-11

Kaul, G., Amiji, M., 2004. Biodistribution and Targeting Potential of Poly (ethylene glycol) -modified Gelatin Nanoparticles in Subcutaneous Murine Tumor Model. J. Drug Target. 12, 585–591. https://doi.org/10.1080/10611860400013451

Khalil, N.M., Mattos, A.C. De, Cristina, T., Moreira, M., Brustolin, D., Mainardes, R.M., 2013. Nanotechnological Strategies for the Treatment of Neglected Diseases 7316–7329.

Kroubi, M., Daulouede, S., Karembe, H., 2010. Development of a nanoparticulate formulation of diminazene to treat African trypanosomiasis. Nanotechnology 505102, 1–8. https://doi.org/10.1088/0957-4484/21/50/505102

Kwofie, K.D., Tung, N.H., Suzuki-Ohashi, M., Amoa-Bosompem, M., Adegle, R., Sakyiamah, M.M., Ayertey, F., Owusu, K.B.A., Tuffour, I., Atchoglo, P., Frempong, K.K., Anyan, W.K., Uto, T., Morinaga, O., Yamashita, T., Aboagye, F., Appiah, A.A., Appiah-Opong, R., Nyarko, A.K., Yamaguchi, Y., Edoh, D., Koram, K.A., Yamaoka, S., Boakye, D.A., Ohta, N., Shoyama, Y., Ayi, I., 2016. Antitrypanosomal activities and mechanisms of action of novel tetracyclic iridoids from Morinda lucida Benth. Antimicrob. Agents Chemother. 60, 3283–3290. https://doi.org/10.1128/AAC.01916-15/ASSET/323443A7-DF80-49DF-92E3-7565B9312037/ASSETS/GRAPHIC/ZAC0051651620005.JPEG

Landfear, S.M., 2011. Nutrient transport and pathogenesis in selected parasitic protozoa. Eukaryot. Cell 10, 483–493. https://doi.org/10.1128/EC.00287-10

Lidani, K.C.F., Bavia, L., Ambrosio, A.R., Messias-reason, I.J. De, Barbosa, A.S., 2017. The Complement System : A Prey of Trypanosoma cruzi. Front. Microbiol. 8, 1–14. https://doi.org/10.3389/fmicb.2017.00607

Luo, Y., 2018. Effects of core size and PEG coating layer of iron oxide nanoparticles on the distribution and metabolism in mice. Int. J. Nanomedicine 13, 5719–5731.

Maniruzzaman, M., Douroumis, D., Boateng, A.D., 2012. Recent advances in Novel drug carrier systems. Intech Open.

Manuja A, Dilbaghi N, Kaur H, Saini R, Barnela M, Chopra M, Manuja B, Kumar R, Kumar S, Riyesh T, Singh S, Y.S., 2018. Nano-Structures & Nano-Objects Chitosan quinapyramine sulfate nanoparticles exhibit increased trypanocidal activity in mice. Nano-Structures & Nano-Objects 16, 193–199.

Manuja A, Kumar S, Dilbaghi N, Bhanjana G, Chopra M, Kaur H, Kumar R, Manuja B, Singh S, Y.S., 2014. Quinapyramine sulfate-loaded sodium alginate nanoparticles show enhanced trypanocidal activity. Nanomedicine 9, 1625–1634.

Maria Jose Morilla, Jorge Montanari, Fernanda Frank, Emilio Malchiodi, Ricardo Corral, Patricia Petray, E.L.R., 2005. Etanidazole in pH-sensitive liposomes : Design , characterization and in vitro / in vivo anti- Trypanosoma cruzi activity. J. Control. Release 103, 599–607. https://doi.org/10.1016/j.jconrel.2004.12.012

Martínez-Luis, S., Félix Gómez, J., Spadafora, C., Guzmán, H.M., Gutiérrez, M., 2012. Antitrypanosomal Alkaloids from the Marine Bacterium Bacillus pumilus. Molecules 17, 11146–11155. https://doi.org/10.3390/molecules170911146

Matthews, K.R., 2005. The developmental cell biology of Trypanosoma brucei. J. Cell Sci. 283–290. https://doi.org/10.1242/jcs.01649

Molina-portela, M.P., Samanovic, M., Raper, J., 2008. Distinct roles of apolipoprotein components within the trypanosome lytic factor complex revealed in a novel transgenic mouse model. https://doi.org/10.1084/jem.20071463

Molina, I., Salvador, F., Serre, N., Almirante, B., 2015. Toxic Profile of Benznidazole in Patients with Chronic Chagas Disease : Risk Factors and Comparison of the Product from Two 59, 6125–6131. https://doi.org/10.1128/AAC.04660-14

Molina, J., Urbina, J., Gref, R., Brener, Z., Maciel, J., Júnior, R., 2001. incorporated into ' stealth ' polyethyleneglycol – polylactide nanospheres. J. Antimicrob. Chemother. 47, 101–104.

Montalvetti, A., Bailey, B.N., Martin, M.B., Severin, G.W., Oldfield, E., Docampo, R., 2001. Bisphosphonates Are Potent Inhibitors of Trypanosoma cruzi Farnesyl Pyrophosphate Synthase * 276, 33930–33937. https://doi.org/10.1074/jbc.M103950200

Montalvetti, A., Fernandez, A., Sanders, M., Ghosh, S., Van, E., Oldfield, E., Docampo, R., Montalvetti, A., Fernandez, A., Sanders, J.M., Ghosh, S., Brussel, E. Van, Oldfield, E., Docampo, R., 2003. Metaboolism and Bioenergetics : Farnesyl Pyrophosphate Synthase Is an Essential Enzyme in Trypanosoma brucei : In-vitro RNA interference and in-vivo inhibition studies Farnesyl Pyrophosphate Synthase. J. Biol. Chem. 278, 17075–17083. https://doi.org/10.1074/jbc.M210467200

Mordt, O.V., 2013. Application to include Nifurtimox-Eflornithine combination as treatment for stage 2 trypanosoma brucei gambiense Human African Trypanosomiasis. Geneva, Switzerland.

Morilla, M.J., Bena, P., Lopez, M.O., Bakas, L., Romero, E.L., 2002. Development and in vitro characterisation of a benznidazole liposomal formulation. Int. J. Pharm. 249, 89–99.

Morilla, M.J., Montanari, J.A., Prieto, M.J., Lopez, M.O., Petray, P.B., Romero, E.L., 2004. Intravenous liposomal benznidazole as trypanocidal agent : increasing drug delivery to liver is not enough. Int. J. Pharm. 278, 311–318. https://doi.org/10.1016/j.ijpharm.2004.03.025

Mugnier, M.R., Stebbins, C.E., Papavasiliou, F.N., 2016. Masters of Disguise : Antigenic Variation and the VSG Coat in Trypanosoma brucei. PLOS Pathog. 1–6. https://doi.org/10.1371/journal.ppat.1005784

Munday, J.C., Eze, A.A., Baker, N., Glover, L., Clucas, C., Andre, D.A., Natto, M.J., Teka, I.A., Mcdonald, J., Lee, R.S., Graf, F.E., Ludin, P., Barrett, M.P., Burchmore, J.S., Turner, C.M.R., Tait, A., Macleod, A., Ma, P., Horn, D., Koning, H.P. De, 2014. Trypanosoma brucei aquaglyceroporin 2 is a high-affinity transporter for pentamidine and melaminophenyl arsenic drugs and the main genetic determinant of resistance to these drugs. J. Antimicrob. Chemother. 69, 651–663. https://doi.org/10.1093/jac/dkt442

Munday, J.C., Settimo, L., Harry, P., Koning, D., 2015. Transport proteins determine drug sensitivity and resistance in a protozoan parasite , Trypanosoma brucei 6, 1–11.

https://doi.org/10.3389/fphar.2015.00032

Muro, S., 2012. Challenges in design and characterization of ligand-targeted drug delivery systems. J. Control. Release 164, 125–137. https://doi.org/10.1016/j.jconrel.2012.05.052

Nenarokova, A., Michels, P.A.M., 2017. A paradigm shift : The mitoproteomes of procyclic and bloodstream Trypanosoma brucei are comparably complex. PLOS Pathog. 1–9. https://doi.org/10.1371/journal.ppat.1006679

Ngantchou, I., Nyasse, B., Denier, C., Blonski, C., Hannaert, V., Schneider, B., 2010. Antitrypanosomal alkaloids from Polyalthia suaveolens (Annonaceae): Their effects on three selected glycolytic enzymes of Trypanosoma brucei. Bioorganic Med. Chem. Lett. 20, 3495–3498. https://doi.org/10.1016/J.BMCL.2010.04.145

Olbrich, C., Gessner, A., Schro, W., Kayser, O., Mu, R.H., 2004. Lipid – drug conjugate nanoparticles of the hydrophilic drug diminazene — cytotoxicity testing and mouse serum adsorption. J. Control. Release 96, 425–435. https://doi.org/10.1016/j.jconrel.2004.02.024

Olliaro, P., Lazdins, J., Guhl, F., 2002. Developments in the treatment of leishmaniasis and trypanosomiasis. Expert Opin. Emerg. Drugs 7, 61–67.

Pathak, K.M.L., Arora, J.K., Kapoor, M., 1993. Short Communication Camel trypanosomosis in Rajasthan , India. Vertirnary Parasitol. 49, 319–323.

Pati, R., Shevtsov, M., Sonawane, A., 2018. Nanoparticle vaccines against infectious diseases. Front. Immunol. 9, 2224. https://doi.org/10.3389/FIMMU.2018.02224/BIBTEX

Pink, R., Hudson, A., Mouriès, M., Bendig, M., 2005. Opprtunities and challenges in anti-parasitic drug discovery. Nat. Rev. 4, 727–740. https://doi.org/10.1038/nrd1824

Press, D., 2012. Nanotechnology-based approaches in anticancer research. Int. J. Nanomedicine 4391–4408.

Priotto, G., Kasparian, S., Ngouama, D., Ghorashian, S., Arnold, U., Ghabri, S., Karunakara, U., 2007. Nifurtimox-Eflornithine Combination Therapy for Second- Stage Trypanosoma brucei gambiense Sleeping Sickness : A Randomized Clinical Trial in Congo. Clin. Infect. Dis. 45, 1435–1442. https://doi.org/10.1086/522982

Rani, R., Kumar, S., Dilbaghi, N., Kumar, R., 2020. Nanotechnology enabled the enhancement of antitrypanosomal activity of piperine against Trypanosoma evansi. Exp. Parasitol. 219. https://doi.org/10.1016/J.EXPPARA.2020.108018

Research, O., Ibezim, A., Debnath, B., Ntie-Kang, F., Chika, •, Mbah, J., Ngozi, •, Nwodo, J., 2017. Binding of anti-Trypanosoma natural products from African flora against selected drug targets: a docking study. Med. Chem. Res. 26, 562–579. https://doi.org/10.1007/s00044-016-1764-y

Ritter, C.S., Baldissera, M.D., Grando, T.H., Souza, C.F., Sagrillo, M.R., da Silva, A.P.T., Moresco, R.N., Guarda, N.S., da Silva, A.S., Stefani, L.M., Monteiro, S.G., 2017. Achyrocline satureioides essential oil-loaded in nanocapsules reduces cytotoxic damage in liver of rats infected by Trypanosoma evansi. Microb. Pathog. 103, 149–154. https://doi.org/10.1016/J.MICPATH.2016.12.023

Riul, B., Campos, P.M., Baruffi, M.D., Marchetti, J.M., 2017. Poly-epsilon-caprolactone nanoparticles enhance ursolic acid in vivo efficacy against Trypanosoma cruzi infection.

Mater. Sci. Eng. C 77, 1196–1203. https://doi.org/10.1016/j.msec.2017.03.266

Road, B., 1988. The pharmacology of isometamidium. J. vet. Pharmacol. Therp. 11, 233–245.

Romero, E.L., Morilla, M.J., 2010. Nanotechnological approaches against Chagas disease. Adv. Drug Deliv. Rev. 62, 576–588. https://doi.org/10.1016/j.addr.2009.11.025

Sahin, A., Asencio, C., Izotte, J., Pillay, D., Coustou, V., Karembe, H., Baltz, T., 2014. Veterinary Parasitology The susceptibility of Trypanosoma congolense and Trypanosoma brucei to isometamidium chloride and its synthetic impurities. Vet. Parasitol. 203, 270–275. https://doi.org/10.1016/j.vetpar.2014.04.002

Salas-sarduy, E., Urán, L., Karpiak, J.X., Madauss, K.P., José, J., 2017. Novel scaffolds for inhibition of Cruzipain identified from high- throughput screening of anti- kinetoplastid chemical boxes. Nature-Scientific Reports 1–12. https://doi.org/10.1038/s41598-017-12170-4

Samo, M., Jannin, J.G., 2012. Monitoring the use of nifurtimox-eflornithine combination therapy (NECT) in the treatment of second stage gambiense human African trypanosomiasis. Res. Rep. Trop. Med. 3, 93–101.

Sanchez, L.M., Knudsen, G.M., Helbig, C., De Muylder, G., Mascuch, S.M., MacKey, Z.B., Gerwick, L., Clayton, C., McKerrow, J.H., Linington, R.G., 2013. Examination of the mode of action of the almiramide family of natural products against the kinetoplastid parasite Trypanosoma brucei. J. Nat. Prod. 76, 630–641. https://doi.org/10.1021/NP300834Q

Saraiva, V.B., Gibaldi, D., Previato, O., Mendonc, L., Bozza, M.T., Freire-de-lima, G., Heise, N., 2002. Proinflammatory and Cytotoxic Effects of Hexadecylphosphocholine (Miltefosine) against Drug-Resistant Strains of Trypanosoma cruzi. Antimicrob. Agents Chemother. 46, 3472–3477. https://doi.org/10.1128/AAC.46.11.3472

Scalise, M.L., Arrúa, E.C., Rial, M.S., Esteva, M.I., Salomon, C.J., Fichera, L.E., 2016. Promising Efficacy of Benznidazole Nanoparticles in Acute Trypanosoma cruzi Murine Model : In-Vitro and In-Vivo Studies. Am. Soc. Trop. Med. Hyg. 95, 388–393. https://doi.org/10.4269/ajtmh.15-0889

Schad, G.J., Allanson, A., Mackay, S.P., Cannavan, A., Tettey, J.N.A., 2008. Development and validation of an improved HPLC method for the control of potentially counterfeit isometamidium products. J. Pharm. Biomed. Anal. 46, 45–51. https://doi.org/10.1016/j.jpba.2007.08.026

Shang, N., Li, Q., Ko, T., Chan, H., Li, J., Zheng, Y., Huang, H., Ren, F., Chen, C., Zhu, Z., Galizzi, M., Li, Z., Rodrigues-poveda, C.A., Gonzalez-pacanowska, D., Veiga-santos, P., Maria, T., Carvalho, U. De, Souza, W. De, Urbina, J.A., Wang, A.H., Docampo, R., Li, K., Liu, Y., Oldfield, E., Guo, R., 2014. Squalene Synthase As a Target for Chagas Disease Therapeutics. PLOS Pathog. 10, 1–16. https://doi.org/10.1371/journal.ppat.1004114

Simarro, P.P., 2014. Epidemiology of human African trypanosomiasis. Clin. epidemology 257–275.

Simarro, P.P., Franco, J., Diarra, A., Postigo, J.A.R., Jannin, J., 2012. Update on field use of the available drugs for the chemotherapy of human African trypanosomiasis. Parasitology 139, 842–846. https://doi.org/10.1017/S0031182012000169

Simarro, P.P., Jannin, J., Cattand, P., 2008. Eliminating Human African Trypanosomiasis : Where Do We Stand and What Comes Next ? 5, 174–180. https://doi.org/10.1371/journal.pmed.0050055

Singh, S., 2016. Synthesis and evaluation of isometamidium-alginate nanoparticles on equine mononuclear and red blood cells. Int. J. Biol. Macromol. 92, 788–794.

Smith, T.K., Bringaud, F., Nolan, D.P., Figueiredo, L.M., 2017. Metabolic reprogramming during the Trypanosoma brucei life cycle. F1000 Res. 6, 1–12. https://doi.org/10.12688/f1000research.10342.1

Souza, C.F., Baldissera, M.D., Cossetin, L.F., Dalla, D.F., Monteiro, S.G., 2017. Microbial Pathogenesis Achyrocline satureioides essential oil loaded in nanocapsules ameliorate the antioxidant / oxidant status in heart of rats infected with Trypanosoma evansi. Microb. Pathog. 105, 30–36. https://doi.org/10.1016/j.micpath.2017.02.005

Souza, W. De, 2002. Basic Cell Biology of Trypanosoma cruzi 269–285.

Steverding, D., 2000. The transferrin receptor of Trypanosoma brucei. Parasitol. Int. 48, 191–198.

Stijlemans, B., Radwanska, M., Trez, C. De, Magez, S., 2017. African trypanosomes undermine humoral responses and vaccine development: Link with inflammatory responses? Front. Immunol. 8, 582. https://doi.org/10.3389/FIMMU.2017.00582/BIBTEX

Suk, J.S., Xu, Q., Kim, N., Hanes, J., En-, L.M., 2016. PEGylation as a strategy for improving nanoparticle-based drug and gene delivery. Adv. Drug Deliv. Rev. 99, 28–51. https://doi.org/10.1016/j.addr.2015.09.012

Tabel, H., Wei, G., Bull, H.J., 2013. Immunosuppression: Cause for Failures of Vaccines against African Trypanosomiases. PLoS Negl. Trop. Dis. 7. https://doi.org/10.1371/JOURNAL.PNTD.0002090

Tachibana, H., Yoshihara, E., Kaneda, Y., Nakae, T., 1988. In Vitro Lysis of the Bloodstream Forms of Trypanosoma brucei gambiense by Stearylamine-Bearing Liposomes 32, 966–970.

Takeara, R., Albuquerque, S., Lopes, N.P., Callegari Lopes, J.L., 2003. Trypanocidal activity of Lychnophora staavioides Mart. (Vernonieae, Asteraceae). Phytomedicine 10, 490–493. https://doi.org/10.1078/094471103322331430

Tessarolo, L.D., Róseo, R., Pessoa, P., Menezes, B. De, Mello, C.P., Lima, D.B., Magalhães, E.P., Bezerra, E.M., Adilson, F., Sales, M., Liberato, I., Neto, B., Oliveira, M.D.F., Pires, R., Albuquerque, E.L., Freire, V.N., Martins, A.M., 2018. Nanoencapsulation of benznidazole in calcium carbonate increases its selectivity to Trypanosoma cruzi. Parasitology 145, 1191–1198.

Thomas, J.A., Baker, N., Hutchinson, S., Id, C.D., Trenaman, A., Id, L.G., Id, S.A., Id, D.H., 2018. Insights into antitrypanosomal drug mode-of- action from cytology-based profiling. PLoS Negl. Trop. Dis. 1–19.

Tiengwe, C., Bush, P.J., Bangs, J.D., 2017. Controlling transferrin receptor trafficking with GPI-valence in bloodstream stage African trypanosomes. PLOS Pathog. 13, e1006366. https://doi.org/10.1371/JOURNAL.PPAT.1006366

Uchiyama, N., 2009. Antichagasic activities of natural products against Trypanosoma cruzi. J. Heal. Sci. 55, 31–39. https://doi.org/10.1248/JHS.55.31

Unciti-broceta, J.D., Arias, J.L., Maceira, J., Soriano, M., 2015. Specific Cell Targeting Therapy Bypasses Drug Resistance Mechanisms in African Trypanosomiasis. PLOS Pathog. 1–20. https://doi.org/10.1371/journal.ppat.1004942

Urbina, J.A., 2015. Recent Clinical Trials for the Etiological Treatment of Chronic Chagas Disease : Advances , Challenges and Perspectives. J. Eukaryot. Microbiol. 149–156. https://doi.org/10.1111/jeu.12184

Urbina, J.A., Docampo, R., 2005. Specific chemotherapy of Chagas disease : controversies and advances. Trends Parasitol. 19, 495–501. https://doi.org/10.1016/j.pt.2003.09.001

Urbina, J.A., Lira, R., Visbal, G., Quı, L. De, 2000. In Vitro Antiproliferative Effects and Mechanism of Action of the New Triazole Derivative UR-9825 against the Protozoan Parasite Trypanosoma (Schizotrypanum) cruzi. Antimicrob. Agents Chemother. 44, 2498–2502.

WHO, n.d. Trypanosomiasis, human African (sleeping sickness) [WWW Document]. URL https://www.who.int/news-room/fact-sheets/detail/trypanosomiasis-human-african-(sleeping-sickness) (accessed 7.3.22a).

WHO, n.d. Chagas disease (American trypanosomiasis).

WHO, n.d. WHO_Trypanosomiasis_Countries at risk [WWW Document]. URL https://www.who.int/trypanosomiasis_african/country/risk_AFRO/en/ (accessed 7.11.19c).

WHO Report on trypansomiasis, 2013, 2001. Control and surveillance of human African trypanosomiasis.

WHO Trypansomiasis, n.d. WHO-Trypansomiasis, International travel & health issue [WWW Document]. URL https://www.who.int/ith/diseases/trypanosomiasis/en/ (accessed 7.10.19).

Wu, D., Kong, Y., Han, C., Chen, J., Hu, L., Jiang, H., Shen, X., 2008. d-Alanine:d-alanine ligase as a new target for the flavonoids quercetin and apigenin. Int. J. Antimicrob. Agents 32, 421–426. https://doi.org/10.1016/J.IJANTIMICAG.2008.06.010

Yamashita, F., Hashida, M., 2013. Pharmacokinetic considerations for targeted drug delivery. Adv. Drug Deliv. Rev. 65, 139–147. https://doi.org/10.1016/j.addr.2012.11.006

Yoshihara, E., Nakac, T., 1986. Cytolytic activity of liposomes containing stearylamine. Biochim. Biophys. Acta 854, 93–101.

Yun, O., Priotto, G., Tong, J., Flevaud, L., 2010. NECT Is Next : Implementing the New Drug Combination Therapy for Trypanosoma brucei gambiense Sleeping Sickness. PLoS Negl. Trop. Dis. 4, 1–5. https://doi.org/10.1371/journal.pntd.0000720

Zhang, R.X., Li, J., Zhang, T., Amini, M.A., He, C., Lu, B., Ahmed, T., Lip, H., Rauth, A.M., Wu, X.Y., 2018. Importance of integrating nanotechnology with pharmacology and physiology for innovative drug delivery and therapy – An illustration with firsthand examples. Acta Pharmacol. Sin. 1–20. https://doi.org/10.1038/aps.2018.33

Zirar, S. Ben, Astier, A., Muchow, M., Gibaud, S., 2008. Comparison of nanosuspensions and hydroxypropyl- b -cyclodextrin complex of melarsoprol : Pharmacokinetics and tissue distribution in mice. Eur. J. Pharm. Biopharm. 70, 649–656. https://doi.org/10.1016/j.ejpb.2008.05.012

Chapter 2: Development and validation of HPLC-based analytical and bioanalytical method for quantification of quinapyramine sulphate

1. Introduction

Quinapyramine sulphate (QS) is an aminoquinalidine derivative that is used to treat *Trypanosomiasis* in animals, a vector-borne disease caused by the Trypanosoma parasite, especially *T. evansi*, which affects animal populations (WHO Report on trypansomiasis, 2001). Its IUPAC name is 6-N-(2-amino-1,6-dimethylpyrimidin-1-ium-4-yl)-1,2-dimethylquinolin-1-ium-4,6-diamine; hydrogen sulphate, and it has a pKa value of 14.16 (Figure 2.1) (National Library of Medicine, n.d.; Prayag et al., 2020). While few antitrypanosomal agents have been approved for clinical use, researchers have not shown much interest in developing novel dosage forms or analytical methods for these drugs. The reported methods often require large amounts of biological fluids or relatively complex sample preparation procedures. For instance, Perschke et al. developed a sensitive method to estimate various trypanocidal agents in about 10 mL of bovine serum/plasma using a silica gel column (Vollner, 2018). Similarly, Chopra et al. developed an HPLC method for estimating QS in rabbit plasma, which uses a complex gradient procedure (Chopra et al., 2015). However, the development of a sensitive, accurate, reliable, and reproducible method to evaluate the quality, safety, and performance of the quinapyramine sulphate formulation requires considerable effort.

The hydrophilic nature of drugs has long posed a challenge for researchers attempting to develop suitable analytical techniques using reverse-phase HPLC and hydrophobic C8 or C18 columns (Mattrey et al., 2017; Sun et al., 2017; Tome et al., 2019). To address this issue, we have developed a rapid and sensitive RP-HPLC method using SLS as an ion-pair agent, which enables the retention of hydrophilic drugs on a hydrophobic column. This method works by treating the stationary column with a mobile phase consisting of an ion-pair agent, which forms a thin layer of ions that enable the retention of counter ions present in the sample. The basis of retention for these hydrophilic drugs lies in this ion-pairing mechanism.

To ensure compliance with the standards set by ICH and USFDA, we evaluated the accuracy, precision, sensitivity, and specificity of the developed method (Sarmento et al., 2010; Schlindwein et al., 2018). The method was then used to estimate the drug content in the newly developed nanoformulations of quinapyramine sulphate. Furthermore, we tested the

applicability of the method to estimate plasma drug concentrations in rats and camels during pharmacokinetic evaluation. The results demonstrated that the developed RP-HPLC method with SLS as an ion-pair agent is suitable for accurate, precise, and sensitive estimation of quinapyramine sulphate in various matrices, including nanoformulations and biological samples.

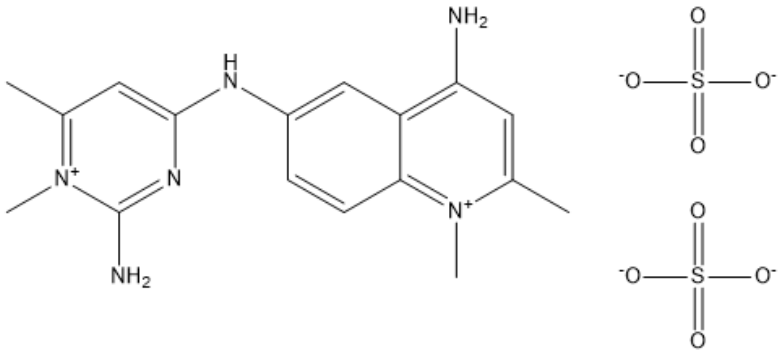

Fig. 2.1 Structure of Quinapyramine sulphate

2. Materials and methods

2.1 Materials

Quinapyramine sulphate was purchased from ProVentus Life Sciences Pvt. Ltd., (Chennai, India). HPLC grade formic acid, acetonitrile and methanol were purchased from Merck Limited (Mumbai, India). Sodium lauryl sulphate was procured from SD Fine-Chem Limited (Mumbai, India). All other chemicals, solvents and reagents utilized, were either HPLC or analytical grade. HPLC grade water was obtained from Milli-Q system (Millipore GmbH, Germany) used throughout the analysis. The solvents and buffers prepared were suitably filtered through 0.22 Millipore^{TM} membrane filter (Merck, Darmstadt, Germany) and suitably degassed using an ultrasonic bath for 30 min.

2.2 Instrument and software

HPLC method for the determination of quinapyramine sulphate in plasma was developed using the Shimadzu HPLC system (Kyoto, Japan) equipped with binary pump (LC-20AD), UV detector (SPD M20A), and auto-sampler (SIL-HTC, Shimadzu, Japan). The hardware control and data processing were done using LC solution software version 2.0. The plasma samples were processed by using Finnpipette™ F2 (ThermoFisher Scientific, USA), Multi Spinix-Vortex shaker (Tarson, USA), Eppendorf Centrifuge (Eppendorf, Germany), and Bath-Sonicator.

Development and validation of analytical method:

1. Chromatographic conditions

A Waters Sunfire® C18 3.5 µm ODS (4.6 x 50 mm) column was used for the separation. A sample injection volume of 20 µL was used. The mobile phase system consisted of reservoir A (acetonitrile) and reservoir B (2.5 mM sodium lauryl sulphate in 0.1% formic acid in water) with a composition of 45:55 (%A: %B) at a flow rate of 1 ml/min in isocratic mode. The study was conducted with a total run time of 8 min and a detection wavelength of 297 nm. The HPLC column was maintained at a constant temperature of 30° C throughout the study.

2. Preparation of standard solutions

A QS standard stock solution (1000 µg/ml) was prepared by dissolving an accurately weighed quantity of QS (25 mg) in a 25 ml volumetric flask, and the volume was made up with methanol. A working standard solution of 100 µg/ml was prepared by diluting 1 mL of the stock solution to 10 mL in a volumetric flask (10 mL) using methanol. To prepare secondary working standard solutions of QS, the working standard solution (100 µg/mL) was suitably diluted with 1:1 acetonitrile: Milli Q water. Specifically, 1.25, 2.5, 5, 10, 20, 40, 80, and 160 µL of the standard stock solution was diluted up to 1.0 mL to obtain a final concentration of 0.125, 0.25, 0.5, 1, 2, 4, 8, and 16 µg/mL, respectively.

3. Preparation of sample solution

The supernatant obtained during separation of QS-loaded solid nanoparticles (QS-DS-SLN) was suitably diluted (10-times) with the methanol and sonicated in water bath for 10 min at room temperature.

4. Analytical Method validation

Developed analytical method was validated according to International Conference on Harmonization (ICH) guideline Q2 (R1)(ICH, 2005) with respect to specificity, linearity, range, limit of detection (LOD), limit of quantitation (LOQ), precision, accuracy and robustness.

4.1 Specificity

To assess the specificity of the developed analytical method, a known concentration of QS (0.5 µg/mL) was spiked in the placebo batch, which contained all the formulation components,

including precirol, docusate sodium, polyvinyl alcohol, sodium cholate, and aluminium monostearate. QS-loaded solid lipid nanoparticles and QS-Na.C complex-loaded oily nanosuspension were analysed separately. Additionally, the release media used during in vitro drug release was spiked with the known concentration of QS (0.5 µg/mL). The resulting chromatograms were carefully analysed to determine if there was any interference from either the formulation components or the release media components.

4.2 Linearity and range

To determine the linearity and range of the developed analytical method, a series of calibration standards with concentrations ranging from 0.125 to 10 µg/mL were injected six times. The peak area for each standard was then plotted against the corresponding concentration to obtain a calibration curve. The linearity of the method was assessed using the ordinary least square regression equation and correlation coefficient previously obtained during the optimization of the analytical method.

4.3 Accuracy

To evaluate the accuracy of the developed RP-HPLC method, known concentrations of QS were spiked into three calibration standards (0.25, 2, and 10 µg/mL), and the samples were analysed in triplicate. The recovery of QS was calculated by comparing the measured concentrations to the expected concentrations of the spiked samples. The accuracy of the method was assessed by calculating the percent relative standard deviation (%RSD) and percent recovery for each calibration standard. This approach provides a reliable and comprehensive assessment of the accuracy of the developed method and ensures the reliability of subsequent analysis.

4.4 Precision

To determine the precision of the developed method, the peak areas of three calibration standards were analysed in triplicate three times a day for intraday precision. Inter-day precision was evaluated by analysing the peak areas of three calibration standards in triplicate for three consecutive days. The precision of the method was assessed by calculating the percent relative standard deviation (%RSD) for each set of triplicate measurements.

4.5 Limit of detection (LOD) and limit of quantitation (LOQ)

The limit of detection (LOD) and limit of quantification (LOQ) of the developed method were determined by measuring the signal-to-noise ratio (S/N) obtained in the chromatogram of blank and standard concentrations of QS. The concentration at which the S/N ratio was greater than 3.3 and 10 was selected as LOD and LOQ, respectively.

4.6 Robustness

To assess the robustness of the developed method, deliberate changes were made to the chromatographic conditions, including variations in flow rate (0.8 and 1.2 mL/min), ion pairing agent concentration (2 and 3 mM SLS), and column temperature (28 and 32°C). The effect of these changes on the accuracy of the method was evaluated by measuring the percent recovery of the three calibration standards.

5. Results and discussion

5.1 Method development

Initially, acidic conditions of the mobile phase were used for the elution of QS due to its high basicity. However, the compound's high hydrophilicity resulted in poor retention of the drug in the hydrophobic C18 column, leading to early elution of the drug with no interaction with the stationary phase (Machairas et al., 2018). Orthophosphoric acid, formic acid, and acetic acid at concentrations of 0.1, 0.3, and 0.5% v/v were added in the aqueous phase to study impact of acidic environment on the retention of QS. It was observed that neither change in type of acid nor the concentration of acid could retain the QS on stationary phase (Filipic et al., 2016; Schlindwein et al., 2018). Furthermore, the addition of various buffering agents such as sodium acetate, ammonium formate, ammonium acetate, and potassium dihydrogen phosphate in the concentration range of 1-10 mM, along with pH adjustment with respective acids, failed to retain QS in the stationary column. In an attempt to improve retention and peak shape and to avoid free silanol group interaction present in the stationary phase, triethylamine was added in varying concentrations in both the aqueous and organic phase, but it did not give the desired results. Despite several attempts to retain the hydrophilic QS in the hydrophobic C18 column, none of the approaches effectively retained the QS in the column. The insufficient interaction of the QS in the column led to quicker elution from the column, as evidenced by the border peaks observed just after the void space.

To address the issues of poor retention of the hydrophilic QS in the hydrophobic C18 column, researchers investigated the addition of counter-ions in the mobile phase to retain ionic, hydrophilic drugs in the column (Brezovska et al., 2010; Varvara et al., 2009). The addition of negatively charged sulfonate ions with different lengths of an alkyl chain, such as sodium lauryl sulphate (SLS), as an ion pair reagent was found to be suitable for increasing the retention time of QS in an octylsilane column (Quintanar-Guerrero et al., 1997; Shervington et al., 2005; TCI, 2016).

The concentration of the ion-pair agent in the aqueous mobile phase was optimised to obtain a reproducible retention time for QS. During the optimisation process, it was discovered that the addition of SLS significantly improved the retention of QS in the C18 column. Increasing the concentration of SLS from 1 to 5 mM, using a 50:50 ratio of buffer and ACN, resulted in a corresponding increase in the retention time from 3.5 to 15 minutes. Moreover, it was observed that increasing the ratio of the aqueous buffer phase led to a significant increase in the retention of QS in the stationary phase.

It was evident that, retention of QS was significantly affected by the concentration of aqueous buffer phase consisting of ion-pair agent. It was observed that the aqueous phase consisting of 2.5mM of SLS in 0.1% v/v formic acid along with acetonitrile at a ratio of 45:55 gave reproducible retention of QS without any interreference at the retention time of QS. Table 2.1 represents various chromatographic parameters obtained at optimized ratio of buffer and organic phase. An increase in the ion-pair agent of the mobile phase contributes to the enhancement in the retention for QS because of increase in active site for the residence by electrostatic interactions which increases the QS residence in the hydrophobic C18 column during analysis. Finally, retention of the QS in the hydrophobic C18 column was achieved using a 55:45 ratio of aqueous buffer to ACN, at a column temperature of 30°C, with a Waters Sunfire® C18 3.5 um ODS (4.6 x 50 mm) column, resulting in peak symmetry (T=1.1±0.05) and a retention time of 7.6 ± 0.5 min. Fig. 2.2 depicts linear regression curve and representative chromatogram of QS (500 ng/mL) spiked in 1:1 ACN: Water.

Table 2.1 Optimization of mobile phase for quantification of QS by RP-HPLC method

Chromatographic conditions	**Acceptance criteria**	**Results**		
A: Acetonitrile, B: 0.1% v/v formic acid	-	30:70	50:50	55:45
Retention of QS	-	15.7 ± 1.23	9.8 ± 0.52	7.5 ± 0.22

Retention factor, *k'*	2<*k'*<10	3.62 ± 0.03	2.51 ± 0.02	1.18 ± 0.01
Tailing factor	0.8-1.5	1.45 ± 0.21	1.22 ± 0.14	1.04 ± 0.08
Number of theoretical plates	>2000	12147 ± 124	9625 ± 363	9986 ± 207
HETP	-	32.56 ± 0.36	23.32 ± 2.14	19.6 ± 0.24

5.2 Method validation

The calibration plots showed a good linear relationship with a high correlation coefficient (R^2) of 0.999 and the equation Y=71372x+11285 over the concentration range of 0.125-16 µg/ml using polynomial regression. The overall % recovery for three different concentration levels was found to be within the acceptable range of 80-120%. The %RSD for the developed method was less than 2%, confirming the inter-day and intra-day precision.

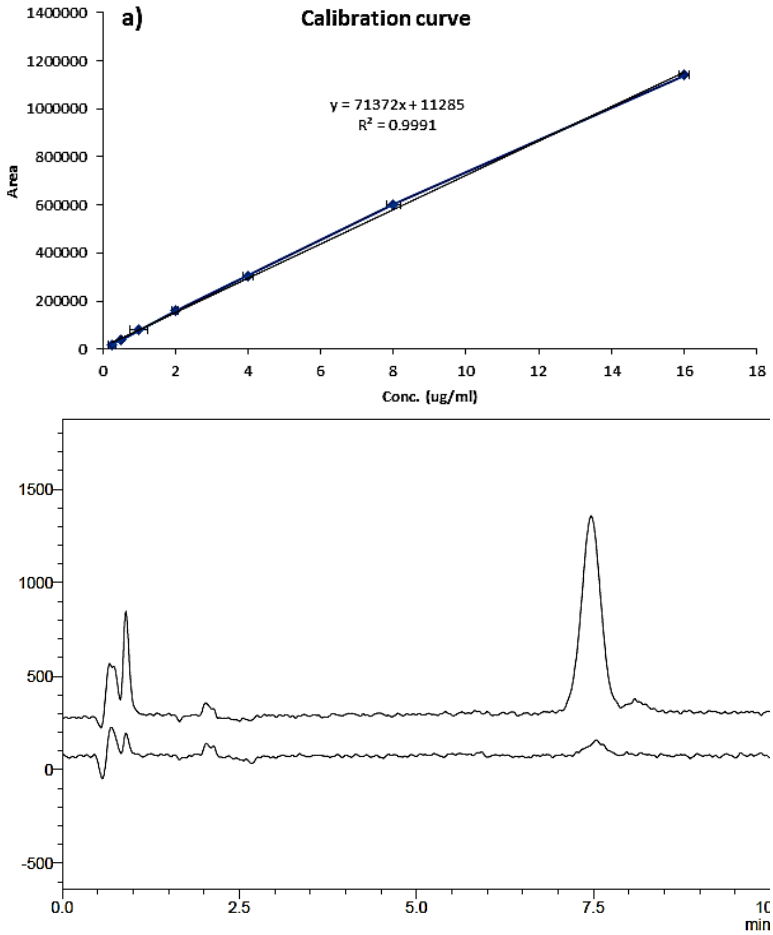

Fig. 2.2 a) linear regression calibration curve, and b) representative chromatogram of blank and QS (500 ng/mL) 2.5 mM sodium lauryl sulphate in 0.1% formic acid: ACN (55:45)

The developed RP-HPLC method for quantification of QS was found to be selective, as demonstrated by the absence of interference from the excipients used in the formulation. Additionally, the % recovery of QS was within the acceptable range of 80-120% upon slight

changes in column temperature, flow rate, and pH of buffer, confirming the robustness of the method. The limit of quantitation (LOQ) and limit of detection were found to be 0.1 µg/ml and 0.18 µg/ml, respectively. Results of the method validation of QS are presented in table 2.2.

The method was also found to be selective, as there was no interference from the excipients used in the formulation observed [(Fig. 2.3 b)]. % Recovery of QS upon slight change in column temperature, flow rate and change in pH of buffer were also found to be within the acceptance criteria of 80-120% at three different concentrations confirmed robustness of developed QS RP-HPLC method. Limit of quantitation (LOQ) and limit of detection were found to be 0.1 µg/ml and 0.18 µg/ml respectively. Results of method validation of QS are presented in table 2.1.

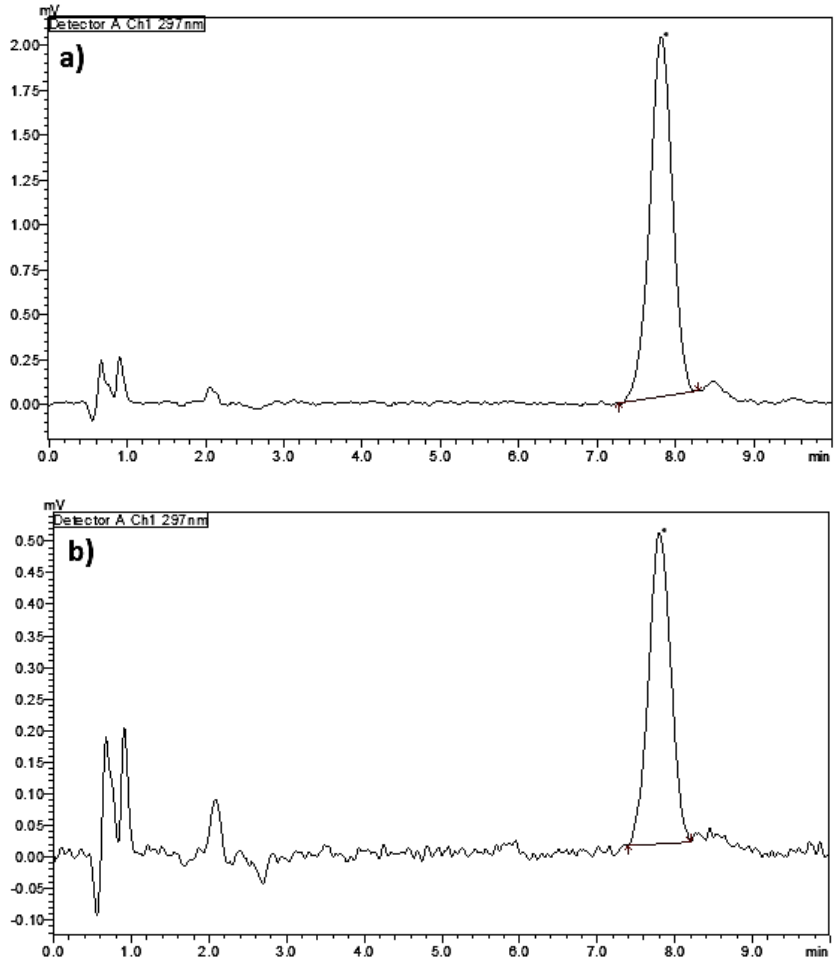

Fig. 2.3 Representative chromatograms of QS spiked in, a) formulation components, and b) release media

Table 2.2: Results for analytical method validation of QS

Accuracy*			
Concentration (µg/ml)	**%Recovery**	**SD**	**% RSD**
0.25	93.50	0.11	0.12
2	94.63	0.08	0.08
10	94.38	0.36	0.38
Intra-day precision*			
Concentration (µg/ml)	**Measured conc. (µg/ml)**	**SD**	**% RSD**
0.25	0.28	0.02	1.58
2	1.83	0.04	0.68
10	9.69	0.09	0.70
Inter-day precision*			
Concentration (µg/ml)	**Measured conc. (µg/ml)**	**SD**	**% RSD**
0.25	0.29	0.11	1.48
2	2.53	0.08	1.44
10	10.84	0.35	1.95

Robustness*			
Condition	**% Recovery ± SD**		
	0.25 µg/ml	**2 µg/ml**	**10 µg/ml**
Column temperature (28°C)	100.24 ± 0.02	98.47 ± 0.03	91.67 ± 0.22
Column temperature (32°C)	98.72 ± 0.01	96.94 ± 0.01	92.78 ± 0.10
Flow rate (1.2 ml/min)	81.94 ± 0.05	81.04 ± 0.01	85.81 ± 0.19
Flow rate (0.8 ml/min)	116.46 ± 0.10	119.28 ± 0.05	115.14 ± 0.21
Conc. of SLS (2 mM)	104.47 ± 0.05	97.91 ± 0.08	92.72 ± 0.19
Conc. of SLS (3 mM)	96.76 ± 0.06	93.82 ± 0.02	90.91 18.75

Bioanalytical method development and validation:

1. HPLC operating conditions

To separate QS from the rat plasma, a Waters Sunfire® C18 3.5 um ODS (4.6 x 50 mm) column was used, with a sample injection volume of 50 µL. The binary mobile phase system comprised of 40% acetonitrile from reservoir A and 60% of 2.5 mM sodium lauryl sulphate in 0.1% formic acid in water from reservoir B, at a flow rate of 1 ml/min in isocratic mode. The separation was carried out for a total run time of 22 min, with detection at a wavelength of 297 nm, and the HPLC column was maintained at 30°C throughout the study. Prior to sample analysis, the HPLC was equilibrated for 30 min.

2. Preparation of stock solution, calibration curve standards and quality control samples

To prepare stock solutions of QS and IS, 100 mg of each was accurately weighed and transferred to volumetric flasks. Methanol was added to make up the volume to 100 ml, and the resulting solutions were stored at 4°C until further analysis. Working solutions of 100 µg/mL were used to prepare calibration curve samples at concentrations of 1, 2, 5, 10, 15, 20, and 40 µg/mL. Quality control (QC) samples were also prepared from stock solutions at concentrations of 1.6, 18, and 32 µg/mL to achieve final concentrations of 80, 900, and 1600 ng/mL, respectively. All working solutions required for plotting the calibration curve and preparing QC samples were prepared by successive dilution with a 1:1 mixture of acetonitrile and water.

3. Extraction procedure

To extract QS from plasma, three methods were evaluated: liquid-liquid extraction (LLE), solid-phase extraction (SPE), and protein precipitation. For LLE, a combination of water-immiscible organic solvents (Dichloromethane, n-Hexane, tert-butyl methyl ether, and Diethyl ether) was attempted. For SPE, the impact of eluting mobile phase with varying concentrations of formic acid was assessed. Additionally, plasma protein precipitation was evaluated using various water-soluble organic solvents (acetonitrile, methanol, tetrahydrofuran, acetone), with varying ratios tested for extraction of QS from plasma.

Protein precipitation was found to be the most effective method and was therefore adopted for further sample processing. The extraction efficiency of the selected method was assessed by comparing chromatographic peak areas of un-extracted non-biological samples with those of spiked plasma (extracted) samples at the same concentration level. Among all the solvents

studied, an equal mixture of acetonitrile and methanol (200 µL) was selected for the drug extraction process during sample preparation.

4. Preparation of plasma samples

To prepare the spiked samples, 5 µL of a known drug concentration and the internal standard (4,7-dichloroquinoline) were added to 90 µL of pooled rat plasma from six healthy animals. After each addition of the drug and the internal standard, vortexing was performed for 30 seconds. The samples were then extracted by adding 200 µL of acetonitrile and methanol (1:1) and vortexed for 30 minutes on a Spinix vertexer. The samples were centrifuged at 15,000 rpm for 15 minutes at 4°C to collect the supernatant, which was then evaporated under a continuous N_2 stream. The resulting residue was reconstituted with 100 µL of a 1:1 mixture of acetonitrile and water and vortexed for 30 minutes before being centrifuged at 15,000 rpm for 15 minutes at 4°C. The supernatant was filtered using a 0.22 µm nylon syringe filter, and 50 µL of the resulting solution was injected into the HPLC system for chromatographic analysis.

5. Method Validation parameters for Quinapyramine sulphate

5.1 Selectivity

To assess the selectivity of the method, potential chromatographic interference from endogenous substances in the blank rat plasma matrix was evaluated. Chromatograms of blank plasma were compared to those of spiked samples to ensure that there was no overlap of peaks from the blank to the analyte. Six randomly selected Wistar rats were used to collect plasma samples, which were then analysed using the aforementioned chromatographic conditions.

5.2 Linearity and range

To construct calibration curves for QS, seven different concentrations (50, 100, 250, 750, 1000, 1500, and 2000 ng/mL) were used in blank rat plasma, with a fixed concentration of IS (1µg/mL). The peak area ratios of drug:IS were plotted on the Y-axis, and the nominal plasma concentrations were plotted on the X-axis to prepare six calibration curves. Samples for the calibration curve and quality control were prepared in replicates (n=6) for analysis.

5.3 Limit of detection (LOD) and limit of quantitation (LLOQ)

Limits of detection (LOD) and quantitation (LOQ) were estimated based on calibration curve using equations below.

$$LOD = \frac{3.3\,\sigma}{S} \quad (2.1)$$

$$LOQ = \frac{10\,\sigma}{S} \quad (2.2)$$

Wherein, σ is the standard deviation of y-intercept of calibration curve and S is the slope of calibration curve.

5.4 Precision and accuracy

The intra-day and inter-day assay precision and accuracy were determined by analysing three replicates at three different QC levels (LQC, MQC, HQC) and LLOQ. For intra-day assay precision and accuracy samples were analysed on same day, while inter-day assay precision and accuracy were determined by analysing samples on three consecutive days. The acceptance criteria for accuracy are within ±15% (expressed as percentage of deviation from nominal concentration, % bias) and for precision within ±15% (expressed as percentage deviation, % CV) except for LLOQ, where it should not exceed ±20% for both accuracy and precision.

5.5 Stability

The stability of QS in plasma was evaluated under four different stress conditions after sample preparation, including auto-injector storage, freeze-thaw, bench-top, and long-term storage. Three QC samples (LQC, MQC, and HQC) were analysed in triplicate under each of the aforementioned conditions to assess stability. Bench-top stability was determined by keeping the QC samples at room temperature (RT) for 24 hours, while auto-injector stability was assessed by analysing the same set of samples at 24 hours. Long-term stability was evaluated by storing the samples at −20 ± 0.5°C for 30 days. Freeze-thaw stability was performed by subjecting the QC samples to three consecutive cycles of freezing (–20 ± 0.5°C for 48 hours) and thawing within 2 days. The stability was assessed by comparing the peak areas of the samples kept under varying stress conditions with those prepared freshly at the same nominal concentrations.

6. Results and discussion

6.1 Optimization of chromatographic conditions

Various chromatographic conditions were screened to determine the optimal mobile phase composition, column selection, flow rate, and injection volume for the analysis of QS in rat plasma. Knowledge gained during the development of the analytical procedure was used to optimize the chromatographic conditions. A significant change in retention time of the analyte QS was observed by changing the buffer concentration from 55% to 60%. The final optimized separation method for quantification of QS involved using a Waters Sunfire® C18 3.5 um ODS (4.6 x 50 mm) column with a mobile phase consisting of 2.5mM SDS in 0.1% formic acid in water and Acetonitrile in a 60:40 ratio, a flow rate of 1.0 mL/min, and an injection volume of 50 µL. With these optimized conditions, QS and IS were retained at 9.5 and 15.3 minutes, respectively, with an overall run time of 22 minutes and a resolution between the two peaks greater than 4.5. Figure 2.4 shows a representative chromatogram of a sample containing QS and IS.

6.2 Optimization of sample preparation method

The plasma sample clean-up procedure is crucial in bioanalytical method development as it affects the sensitivity and selectivity of the developed method. The extraction efficiency of the analytical process refers to the recovery of a known concentration of the analyte after sample extraction procedures. A higher extraction efficiency leads to a more accurate method. However, the hydrophilic nature of QS made it difficult to extract using various water-insoluble organic solvents in liquid-liquid extraction (LLE) methods. The affinity of QS towards plasma was greater than the organic solvents due to the drug's plasma protein binding ability. The extraction efficiency in LLE ranged from 8-15%, which was significantly lower than the analytical chromatograms of the same concentrations. Similarly, solid-phase extraction (SPE) method of drug extraction also yielded low extraction efficiency of 13-22%. Ultimately, a single-step protein precipitation technique gave the highest recovery (~80%), making it an easier and widely applicable technique for extracting hydrophilic drugs like QS. Table 2.3 shows various solvents and their combinations used to maximize the extraction efficiency of the drug from plasma. Amongst the various solvents studied, an equal mixture of acetonitrile and methanol was chosen for further sample processing.

Table 2.3 Optimization of the protein precipitation method for sample preparation

Plasma protein precipitating solvent	Qty added (µL)	Vortex time (min)	Centrifugation [speed (rpm), time (min)]	% Recovery	Remarks
Acetonitrile	200-400	10 30	10000, 10	52-86%	Variable recovery observed for both the analytes. Least interference of proteins in methanol as a solvent
Methanol	500	10 30	10000, 15	72-83 %	
Acetone	500	10 30	10000, 15	52-63 %	Although lesser time required for evaporation of solvent, % recovery was not up to mark
0.1% trichloroacetic acid, 0.1M hydrochloric acid	400	30	10000, 15	NC*	*After reconstitution of the samples, filtration was required with 0.22 µm filter indicating some of the proteins got extracted in these solvents. Resulting samples were not run in HPLC system.
Tetrahydrofuran	400	10	10000, 15	73-79%	Longer time for evaporation of the solvent
Acetonitrile: Methanol (1:1 v/v)	200	20	10000, 15	78-82%	Equal mixture of ACN: MeOH gave maximum extraction efficiency of QS and IS

6.3 Method validation

6.3.1 Specificity

The HPLC analysis of a sample containing both QS and IS, as depicted in Fig. 2.4, showed a clear separation between the two analytes, indicating that the chosen chromatographic conditions were suitable for the detection of the QS. The peak shape of both compounds was symmetrical, suggesting that the extraction and sample preparation procedures were effective in removing any potential matrix interference.

6.3.2 Selectivity

The developed and validated method showed no matrix interference at the retention time of the analyte and internal standard (I.S.) when analysed using blank plasma samples from six healthy rats. This was confirmed by the representative chromatograms obtained after the extraction and analysis of blank rat plasma, blank rat plasma spiked with I.S. (Zero blank), and plasma spiked with QS (750 ng) and IS as shown in Figure 2.4.

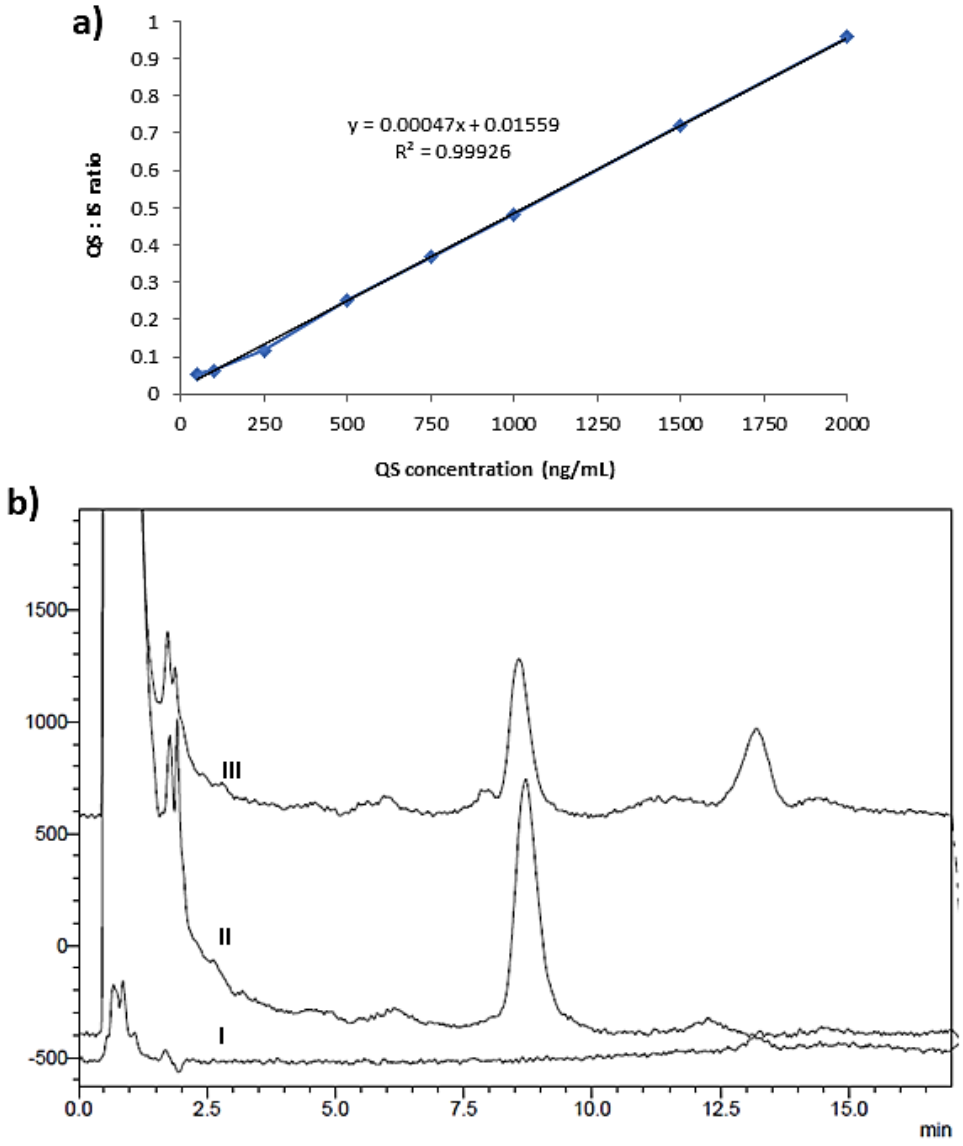

Fig. 2.4. a) Calibration curve for QS in plasma, b) representative chromatograms of QS spiked in rat plasma, I) blank plasma without QS and IS, II) blank plasma spiked with IS (zero blank), and III) known conc. of QS spiked in rat plasma (750 ng/mL).

The chromatogram of the zero blank, the blank plasma spiked with IS, and the plasma spiked with QS and IS demonstrated excellent resolution between the peaks of the analyte QS and IS. These peaks were well distinguished from the peaks of plasma components, such as proteins and enzymes, indicating the absence of any interfering matrix effects.

6.3.3 Linearity and range

The peak area ratios of QS to IS at different concentrations of QS in plasma were plotted to generate a calibration curve that exhibited linearity in the concentration range of 50-2000 ng/mL with a high regression coefficient of 0.999, indicating good reproducibility. Table 2.4 displays the regression data.

Table 2.4: Linear regression data for the calibration curve of QS in rat plasma (n = 6).

Parameters	Values
Range (ng/mL)	50-2000
Correlation coefficient (r^2)	0.99926 ± 0.0081
Slope	0.00047 ± 0.0062
Intercept	0.01559 ± 0.0173
LLOQ (ng/mL)	50

6.3.4 LOD and LOQ

The LOD and LOQ value for QS in plasma was found to be 46.21 ng/mL and 34.71 ng/mL, respectively.

6.3.5 Precision and accuracy

Table 2.5 shows that the inter and intra-day precision and accuracy values for the QC levels of LQC, MQC, and HQC, including LLOQ, were within the acceptable range. The inter-day precision ranged from 1.42% to 11.59% for %CV, while the intra-day precision ranged from 2.13% to 9.07%. The accuracy, when calculated in terms of % bias from nominal concentration, yielded acceptable values ranging from (-)2.18% to 4.61%.

Table 2.5: Precision (% CV) and accuracy (% bias) of the QS in rat plasma samples at quality control concentrations of the calibration ranges (n=5)

Level	Nominal conc. (ng/mL)	Inter-day		
		Measured conc.	Precision (%CV)	Accuracy (% Bias)
LLOQ	50	52.30 ± 8.06	11.59	4.61
LQC	80	78.26 ± 2.01	2.58	-2.18
MQC	900	914.04 ± 29.89	3.27	3.96
HQC	1800	1807 ± 25.75	1.42	0.44
Level	**Nominal conc. (ng/mL)**	**Intra-day**		
		Measured conc.	**Precision (%CV)**	**Accuracy (% Bias)**
LLOQ	50	53.36 ± 4.84	9.07	6.73
LQC	80	77.38 ± 3.41	4.41	-3.27
MQC	900	932.03 ± 46.43	4.98	3.56
HQC	1600	1814.58 ± 38.79	2.13	0.81

6.3.6 Stability

Table 2.4 shows the stability results of QS in rat plasma under different stress conditions. The results indicate that the analyte is stable in rat plasma under various storage conditions that may be encountered during routine study sample analysis. The samples subjected to different stability conditions showed results well within the assay variability limits throughout the process, indicating that the integrity of the samples was not compromised significantly. These findings suggest that quinapyramine sulphate can be stored under the tested conditions without affecting the quality of the samples.

Table 2.6: Stability of QS in different operating conditions

Type of stability	Nominal concentration (ng/mL)	Measured concentration (ng/mL)	Precision (%CV)	Accuracy (% Bias)
Bench-top stability	80	77.68	1.99	-2.90
	900	927.67	6.05	3.07
	1600	1806.12	1.35	0.34
Auto-sampler stability	80	78.31	3.36	-2.11
	900	939.86	6.32	4.43
	1600	1814.55	1.88	0.81
Freeze-thaw stability	80	77.41	4.12	-3.24
	900	933.33	5.65	3.70
	1600	1826.52	1.71	1.47
Long term stability	80	79.06	3.09	-1.17
	900	913.56	1.75	1.50
	1600	1808.35	1.19	0.46

7. Conclusion

A validated and sensitive ion pair-reverse phase high-performance liquid chromatography (HPLC) method was developed to quantify the anti-trypanosomal drug QS in rat plasma. The method involves a simple sample preparation process with adequate recovery using a one-step protein precipitation method. The developed method has significant therapeutic importance in anti-trypanosomal therapy of animals and can be extensively used to study drug exposure, in vivo drug-drug interactions, and pharmacokinetic-pharmacodynamic (PK-PD) parameters. It requires a very small plasma sample volume of 90 µL and can analyse a wide concentration range of 50-2000 ng/mL in a short overall run time of 22 minutes without the need for advanced, sophisticated techniques. The study also demonstrated that QS remains stable in plasma when stored under different working and storage conditions.

References:

Brezovska, K., Dimitrovska, A., Kitanovski, Z., Petrusevska, J., Ribarska, J.T., Jolevska, S.T., 2010. Development of an ion-pair reversed-phase HPLC method with indirect UV detection for determination of phosphates and phosphites as impurities in sodium risedronate. J. AOAC Int. 93, 1113–1120. https://doi.org/10.1093/jaoac/93.4.1113

Chopra, M., Rathore, N.S., Kumar, S., Kumar, B., Pandita, D., Manuja, A., 2015. Development and validation of high performance liquid chromatography uv-visible spectrometry method for the detection of quinapyramine sulfate 4, 666–673.

Filipic, S., Elek, M., Popović, M., Nikolic, K., Agbaba, D., 2016. Development of Hydrophilic Interaction Liquid Chromatography Method for the Analysis of Moxonidine and Its Impurities. J. Anal. Methods Chem. 2016. https://doi.org/10.1155/2016/3715972

ICH, 2005. ICH harmonised tripartite guideline validation of analytical procedures : 1994.

Machairas, G., Panderi, I., Geballa-Koukoula, A., Rozou, S., Antonopoulos, N., Charitos, C., Vonaparti, A., 2018. Development and validation of a hydrophilic interaction liquid chromatography method for the quantitation of impurities in fixed-dose combination tablets containing rosuvastatin and metformin. Talanta 183, 131–141. https://doi.org/10.1016/J.TALANTA.2018.02.068

Mattrey, F.T., Makarov, A.A., Regalado, E.L., Bernardoni, F., Figus, M., Hicks, M.B., Zheng, J., Wang, L., Schafer, W., Antonucci, V., Hamilton, S.E., Zawatzky, K., Welch, C.J., 2017. Current challenges and future prospects in chromatographic method development for pharmaceutical research. TrAC Trends Anal. Chem. 95, 36–46. https://doi.org/10.1016/J.TRAC.2017.07.021

National Library of Medicine, n.d. Quinapyramine sulphate - Compound Summary [WWW Document]. Pubchem. URL https://pubchem.ncbi.nlm.nih.gov/compound/Quinapyramine-sulfate

Prayag, K., Surve, D.H., Paul, A.T., Kumar, S., Jindal, A.B., 2020. Nanotechnological interventions for treatment of trypanosomiasis in humans and animals. Drug Deliv. Transl. Res. 10, 945–961.

Quintanar-Guerrero, D., Allémann, E., Fessi, H., Doelker, E., 1997. Applications of the ion-pair concept to hydrophilic substances with special emphasis on peptides. Pharm. Res. 14, 119–127. https://doi.org/10.1023/A:1012076022420/METRICS

Sarmento, B., Amiji, M.M., Fernanda, M., 2010. Journal of Pharmaceutical and Biomedical Analysis Development and validation of a rapid reversed-phase HPLC method for the determination of the non-nucleoside reverse transcriptase inhibitor dapivirine from polymeric nanoparticles 52, 167–172. https://doi.org/10.1016/j.jpba.2010.01.007

Schlindwein, W., Bezerra, M., Almeida, J., Berghaus, A., Owen, M., Muirhead, G., 2018. In-line uv-vis spectroscopy as a fast-working process analytical technology (Pat) during early phase product development using hot melt extrusion (hme). Pharmaceutics 10, 1. – 25. https://doi.org/10.3390/pharmaceutics10040166

Shervington, L.A., Abba, M., Hussain, B., Donnelly, J., 2005. The simultaneous separation and determination of five quinolone antibotics using isocratic reversed-phase HPLC: Application to stability studies on an ofloxacin tablet formulation. J. Pharm. Biomed. Anal. 39, 769–775. https://doi.org/10.1016/j.jpba.2005.04.039

Sun, W.Y., Lu, Q.W., Gao, H., Tong, L., Li, D.X., Zhou, Z.Q., Jiang, Z.J., Sun, H., Bi, K.S., 2017. Simultaneous determination of hydrophilic and lipophilic constituents in herbal medicines using directly-coupled reversed-phase and hydrophilic interaction liquid chromatography-tandem mass spectrometry. Sci. Rep. 7, 1–12. https://doi.org/10.1038/s41598-017-07087-x

TCI, 2016. Ion-Pair Reagents for HPLC 7.

Tome, T., Žigart, N., Časar, Z., Obreza, A., 2019. Development and Optimization of Liquid Chromatography Analytical Methods by Using AQbD Principles: Overview and Recent Advances. Org. Process Res. Dev. 23, 1784–1802. https://doi.org/10.1021/ACS.OPRD.9B00238/ASSET/IMAGES/LARGE/OP9B00238_0009.JPEG

Varvara, A., Monciu, C.M., Aramă, C., Popescu, C., 2009. Ion-pair reversed-phase high-performance liquid chromatography of ondansetron hydrochloride using sodium heptanesulphonate as a counterion. Farmacia 57, 442–451.

Vollner, H., 2018. Determination of the trypanocidal drugs Homidium , Isometamidium and Quinapyramine in bovine serum or plasma using HPLC Isometamidium and Quinapyramine in bovine serum or plasma Vollner.

WHO Report on trypansomiasis, 2013, 2001. Control and surveillance of human African trypanosomiasis.

Chapter 3: Development and Evaluation of Quinapyramine Sulphate Loaded Lipidic Nanoparticles

1. Introduction

Animal *trypanosomiasis* is caused mostly by the *T. evansi* parasite where, quinapyramine sulphate (QS) is considered a drug of choice for the treatment in domestic animals (Surve and Jindal, 2021). It is an aminoquinaldine derivative, a highly hydrophilic cationic drug used for the treatment of *trypanosomiasis* in camels, horses, buffaloes, sheep, and goats.(Desquesnes et al., 2013; Prayag et al., 2020) It is freely soluble in water and almost insoluble in organic solvents.(Yashica Pharmaceuticals Pvt. Ltd., n.d.) Commercially, QS is available as a powder for reconstitution, which exhibits dose-dependent side effects, including salivation, tremors, and tachycardia, after parenteral administration of quinapyramine sulphate formulation available in the market (Desquesnes et al., 2013). However, it could result in subtherapeutic plasma concentration of the QS, leading to the development of drug resistance and relapse of the infection.

In order to minimise theses dose-related side effects, incorporation of QS in nanocarriers showed significant improvement in efficacy with a reduction in side effects during preclinical studies (Manuja A, et.al. 2016). For instance, Manuja and co-workers reported that QS when encapsulated in sodium alginate nanoparticles has shown significant improvement in therapeutic efficacy with a 2-fold reduction in cytotoxicity as compared to free QS. Moreover, QS loaded sodium alginate nanoparticles showed higher cytotoxicity when compared with the free QS at the concentration almost 300-fold higher than that of the therapeutic dose (Manuja A, et.al. 2014). In an attempt to decrease the cytotoxicity of QS, polymeric nanoparticles composed of chitosan were prepared by the same research group. The chitosan nanoparticles were found to be safe against mammalian cells even at a concentration significantly higher than the recommended dose with 2-fold higher trypanocidal activity (Manuja A, et.al. 2018). Although, polymeric nanoparticles have shown significant improvement in trypanocidal activity of QS, the safety and biocompatibility of sodium alginate and chitosan polymers have not yet been fully established since these polymers (chitosan/ sodium alginate) are not approved for parenteral use by the regulatory agencies. Moreover, chitosan when used to prepare polymeric nanoparticles requires the addition of toxic crosslinking agents such as glutaraldehyde and epichlorhydrin to enhance the drug loading(Bellich et al., 2016). Whereas,

the use of sodium alginate could enhance the viscosity of nanodispersion, which may lead to additional challenges associated with the syringability and parenteral administration during clinical use(Fu et al., 2010). Furthermore, QS-loaded sodium alginate polymeric nanoparticles also revealed significantly low drug loading of 3.70 ± 1.80 (Manuja A, et.al. 2014). It is also well reported that natural polymers on storage loses structural integrity(Emilia S, 2015), which may lead to the reduction in % entrapment efficiency and drug loading during storage. Therefore, a safe and effective QS formulation for the treatment of animal *trypanosomiasis* is the need for an hour.

Although lipid-based nanocarriers offer additional advantages including biocompatibility, reduced toxicity, and scale-up feasibility over other types of carrier systems(Gohla et al., 2000; Mehnert and Mäder, 2012), yet the incorporation of hydrophilic drugs into lipid nanoparticles poses a significant challenge in attaining high drug loading.(Peres L, Peres La, Henrique P, 2016). The use of an ionic complexation approach to enhance the loading of the charged drugs into nanocarriers have been attempted by several researchers (Battaglia L, et.al. 2014; Ijaz M, et.al. 2016; Ristroph and Prud, et.al. 2019; Schouenborg, 2016; Silva E, et.al. 2016; Tang et al., 2017). The objective of the present work is to prepare and evaluate ionically complexed QS-DS loaded solid lipid nanoparticles (QS-DS-SLN) using an ion-pairing approach to obtain high drug loading of cationic hydrophilic drug.

Moreover, study consisted of the rationale scale-up of QS-DS-SLN using the geometric similarity approach where, we have utilized the equal liquid motion and scale of agitation principles (Sidney H Wiling, n.d.). Further, study consisted the pre-clinical evaluation of QS-DS-SLN for the trypanocidal effect against *T. evansi* parasite.

2. Materials and methods

2.1 Materials

Quinapyramine sulphate was procured from ProVentus Life Sciences Pvt. Ltd. (Chennai, India). Glyceryl monostearate, compritol and precirol ATO was kind gift from Gattefosse (Mumbai, India). Palmitic acid and stearic acid were procured from SD Fine chem. (Mumbai, India). Polyvinyl alcohol was purchased from Sigma-Aldrich Chemicals Company (Missouri, United States) whereas, precirol ATO was kind gift from Gattefosse (Mumbai, India). Docusate sodium was purchased from SD Fine Chem (Mumbai, India). Branched polyethyleneimine, and Coumarin 6 was purchased from Sigma-Aldrich Chemicals Company (Missouri, United States). MitoTracker™ Red CMXRos was purchased from ThermoFisher Scientific (USA). Thiazolyl blue tetrazolium bromide (MTT) was obtained from Sisco Research Laboratories Pvt. Ltd. (Mumbai, India). DAPI, RPMI 1640 was purchased from HiMedia Laboratories Pvt. Ltd. (Mumbai, India). Sodium resarzurin salt was purchased from Tokyo Chemical Industry (India) Pvt. Ltd (Hyderabad, India). β-cyclodextrin (β-CD), nystatin (NYS), and amiloride (AMD), were purchased from Himedia Laboratories Pvt. Ltd. (Mumbai, India) whereas, chlorpromazine (CPZ) was obtained from Yarrow Chem Products (Mumbai, India), respectively. Ficoll-paque Plus was procured from GE Healthcare (Chicago, United States). Ethanol from Jabsen and Jabsen Co. (GmbH, Germany), and foetal bovine serum (FBS) was procured from Gibco Biosciences (New York, United states). Phorbol-12-myristate-13-acetate (PMA) was procured from Cayman chemical (Michigan, USA). HPLC grade acetonitrile, methanol, dichloromethane was purchased from Merck (Darmstadt, Germany). HPLC grade water was obtained from Milli-Q system (Millipore GmbH, Germany).

2.1 Screening of lipids based on total solubility parameter and polarity

Two thermodynamic parameters namely total solubility parameter and polarity of different lipids and QS-DS complex were used to screen the lipid for preparation of QS-DS-SLN.(Hansen, 2004; Jindal and Devarajan, 2015; Krevelen, 2019; Raina et al., 2017)

2.1.1 Total solubility parameter

The total solubility parameter was calculated using equation 3.1

$$\delta_{total} = [\,(\delta_d)^2 + (\delta_p)^2 + (\delta_h)^2]^{1/2} \qquad (3.1)$$

Wherein, δ_d, δ_p and δ_h represents partial solubility parameter associated with dispersion forces, polar interactions and hydrogen bonding and were calculated using equations 3.2, 3.3 and 3.4, respectively.

$$\delta_d = \frac{\sum F_d}{\sum V} \quad (3.2)$$

$$\delta_p = \frac{(\sum F_p)^{1/2}}{\sum V} \quad (3.3)$$

$$\delta_h = (\frac{\sum E_h}{\sum V})^{1/2} \quad (3.4)$$

Where F_d, F_p, and E_h indicate group contribution by dispersion forces, polar forces, and hydrogen bond energy respectively and V is molar volume.

2.1.2 Polarity

The polarity of each component in the study can be evaluated by the following equation –

$$Polarity = 1 - (\frac{\delta_d}{\delta_{total}})^2 \quad (3.5)$$

The polarity calculation for each component under can be evaluated by difference in polarities of both components.

2.2 Screening of anionic complexing agents

Different anionic agents including docusate sodium, sodium tripolyphosphate, sodium alginate, and sodium carboxymethylcellulose were screened to prepare QS–ionic complex by modified solubility method as described previously with some modifications (Wong et al., 2004). Briefly, an aqueous solution of QS (1 mg/mL) was prepared and different anionic agents were added to it to obtain QS to anionic agent molar ratio of 1:0.5, 1:1, 1:2, and 1:4. The above solutions were vortexed for 5 min. using Tarson multispin vortex mixer and were centrifuged at 12,000 rpm for 15 min. Thereafter, the supernatant was separated and analysed at λ_{max} of 297 nm using a UV-visible spectrophotometer (Shimadzu, Japan) to determine QS. The pellet obtained after centrifugation was dissolved in n-octanol (2.0 mL) by vortexing for 10 min followed by bath sonication for 5 min. Aliquot (20 µL) was withdrawn and the QS was extracted using 2.0 mL of warm mixture of methanol: 0.3 M $CaCl_2$ (80:20). The concentration of QS was analysed by measuring absorbance at λ_{max} of 297 nm using a UV-spectrophotometer. All samples were analysed in triplicate.

2.3 Preparation of QS-DS-SLN

QS-DS-SLN were prepared by the solvent evaporation method using an in-situ complexation approach as reported previously with some modifications (Poudel B, Gupta B, Ramasamy T, Thapa R, Youn Y, Choi H, Yong C, 2016).

Briefly, the organic phase was prepared by dissolving docusate sodium (9.0 mg), and precirol (20.0mg) in dichloromethane (2.0 mL). The organic phase was dispersed in the aqueous phase (10.0 mL) consisting of quinapyramine sulphate (5.0 mg) and polyvinyl alcohol (1% w/v) using a high shear homogeniser (T10 ULTRA-TURRAX, IKA). The resulting dispersion was sonicated using a probe sonicator (Sonics & Materials, Inc., US) at 500 W and an amplitude of 25% for 180 s (30 s: ON and 10 s: OFF). Thereafter, the organic solvent was removed under reduced pressure using a rotary evaporator (Buchi Rotavapor®, USA) and the nanoparticles were separated using Sorvall™ Ultracentrifuge (Thermo Scientific, Waltham, USA) at 20,000 rpm for 20 min. The pellet of QS-DS-SLN obtained after centrifugation was freeze-dried using FreeZone Triad Benchtop Freeze Dryer (Labconco, USA). Briefly, pellet was redispersed in 10% w/v aqueous solution of trehalose: mannitol (1:1 ratio) and stirred to get uniform dispersion. The mixture was then pre-frozen at -80°C for 12 h, vacuum dried from -50°C to 4°C for 19 h at 0.164 mbar thereafter, the temperature was slowly raised to 20°C in 7 h to evaporate traces of moisture. The ramp was kept constant at 0.25°C

The nanoparticles were characterized for particle size, polydispersity index (PDI), and zeta potential using Malvern Nano ZS (Malverns instrument Ltd., UK). % Entrapment efficiency (%EE) and % drug loading (%DL) were determined using HPLC based analytical method as described earlier. Furthermore, the optimised formulation was stored under different stability conditions, for 2 months at 4°C and 1 month at ambient conditions (25±5°C, 60±5%RH) to ensure the storage stability by evaluating for particle size, PDI, and %EE, respectively.

2.4 Characterization of QS-DS-SLN

2.4.1 Particle size, Polydispersity Index (PDI), and zeta potential

The pellet obtained after centrifugation was redispersed and appropriately diluted using Milli Q water. Nanodispersion was analysed for particle size, PDI, and zeta potential using Malvern Nano ZS (Malverns instrument Ltd., UK) at 25^{o}C.

2.4.2 % Entrapment Efficiency and % Drug Loading

The supernatant obtained after centrifugation was diluted appropriately and QS present in the supernatant was analysed by HPLC. % Entrapment efficiency and drug loading of QS loaded lipid nanoparticles were calculated using equations 3.6 and 3.7 respectively.

$$\%\ \text{entrapment efficiency} = \frac{\text{Total amount of drug added} - \text{amount of drug in supernatant}}{\text{Total amount of drug added}} \times 100 \quad (3.6)$$

$$\%\ \text{drug loading} = \frac{\text{Weight of drug in nanoparticle}}{\text{Total weight of nanoparticles}} \text{ x } 100 \quad (3.7)$$

2.4.3 Field-emission Scanning Electron Microscopy (FESEM)

Scanning electron microscopic images were taken to study morphological behaviours like aggregation and surface sphericity. Briefly, nanoparticles obtained after centrifugation were placed onto the carbon tape attached to metal stub and gold-coated using Quorum Technologies Q150TES sputter coater (East Sussex, England). Gold-coated nanoparticles were then analysed by FEI™ scanning electron microscope (Hilsboro, Washington) at 20KV high vacuum, 25000X magnification, and scale of 1-3 µm.

2.4.4 Differential Scanning Calorimetry

Differential Scanning Calorimetry (DSC) was performed by adding 10.0 mg of sample in a hermetically sealed aluminum pan. An empty aluminum pan was used as a reference. DSC thermogram of QS, docusate sodium, precirol, QS-DS complex, and QS-DS-SLN was obtained using DSC-60 Plus (Shimadzu, Japan) by supplying constant heating of 10ºC/min between 30-300ºC under inert atmosphere maintained by purging nitrogen gas at a flow rate of 100 mL/min.

2.4.5 Fourier Transform Infrared Spectroscopy

Fourier Transform Infrared Spectroscopy (FTIR) of QS-DS ionic complex was carried out to study the interaction between QS and DS. The spectra of QS, DS and QS-DS ionic complex were obtained using Bruker alpha-one FTIR spectrophotometer (Bruker Optik, Germany) after placing individual sample (about 10 mg) on ZnSe sample crystal and scanning the spectra from 3800- 600 cm^{-1}.

2.4.5 X-ray Diffraction

X-ray Diffraction (XRD) patterns were recorded at room temperature using an X-ray diffractometer (Rigaku Miniflex II, Tokyo, Japan), with nickel filtered Cu K radiation operated at a voltage of 3 kV, 5 mA current, 4°/min scanning speed, and 5–40° 2θ range. PXRD diffraction patterns were recorded for pure drug, QS-DS physical mixture, QS-DS complex and QS-DS-SLNs. The SLNs were dried at room temperature for removing water before PXRD studies.

2.5 *In vitro* drug release

The *in vitro* release profile of QS-DS-SLN was determined by using Franz diffusion cell as reported previously with some modifications (Bonferoni et al., 1999). The nanodispersion of QS loaded lipid nanoparticles obtained after centrifugation (equivalent to 1 mg of QS) was placed in donor compartment of Franz diffusion cell separated by SnakeSkin™ dialysis membrane (M.W.CO. 3.5Da) (ThermoFisher Scientific, USA) from acceptor compartment. The acceptor compartment was filled with 5.0 mL of phosphate-buffered saline of pH 7.4 maintained at 40°C and stirred at 200 rpm. At predetermined time points, 500µL of sample was withdrawn from the sampling arm and replaced with an equivalent quantity of PBS. The above aliquots were analysed by HPLC to determine the amount of QS released.

2.6 Effect of ionic strength and physiological media on the stability of nanoparticles

To determine stability of nanoparticles in various physiological media, nanoparticle dispersion was incubated with normal saline (0.9% w/v NaCl), 0.05M $CaCl_2$, phosphate-buffered saline (PBS) of pH 7.4, 5% w/v dextrose, and foetal bovine serum (1:1 with PBS) in the ratio of 1:1 at 37 ± 0.5°C. The stability of QS-DS-SLN was evaluated by determining the change of the particle size following incubation in different media for 6 h.

Milli-Q system (Millipore GmbH, Germany). The solvents and buffers prepared were suitably filtered through 0.22µ Millipore™ membrane filter (Merck, Darmstadt, Germany) and suitably degassed in an ultrasonic bath for 30 min. All other chemicals, solvents, and reagents utilized, were either HPLC or analytical grade.

2.7 Hemocompatibility studies

2.7.1 Haemolysis

Haemolytic effect of quinapyramine sulphate and QS-DS-SLN was studied as reported previously, with some modifications (K.S. et al., 2017). Fresh blood (1.0 mL) was withdrawn from healthy Wistar rats by retroorbital puncture and red blood cells (RBCs) were separated by centrifuging at 1200 rpm for 5 min in Eppendorf containing EDTA solution (10%w/v). After centrifugation, RBCs were collected and washed twice with normal saline and diluted in a fresh 1.5 mL Eppendorf, 50 µL of diluted RBC pellet was incubated with different concentrations including 0.5, 10, 15, 20 and 50 µg/mL of quinapyramine sulphate (free drug), blank solid lipid nanoparticles (without drug) and QS-DS-SLN (quinapyramine sulphate equivalent to 0.5, 10, 15, 20 and 50 µg/mL) at 37°C for 30 min. Distilled water and normal saline were used as a positive and negative control, respectively. After 30 mins of incubation, the above dispersion was diluted up to 1.0 mL with normal saline and centrifuged at 1200 rpm for 5 min. The supernatant (200 µL) was analysed using Epoch Elisa plate reader (BioTek U.S., Winooskii) at 540 nm and, % haemolysis was calculated using equation 3.8.

$$\%\ \text{Hemolysis} = \frac{\text{OD of sample} - \text{OD of negative control}}{\text{OD of positive control} - \text{OD of negative control}} \text{x}100 \qquad (3.8)$$

2.7.2 Red Blood Cells (RBC), White blood cells (WBC) and platelet aggregation studies

RBC (50µL) were treated and incubated with blank nanocarrier (without drug) or QS-DS-SLN (20µg/mL) at 37ºC for 30 min. Thereafter, RBCs were separated by centrifugation and fixed using 2.5%v/v glutaraldehyde. Aliquot of the sample was placed on a coverslip, washed with normal saline and dehydrated using 50%, 70%, 90% and 100% ethanol and allowed to air dry. Samples were mounted on metal stubs and attached with carbon tape for gold coating using Quorum Technologies Q150TES sputter coater (East Sussex, England). Gold coated slides were then analysed by FEI™ scanning electron microscope (Hilsboro, Washington) at 20 x KV high vacuum, 5000 x magnification.

Platelets and WBCs were separated using Ficoll-Paque® Plus density gradient method as described by manufacturer (Seeligmüller, 2016). Briefly, rat blood was diluted with normal saline (1:1 ratio) was layered on 3 mL Ficoll-Paque Plus and centrifuged at 400g for 30min. Different layers were separated carefully to collect platelets and WBC. 50µL of platelet or WBC suspension was treated with blank nanocarriers (without drug) or QS-DS-SLN (quinapyramine sulphate equivalent to 20 µg/mL) for 1h at 37ºC. Normal saline and

polyethylenimine (PEI) were kept as a negative and positive control, respectively. Aliquots of the sample were loaded onto the coverslip and FESEM analysis was performed the same as described earlier for RBC.

2.8 Cytotoxicity and cellular uptake studies

2.8.1 Maintenance of cell line

THP-1 cells were suspended in RPMI-1640 media enriched with 10 %w/v foetal bovine serum (FBS) and 0.002% v/v of Gentamicin solution in a culture flask and incubated at 37ºC and 5% CO_2 for 15 days, and culture media was changed at regular intervals when required.

2.8.2 Cytotoxicity

The cytotoxicity of quinapyramine sulphate and QS-DS-SLN was determined using THP-1 monocyte-macrophage cell lines by MTT assay. THP-1 cells were seeded in 96 well plate at a density of $5x10^4$ cells per well in 100µL of RPMI 1640 cell culture medium enriched with 10%v/v FBS containing Phorbol 12-myristate 13-acetate (PMA) (0.1 ng/mL) for 48h in an incubator at 37ºC and 5% CO_2. Thereafter, the media was removed, and cells were incubated with free quinapyramine sulphate or QS-DS-SLN equivalent to different concentration of quinapyramine sulphate including1.56, 3.12, 6.25, 12.5, 50, 100 and 200 µM for 24 h. After 24h of incubation, the supernatant was removed and cells were washed with phosphate buffered saline (PBS). Thereafter, cells were treated with 100µL of MTT reagent (500 µg/mL) and incubated in an incubator at 37ºC and 5% CO_2 for 4 h. After 4 h of incubation, the MTT reagent was removed, 100 µL of DMSO was added and kept on horizontal shaker for 2 h to dissolve formazan crystals.

Thereafter, absorbance of the plate was measured at 570 nm using Epoch Elisa plate reader (BioTek U.S., Winooskii), and the %cell viability was estimated using equation 3.9 where, the wells with THP-1 cells without any treatment group represents control (100% viable) and the wells without cells but having treatment as that of sample are considered as a blank, respectively.

$$\%\ \text{Cell viability} = \frac{\text{Absorbance of sample} - \text{Absorbance of blank}}{\text{Absorbance of control} - \text{Absorbance of blank}} \text{x} 100 \qquad (3.9)$$

2.8.3 Cellular uptake

Coumarin-6 (C6) loaded SLN were used as a surrogate to study time-dependent qualitative and quantitative cellular uptake of nanoparticles in THP-1 monocyte-macrophage cell lines. In a 6-well cell culture plate, cells were seeded at a density of $1x10^5$ cells per well with RPMI 1640 containing PMA (0.1 ng/mL) for 48h in an incubator at 37ºC and 5% CO_2.

2.8.3.1 Confocal laser scanning microscopy (CLSM)

Briefly, cells were treated with free C6 (50 nM) or C6 SLNs (equivalent to 50 nM) for 1, 3 and 6h. After incubation, cells were fixed with 2%w/v paraformaldehyde (PFA) for 5min. Thereafter, cells were washed to remove PFA and counter-stained with DAPI (1µg/mL) and observed under a 40x oil immersion lens in CLSM.

2.8.3.2 Flow Cytometry

THP-1 cells were treated with C6 or C6 SLNs and incubated for 1, 3 and 6h in an incubator at 37ºC and 5% CO_2. After incubation, cells were washed in PBS, trypsinized, centrifuged, and the pellet was resuspended with 0.5 mL PBS and sample was analysed using FACS (Cytoflex, Beckman Coulter, USA) at an excitation and fluorescence wavelength of 488 and 525 nm, respectively. The data was analysed using CytExpert® software.

2.8.3.3 Cellular uptake mechanism

Cellular uptake mechanism of nanoparticles was studied by incubating THP-1 cells with different endocytic pathway inhibitors. Briefly, THP-1 cells were incubated with Methyl-β-cyclodextrin (M-β-CD; 20mM), nystatin (NST; 150µM), chlorpromazine (CPZ; 10µg/mL) and amiloride (AMD; 10mM) for 1 h. After 1h of incubation, the supernatant was removed and cells were washed with PBS. Subsequently, cells were treated with C6 SLN and incubated for 6h. After 6h of incubation, samples were analysed by FACS and CLSM.

2.9 Scale up of QS-DS-SLN

In order to cope with the increasing demands of production and to reduce the cost of multiple batches, it is extremely important to enhance the scale of production (Colby et al., 2021). Moreover, the translation of the lab scale to a large manufacturing scale is a challenging task for skilled personnel (Block, 2005; Kumar et al., 2022; Muthu and Wilson, 2012). The

scientific manufacturing process involving homogenous or heterogeneous systems utilizes a number of scale-up parameters while designing large-scale production. The skilled person involved in designing the scale-up process has to consider various parameters across scales prior to the actual execution of the process (Hernández K, Rodríguez R, Gutiérrez C, Peñuñuri O, Zavala P, Guerrero P, 2020).

Considering the target animal population i.e., camels, in the treatment of *T. evansi*, production of larger dosages becomes challenging. In order to meet the higher dosing requirements, the developed lab scale nanoformulation was scaled-up. For instance, the use of scientific geometric similarity principle was adopted to design 20-times of lab scale batch to attain similar characteristics in terms of particle size, PDI, and other physicochemical properties equivalent to lab-scale.

2.9.1 Methodology and scale-up parameter calculations of QS-DS-SLN

Preparation of pilot-scale QS-DS-SLN

The pilot-scale batch (20 times of lab-scale) of QS-DS-SLN was prepared by the method used for the preparation of lab-scale batches. Briefly, the aqueous phase was prepared by dissolving QS (100.0 mg) and polyvinyl alcohol (1% w/v) in 200.0 mL of Milli Q water. The organic phase was prepared by dissolving docusate sodium (180.0 mg) and precirol (400.0. mg) in 80.0 mL of dichloromethane. Initially, 40.0 mL of the organic phase was added dropwise into the aqueous phase under constant stirring using 50.0 mL of syringe mounted onto stand and clamp assembly. The resulting dispersion was sonicated using a probe for 150 sec at 25% amplitude and 500 watts (30 sec: ON, 10 sec: OFF). Thereafter, the remaining 40.0 mL of the organic phase was added in the aqueous phase and probe sonicated as stated above. The resulting aqueous dispersion was then subjected to removal of the organic phase by using a round bottom flask at 30°C under reduced pressure using a rotary evaporator and subsequently centrifuged at 15,000 rpm for 25 min using Sorvall™ Ultracentrifuge.

To overcome scale-up effects and simulate lab-scale and pilot-scale batches, rotational speed was calculated using various approaches based on geometric similarity approach, scale of agitation, and dimensionless number approach. Nanoparticles were characterized for physicochemical evaluation like particle size and entrapment efficiency.

Calculation of rotational speed for the production of pilot-scale batch

The geometric similarity approach was used to calculate rotational speed during pilot-scale batches. The diameter of impeller/ magnetic bead (D), the internal diameter of vessel (T), working height of vessel i.e. height of the liquid in vessel (Z) are presented in Table 3.1. Whereas, $^{D}/_{T}$ and $^{Z}/_{T}$ ratios were calculated (Table 3.1). Following strategies were adopted for calculation of rotational speed for pilot scale batch as described earlier with some modifications (Sidney H Wiling and Levin, 2003).

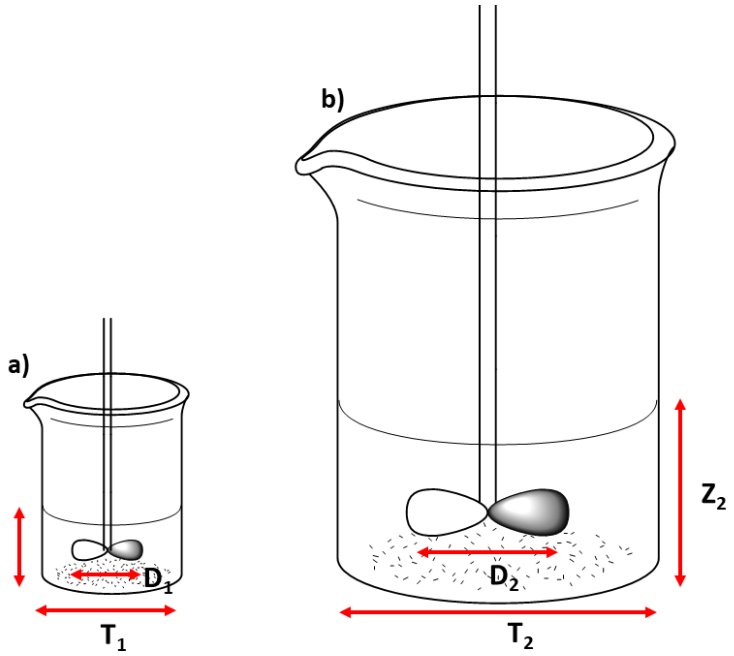

Fig. 3.1 Representation of a) lab-scale and b) pilot-scale equipment used during production of QS-DS-SLN

Table 3.1: Geometric parameters of glass apparatus and instruments

Parameters	**Lab-scale batch**	**Pilot-scale batch**
Diameter of impeller (D) (cm)	2.06	4.15
Diameter of tank/ vessel (T) (cm)	3.10	7.83
Height of liquid in vessel (Z) (cm)	1.92	5.91
$^{D}/_{T}$	0.64	0.53
$^{Z}/_{T}$	0.61	0.75
Volume of round bottom flask (mL)	50.0	1000.0
Probe diameter (mm)	3.0	13.0

A. Scale of agitation approach

Scale of agitation approach is based upon equal liquid motion principle during the preparation of nanoparticles at lab and pilot scale. Equal liquid motion was confirmed by maintaining equal bulk fluid velocity across the scales (Sidney H Wiling and Levin, 2003). Dimensions of vessels and impeller, physical properties of liquid such as density and viscosity were considered during the preparation of pilot-scale batch using scale of agitation approach. Rotational speed (N) was determined by calculating terminal pumping number (N_Q), effective pumping capacity (Q), bulk fluid velocity (V_b) and cross-sectional area (A) of the vessel (Table 3.6).

B. Dimensionless number approach

Froude number (combines the inertial and gravitational forces) was determined using equation 3.11 to calculate the rotational speed for the pilot batch.

$$N_{Fr} = \frac{DN^2}{g} \tag{3.11}$$

Where, D is the diameter of the impeller

N is the rotational speed of the impeller and

g is acceleration due to gravity

C. Equal mixing parameters approach

Rotational speed was calculated based on the different considerations namely 1) equal blending time, 2) equal surface motion and 3) equal % of solids under equal liquid motion and calculated using the following equation -

$$R = \frac{T_2}{T_1} \tag{3.12}$$

$$N_2 = N_1(1/R)^n \tag{3.13}$$

Where, R is geometric scaling factor and T_2, T_1 are diameters of vessel and N_2 and N_1 are rotational speed used in pilot-scale and lab-scale respectively. In equation 3.13 value of "n" was calculated based upon physical interpretation as stated in Table 3.2.

Table 3.2: Calculation of rotational speed for lab-and pilot scale batches using scale of agitation approach

Parameters (Unit)	Equation	Lab-scale batch	Pilot-scale batch
Terminal pumping number (N_Q)	$N_Q = 1.1283 - 1.07118\ (^{D}/_{T})$	0.443	0.561
Cross-sectional area of tank (A) (cm^2)	$A = \frac{\pi T^2}{4}$	7.554	48.175
Effective pumping capacity (Q) (cm^3/sec)	$Q = N_Q * N * D^3$	45.163	288.423
Bulk fluid velocity (V_b) (cm/sec)	$V_b = \frac{Q}{A}$	5.987	5.987
Impeller speed (rpm)	-	700	430

2.10 *In vitro* antitrypanosomal efficacy studies

2.10.1 Trypanotoxicity assay

In vitro trypanocidal effect of quinapyramine sulphate and QS-DS-SLN was studied against *T. evansi* parasite using Alamar Blue assay method as described previously with some modifications (Juan et al., 2013; Räz et al., 1997). *T. evansi* parasites were freshly collected from the infected mice by cardiac puncture, was harvested and added into the 96-well plate (50µL) at an initial density of 10^4 parasite/well in phosphate buffered saline with 10mM glucose (PSG). Thereafter, the parasites were treated with quinapyramine sulphate or QS-DS-SLN at quinapyramine sulphate concentration of 0.05, 0.5, 5, 10, 50, and 100µM for 20h in an incubator at 37ºC and 5% CO_2. 20µl of 0.5mM sodium resarzurin dye was added to the above plate and incubated for 4h. Thereafter, 50µl of 3%w/v sodium lauryl sulphate was added to seize the reaction. Samples were analysed using Epoch Elisa plate reader at 535 nm and 590 nm excitation and emission wavelengths, respectively. %Viability of trypanosomes were calculated using equation 3.10.

$$\%\ \text{viability of trypanosome} = \frac{\text{Absorbance of sample} - \text{Absorbance of blank}}{\text{Absorbance of control} - \text{Absorbance of blank}} \text{x} 100 \qquad (3.10)$$

2.10.2 Assessment of morphological changes in *T. evansi* parasite

2.10.2.1 *Confocal laser scanning microscopy*

T. evansi parasites were treated with quinapyramine sulphate or QS-DS-SLN at quinapyramine sulphate concentration of 0.25, 0.5 and 5µM in 2.0mL of Eppendorf tube and incubated at 37ºC

and 5% CO_2 in an incubator for 24h. After incubation, parasites were separated by centrifugation at 3000 rpm for 7min and resuspended in 1.0mL of PBSG. Thereafter, 10µL of MitoTracker Red CMXRos (80nM) was added and incubated at room temperature for 30 min. Thereafter, the parasites were separated by centrifugation, resuspended, and fixed using 4%w/v PFA. 40µL of the above trypanosome suspension was placed on a glass slide precoated with poly-l-lysine solution and air dried. Thereafter, the slide was washed with PBS and stained with DAPI (1µg/mL). The samples were analysed using CLSM at 63x oil immersion lens.

2.10.2.2 *Field-emission high-resolution scanning electron microscopy*

Localization of the nanoparticles onto the *T. evansi* parasite were studied by FESEM (Arias et al., 2015). Approximately 10^5 parasites were incubated with QS-DS-SLN (0.25 or 0.5 µM) for 30 min at 37ºC. After 30 min of incubation, it was centrifuged and resuspended in 0.5mL of PBS and 200µL of 2.5%v/v glutaraldehyde solution was added and incubated at 4°C for 24 h. 50µL of samples was then mounted onto poly-L-lysine coated slides and incubated at 4°C for 6 h followed by air drying at room temperature. Thereafter, samples were dehydrated using varying concentrations of ethanol including 50%, 70%, 90%, and 100% at room temperature. Slides were mounted on metal stubs and attached with carbon tape for chromium coating using Quorum Technologies Q150TES sputter coater (East Sussex, England). Chromium coated slides were then analysed by FEI™ scanning electron microscope (Hilsboro, Washington) at 20 x KV high vacuum, 20000 x magnification.

2.11 Pharmacokinetic study

The study protocol was approved by the Institutional Animal Ethics Committee of Birla Institute of Technology and Science, Pilani campus, Pilani, with Protocol no.: IAEC/RES/31/16. Female Wistar rats weighing 290.0±40.0g were acclimatized for a week on a regular 12 h light-dark cycle, housed in a well-ventilated cage with access to food and water ad libitum. The animals were divided into two different groups (n=4) such as free QS in water (I), and QS-DS-SLN at a dose of 7.5 mg/kg body weight.

300 µl of blood was collected from retro-orbital plexus of rat at pre-determined time points including 0, 1, 3, 6, 12, 24, 36, 48, 72, and 120 h in an Eppendorf centrifuge tube containing 10% w/v EDTA solution. Plasma was separated from the blood by centrifugation at 7000 rpm for 10 minutes using REMI cooling centrifuge and stored at -20ºC until further use. QS was analysed by developed and validated RP-HPLC method of analysis. Further, the

pharmacokinetic parameters were calculated by non-compartmental analysis using WiNonlin software version 6.3.

2.12 *In-vivo* antitrypanosomal efficacy in *T. evansi* infected mouse model

Total 35 Swiss albino mice (25-30g) of either sex was used for the antitrypanosomal efficacy study. *T. evansi* initially isolated from the infected camel was maintained in Swiss albino mice by intraperitoneal inoculation of approximately 1×10^3 viable *trypanosome* suspension in PSG. Infection was confirmed by the observation of blood smear for the presence of *T. evansi* parasite and the level of parasitaemia was monitored by using matching method described earlier with some modification (Herbert and Lumsden, 1976). The *in vivo* experimental protocol were approved by the Institutional Animal Ethics Committee of National Research Centre on Camel, Bikaner (NRCC/PSME/6/(141)2000-Tech). The animals were maintained at ICAR-NRCC, and provided with laboratory cooked wheat dalia in camel milk and water *ad libitum*. Those mice which showed parasitemia after 2-3 days of inoculation were considered as infected and divided into 7 different groups of 5 animals and treatment was given by subcutaneous route. Prior to the administration of the treatment, an aqueous solution of lyophilized nanoformulation was treated with UV light for sterilization whereas, the free drug solution was filtered aseptically using membrane filter.

Group I vehicle control (0.2mL normal saline solution), group II free quinapyramine sulphate (2.5mg/kg), group III free quinapyramine sulphate (5.0mg/kg), group IV free quinapyramine sulphate (7.5mg/kg), group V QS-DS-SLN (2.5mg/kg), group VI QS-DS-SLN (5.0mg/kg) and group VII QS-DS-SLN (7.5mg/kg). After the treatment, approximately 2µL of blood was withdrawn from each animal from the tail vein and evaluated for the presence of parasites twice a week for 60 days (Herbert and Lumsden, 1976). The efficacy of the treatment was assessed by observation for the presence of parasite and the survival rate of the animal as compared to the control group. At the end of 60 days post treatment blood and organs were collected in group VII and were processed for further presence or absence of parasite residues which was confirmed by polymerase chain reaction (PCR) assay method.

2.12.1 Extraction of DNA from Blood and organs

Infected mice and parasitologically negative mice (post treatment with 7.5 mg/kg of QS-DS-SLN) were sacrificed, dissected and organs, viz. spleen, liver, kidney, lungs and brain were collected and processed for extraction of DNA using blood DNA extraction kit spin-column

(Thermo-fisher, USA), following the manufacturer's instructions. The concentration of DNA in 1 µg/mL was measured at 260 and 280 nm by ultra-violet spectrophotometer and then diluted to 50 ng/µL and was stored at -20°C for later use for PCR. The quality and integrity of the DNA were checked by ethidium bromide stained 0.8% TAE – agarose gel.

Primer Selection in PCR assay was carried out targeting internal transcribed spacer (ITS) region of rDNA using the primers Kin1, 5'- GCG TTC AAA GAT TGG GCA AT-3' (reverse) from the 5.8S gene and Kin2, 5'- CGC CCG AAA GTT CAC C -3' (forward) near the end of the 18S gene (Desquesnes et al., 2001).

2.12.2 DNA Amplification and Detection

PCR amplification reaction was performed in a total reaction volume of 50µl containing, 5X GoTaq® Colored reaction Mix, (Promega Co. USA) 2 mM $MgCl_2$, 200 µM of each of the four deoxynucleoside triphosphates (dNTPs), primers at 1 µM and 1.25 U of *Taq* DNA polymerase (GoTaq®, Promega Co. USA).The PCR amplification was performed as an initial cycle at 94ºC for 4 min and then 35 cycles of denaturation at 94ºC for 15 sec, annealing at 52ºC for 45 sec and extension at 72°C for 1 min and finally one cycle at 72ºC for 10 min. The PCR products were then electrophoresed on a 1.0 % agarose gel containing ethidium bromide (0.5 g/mL) and the image of the amplified DNA was captured using a gel documentation system (Alpha imager, USA) as evident in the ethidium bromide-stained gels, compared with the molecular size marker (O'GeneRuler 100 bp DNA Ladder, Thermo Scientific, USA).

3. Results and discussion

3.1 Screening of lipids based on solubility parameters

Drug loading into nanoparticles is the result of the affinity of the cargo with the matrix material. Thermodynamic parameters including total solubility parameter and polarity are used as a measure of the affinity of two molecules. Therefore, these parameters were used to screen various lipids to enable maximum loading of ionically complexed QS into lipid carriers. Table 3.3 represents the partial solubility parameter, total solubility parameter and polarity of different lipids and QS-DS complex.

The total solubility parameter comprises three components that represent intra-atomic or intermolecular forces and is a measure of cohesive energy between two substances. Cohesive energy is the amount of energy required to separate atoms or molecules of the substances to an infinite distance (Taylor et al., 1987).

The total solubility parameter is the combinatorial effect of dispersion, polar and hydrogen bond forces. In general, dispersion forces are the result of presence of alkyl groups (-CH_3, -CH_2 and >CH<) in the chemical structure of the molecule whereas, polar groups such as -OH, -COOH, -O- and –COO are responsible for interaction between molecules due to formation of hydrogen bond or presence of polar forces.(Kitak and Dumiˇ, 2015) The polarity decides the hydrophilic or hydrophobic nature of the molecule. For instance, QS exhibited highest polarity value (0.367), indicating the hydrophilic nature of the drug whereas, the QS-DS complex had reduced polarity of 0.226 indicating significant decrease in hydrophillicity of the QS.

Table 2 represents the difference between total solubility parameter and polarity between QS-DS complex and various lipids. Generally smaller the values of $\Delta\delta_{total}$ and ΔP greater are the affinity between two mixing components. As $\Delta\delta_{total}$ and ΔP value between QS-DS complex and three lipids mainly glyceryl tripalmitostearate, glyceryl tristearate and glyceryl tripalmitate and were found to be minimum, these lipids were considered suitable for loading of QS-DS complex. Precirol is a mixture of 8-22% mono-, 40-60% di-, and 25-35% triglycerides of palmitic acid and stearic acid, fatty acids other than palmitic acid and stearic acid account for less than 10%. Therefore, considering the $\Delta\delta_{total}$ and ΔP values of different lipids and composition of precirol, it was concluded that precirol could be suitable lipid carrier. Although glyceryl tribehenate showed minimum ΔP value, it presents in small proportion (35%) of compritol ATO (other component includes 15% mono and 50% diglycerides of behenic acid).

Table 3.3: Partial solubility parameters, total solubility parameter and polarity of various lipids and QS-DS complex

Compound	Chemical formula	δ_d	δ_p	δ_h	δ_{total}	Polarity
Quinapyramine sulphate	$C_{19}H_{28}N_6O_8S_2$	11.138	2.421	8.123	13.966	0.367
DCM	CH_2Cl_2	18.253	12.134	3.533	22.201	0.324
Docusate sodium	$C_{20}H_{37}NaO_7S$	15.476	2.358	7.261	17.257	0.196
Palmitic acid	$CH_3(CH_2)_{12}COOH$	16.458	1.461	5.899	17.544	0.120
Stearic acid	$CH_3(CH_2)_{16}COOH$	16.489	1.314	5.594	17.462	0.109
Glyceryl monostearate	$CH_3(CH_2)_{16}COOCHOHCH_2OH$	17.125	2.077	11.421	20.688	0.314
Glyceryl distearate	$[CH_3(CH_2)_{16}COOCH_2]_2CHOH$	16.818	1.213	7.181	18.327	0.158
Glyceryl tristearate	$CH_3(CH_2)_{16}COOCH_2]_3CH$	16.703	0.885	4.681	17.369	0.075
Glyceryl monopalmitate	$CH_3(CH_2)_{15}COOCHOHCH_2OH$	17.141	2.174	11.685	20.859	0.325
Glyceryl dipalmitate	$[CH_3(CH_2)_{15}COOCH_2]_2CHOH$	16.886	1.404	9.206	19.284	0.233
Glyceryl tripalmitate	$[CH_3(CH_2)_{15}COOCH_2]_3CH$	16.700	0.932	4.803	17.402	0.079
Glyceryl monopalmitosterate	-	17.133	1.502	11.551	20.718	0.316
Glyceryl dipalmitosterate	-	16.820	0.879	7.270	18.345	0.160
Glyceryl tripalmitosterate	-	16.701	0.642	4.741	17.317	0.075

Glyceryl monobehenate	$CH_3(CH_2)_{20}COOCH_2CHOHCH_2OH$	17.071	1.762	10.520	20.129	0.281
Glyceryl dibehenate	$[CH_3(CH_2)_{20}COOCH_2]_2CHOH$	16.810	1.015	6.568	18.076	0.135
Glyceryl tribehenate	$[CH_3(CH_2)_{20}COOCH_2]_3CH$	16.714	0.737	4.270	17.627	0.063
QS-DS. complex (1:2mole)	-	14.160	1.374	7.535	16.098	0.226

Table 3.4: The difference of partial solubility parameters, total solubility parameter and polarity between various lipids and QS-DS complex

Compound	$\Delta\delta_d$	$\Delta\delta_p$	$\Delta\delta_h$	$\Delta\delta_{total}$	**ΔPolarity**
Palmitic acid	2.298	0.087	-1.636	1.446	-0.106
Stearic acid	2.329	-0.060	-1.941	1.364	-0.117
Glyceryl monostearate	2.965	0.703	3.886	4.590	0.088
Glyceryl distearate	2.658	-0.161	-0.354	2.229	-0.068
Glyceryl tristearate	2.543	-0.489	-2.854	1.271	-0.151
Glyceryl monopalmitate	2.981	0.800	4.150	4.761	0.099
Glyceryl dipalmitate	2.726	0.030	1.671	3.186	0.007
Glyceryl tripalmitate	2.540	-0.442	-2.732	1.304	-0.147
Glyceryl monopalmitosterate	2.973	0.128	4.016	4.620	0.090
Glyceryl dipalmitosterate	2.660	-0.495	-0.265	2.247	-0.066
Glyceryl tripalmitosterate	2.541	-0.732	-2.794	1.219	-0.151
Glyceryl monobehenate	2.911	0.388	2.985	4.031	0.055
Glyceryl dibehenate	2.650	-0.359	-0.967	1.978	-0.091
Glyceryl tribehenate	2.554	-0.637	-3.265	1.529	-0.163

3.2 Screening of complexing agent

QS is a positively charged divalent basic compound which is freely soluble in water. To enhance the drug loading of such a hydrophilic compound in hydrophobic lipid core, different anionic agents were screened to form water insoluble complex by electrostatic interaction. To characterize the extent of hydrophobic nature exhibited by ionically complexed QS solubility of ionically complexed QS in 1-octanol was determined (Fig.3.2(a)). Solubility of QS-anionic complex in 1-octanol was found to be in order of docusate sodium > sodium tripolyphosphate> sodium alginate > sodium carboxy methylcellulose (CMC). In general, higher the solubility of ionically complexed QS in 1-octanol more the hydrophobic nature of complex. QS-DS complex at molar ratio of 1:2 showed maximum complexation efficiency than at any other molar ratio owing to monovalent nature of docusate sodium and divalent nature of QS. It is prevalent from data that as molar ratio increases from 1:2 to 1:4, almost 4-fold decrease in

complexation occurred probably due to micelle formation exhibited by anionic surfactant which might have solubilized the hydrophobic QS-DS complex in it.

3.3 Characterization of QS-DS complex using FTIR

Fig. 3.2(b) depicts FTIR spectra of QS, DS, QS-DS complex. In FTIR spectra of QS, peaks at 3846 cm^{-1}, 3743 cm^{-1} and shoulder at 3618 cm^{-1} corresponds to N-H stretch and overtone due to N-H bending vibrations of primary amine. FTIR spectra of DS depicted sharp S=O stretch at 1461 cm^{-1} and ketone carbonyl stretch at 1728 cm^{-1}. Whereas, FTIR spectra of QS-DS complex revealed absence of two N-H stretches at 3846 and 3743 $cm^{-1}$and presence of strong, broad peak around 2925 cm-^{1} probably due to formation of amine salt by electrostatic interaction between QS and DS.

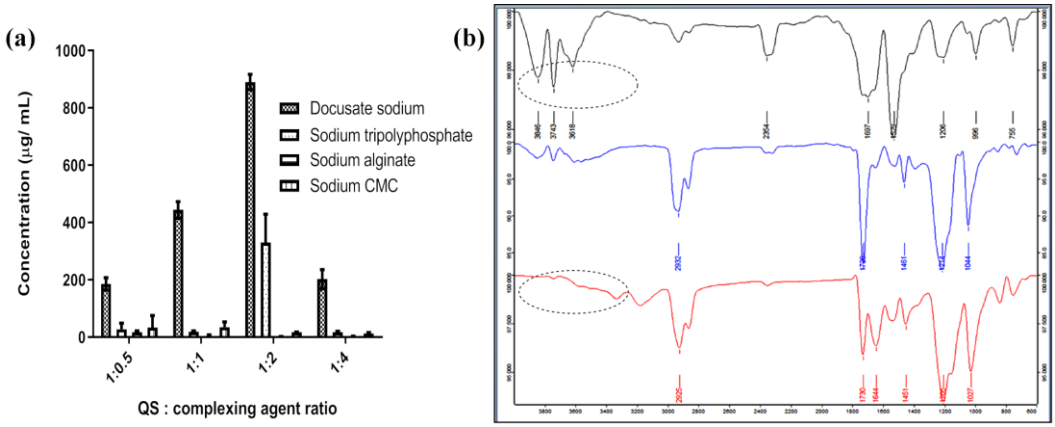

Fig. 3.2. Characterization of QS-DS complex (a) Screening of complexing agent and (b) FTIR spectra of QS, DS and QS-DS ionic complex

3.4 Development of lab scale QS-DS-SLN

Effect of amount and type of lipids, and amount of drug on particle size and % entrapment efficiency of QS-DS-SLN are presented in Table 3.5. The type and amount of lipid used during preparation of nanoparticles showed significant impact on particle size. When amount of precirol was reduced from 50.0 mg to 20.0 mg almost 1.4-fold decrease in particle size was observed (Table 3.5). Drug: lipid ratio was kept constant in all formulations. Moreover, significantly low % EE (13.21±7.23%) was observed, when DS was not used in formulation. Particle size evaluation by zetasizer is presented in Fig. 3.3(c).

The mechanism of high entrapment of hydrophilic drug QS in hydrophobic environment could be attributed to instantaneous formation of hydrophobic complex between QS and DS by electrostatic interaction between negatively charged sulphonyl group of DS and positively charged amino nitrogen group present on QS. The addition of lipid and DS in the organic phase

to the aqueous phase consisting of drug and surfactant resulted in the formation of emulsion and subsequent evaporation of the solvent resulted in nano-precipitation of the lipid entrapped QS-DS complex.

Furthermore, theoretical considerations adopted during screening of lipids can be used in conjunction with experimentally determined values for scientific justification of obtained results. Table 3.3 depicts polarity of various lipids used for screening of the cargo matrix for loading of QS-DS complex. Although ionic complexation of QS with DS has shown significant reduction in hydrophillicity, the polarity value of 0.226 still suggests sufficient retention of hydrophillicity of molecule. Amongst various lipids screened during manufacturing of QS-DS-SLN, precirol has accounted for maximum drug loading along with persistently lower particle size.

3.5 Characterization of QS-DS SLN

3.5.1 DSC

The DSC thermograms of QS, DS, precirol, QS-DS complex and QS-DS-SLN are shown in Fig. 3.3a. Thermogram of QS revealed melting endotherm at 253ºC, corresponding to melting point of drug. Furthermore, QS-DS complex showed sharp endotherm at 153 ºC, probably due to the cleavage of ionic bond between appositively charged QS and DS corresponding to melting point of DS whereas, a small endothermic peak at 249°C in QS-DS complex represented presence of QS. Furthermore, DSC thermogram of QS-DS-SLN showed presence of precirol at 63°C, DS at 121°Cwhile absence of any sharp peak representing QS, depicting probable amorphization of QS.

Table 3.5: Composition and physicochemical parameters of various QS-DS-SLN batches

Formulation code	**Lipids (mg)**				**Particle size (nm)**	**PDI**	**Zeta potential (mV)**	**% EE**
	Palmitic acid	**GMS**	**Precirol**	**Compritol**				
QS-DS-SLN: Formulation variable; type of lipid*								
QS-PA	50.0	-	-	-	1062±23.0	0.59±0.04	-24.3±6.05	89.79±0.44
QS-GMS	-	50.0	-	-	646.3±35.7	0.33±0.09	-17.3±3.13	85.24±1.28
QS-Prec.	-	-	50.0	-	361.3±30.57	0.27±0.05	-12.8±3.93	86.79±0.63
QS-Comp.	-	-	-	50.0	592.7±56.41	0.31±0.17	-14.6±3.54	86.03±3.86
QS-DS-SLN: Formulation variable; amount of lipid **								
QS-Prec.30	-	-	30.0	-	350.8±25.05	0.25±0.01	-22.53±6.17	84.83±3.75
QS-Prec.20	-	-	20.0	-	250.10±26.04	0.12±0.05	-27.41±4.18	81.26±4.67
QS-Prec.20 (Without DS)	-	-	20.0	-	289.13±19.23	0.16±0.03	-11.0±3.17	13.21±7.23

All formulations contained Polyvinyl alcohol (1% w/v), QS:DS (1:2 molar ratio).

*****QS-10.0 mg and ** 5.0 mg

3.5.2 X-ray Diffraction

Fig. 3.3(b) represents the X-ray diffraction spectra of QS, QS-DS complex and QS-DS-SLN.X-ray diffraction pattern of QS depicts sharp peaks at a diffraction angle (2θ) of 7.40°, 14.42°, 15.84°, 19.54°, 20.33°, 26.43° and 28.83° representing crystalline nature of the drug. XRD spectra of QS-DS physical mixture depicted presence of characteristic peaks corresponding to crystalline nature of drug. On the other hand, QS-DS complex showed absence of sharp peak indicating amorphous nature of QS. Furthermore, XRD spectra of QS-DS-SLN did not showed any peak related to QS, indicating amorphous state of QS in the nanoparticles. To conclude, these results represent that there was no significant crystallization of drug inside the lipid nanocarrier matrix.

3.5.3 Field-emission Scanning Electron Microscopy (FESEM)

Fig. 3.3(d) depicts the SEM image of QS-DS-SLN. QS-DS-SLN were found to be spherical in shape. SEM images reveled lower particle size of QS-DS-SLN than the size obtained from zetasizer. This could be attributed due to the fact that zetasizer determined the hydrodynamic diameter of QS-DS-SLN.

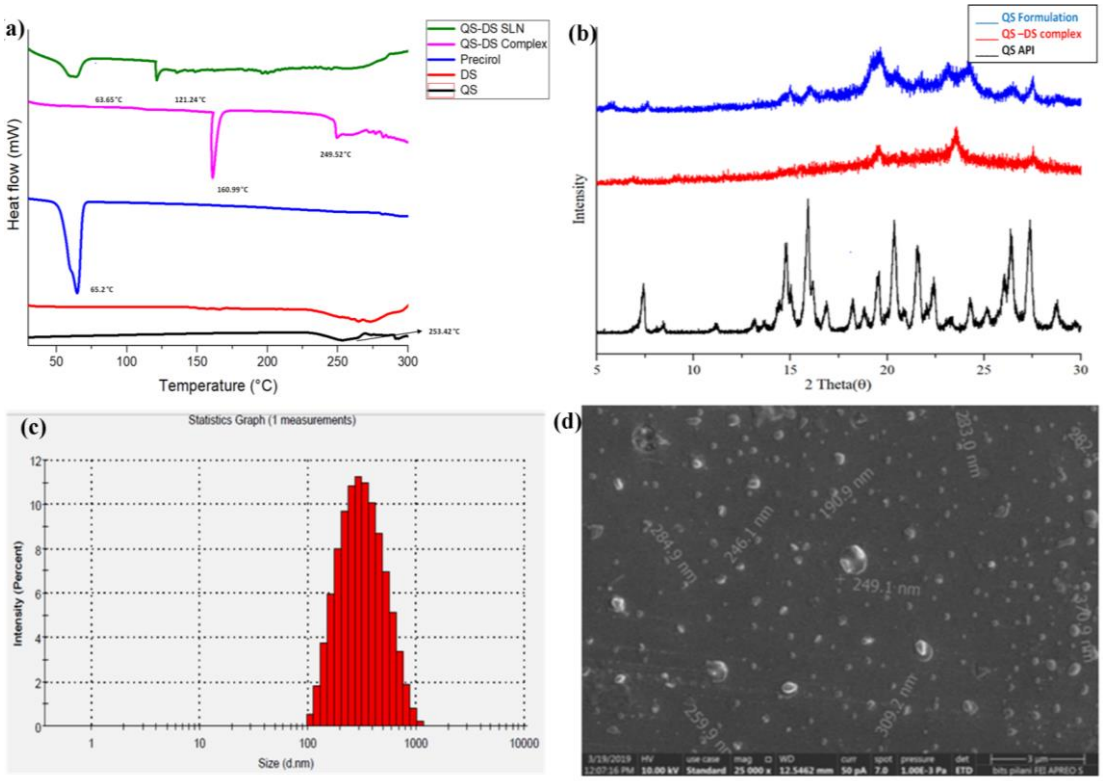

Fig. 3.3. Characterization of QS-DS-SLN (a) DSC thermograms of QS, DS, precirol, QS-DS complex and QS-DS-SLN, (b) XRD spectras of QS, QS-DS complex and QS-DS-SLN, (c) particle size by zetasizer and (d) FESEM image of QS-DS-SLN.

3.6 *In vitro* drug release

The rate and extent of drug release dictates the therapeutic potential of nanoformulations. Release profile of QS and QS-DE SLN are depicted in Fig. 3.4(a). At the end of 12 h, almost 80% of free QS was released while, only 40% QS was found to be released from QS-DS-SLN. Moreover, almost 95% QS was released from QS-DS-SLN at the end of 60 h, suggesting sustained drug release potential of QS-DS-SLN. In chronic parasitic infections like *trypanosomiasis*, sustained release of drug from formulation is desirable to avoid multiple dosing and drug associated side effects. Although, QS is highly water-soluble compound, QS-DS-SLN showed prolonged drug release profile which could be due to the release of QS from QS-DS complex followed by partitioning of QS into the surrounding medium after the diffusion through lipid matrix.

3.7 Stability of QS-DS-SLN in various physiological medias

Due to the ionic and hydrophobic nature of the QS-DS complex in QS-DS-SLN, the stability of the complex was assessed in various physiological media of different ionic strength [Fig. 3.4(b)]. No significant change in particle size was observed with 5% w/v dextrose solution as well as PBS of pH 7.4. Moreover, significant increase in particle size was observed when nanoparticles were incubated with 0.9% w/v NaCl and 0.05 M $CaCl_2$. Furthermore, QS-DS-SLN in FBS has shown a significant increase in particle size at the end of 6 h.

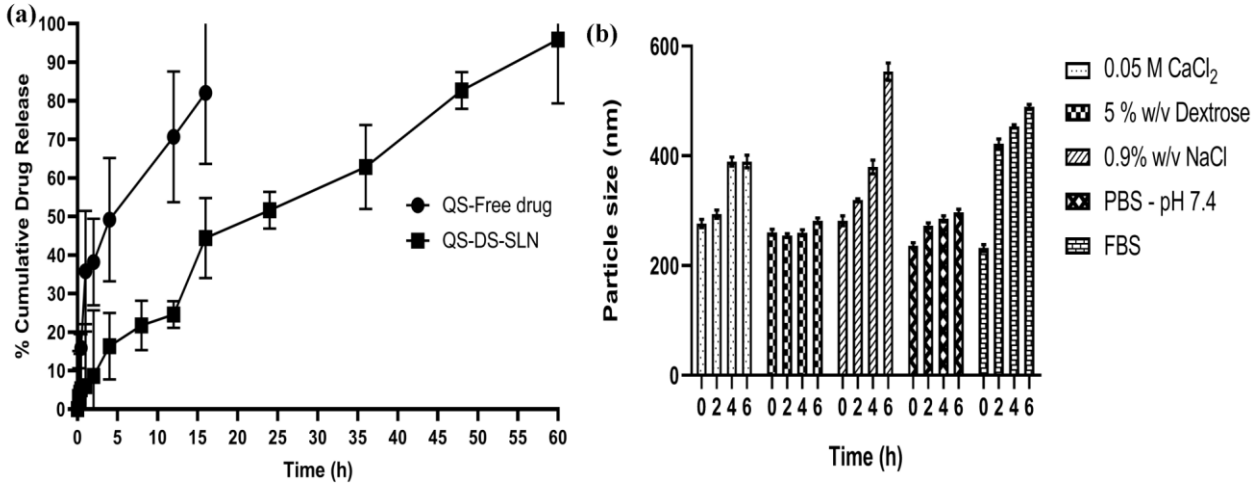

Fig. 3.4. *In-vitro* evaluation of QS-DS-SLN (a) *In-vitro* drug release of QS and QS-DS-SLN,(b) Stability of QS-DS-SLN in different physiological media.

3.8 Hemocompatibility studies

After parenteral administration, nanoparticles interact with the different blood cells including red blood cells, white blood cells and platelets during their presence in circulation which could induce hemolysis and exert morphological changes in the cells. Hence, it is essential to study the hemocompatibility of parenteral nanoformulations. %Hemolysis of QS, blank nanoparticles and QS-DS-SLN is depicted in (Fig. 3.5). At lower concentration of quinapyramine sulphate (0.5-20 µg/mL), there was no significant difference in hemolysis observed between free QS and QS-DS-SLN. However, at QS equivalent to 50µg/mL QS-DS-SLN showed significantly lower %hemolysis as compared to free quinapyramine sulphate ($p<0.0001$). Moreover, QS-DS-SLN showed <10% of hemolysis at the entire concentration range used in the study.

At an early stage of infection, the parasite growth rate is significantly high leading to an increase in parasite burden in the blood. The important consequences of higher parasite load in the blood are rupture and destruction of RBCs which results in release of hemoglobin, anemia and other hematological effects ("How Human Body Fights Off African Parasite -- ScienceDaily," n.d.; Sivajothi et al., n.d.). To study the impact of QS-DS-SLN on blood cell morphology after parenteral administration, cell surface was observed under SEM after incubating nanoformulation (quinapyramine sulphate equivalent to 20µg/mL) with different blood cells at 37ºC for 30 min. There was no significant change in RBC cell morphology was observed when incubated with blank nanocarriers or QS-DS-SLN. Similarly, there were no changes in the morphology of WBC and platelets observed after incubation with blank/ QS-DS-SLN indicating there would be no or minimal inflammatory response after administration [Fig. 3.6].

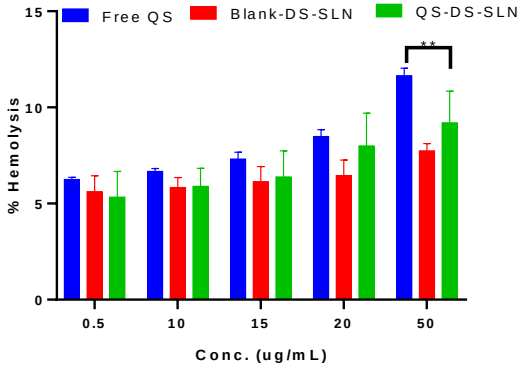

Fig. 3.5 % hemolysis of rat erythrocytes after treatment with QS, blank SLN and QS-DS-SLN (data represented as mean ± SD (n=3). Statistical comparison was done using Tukey's two-way ANOVA multiple comparison test **$p<0.01$)

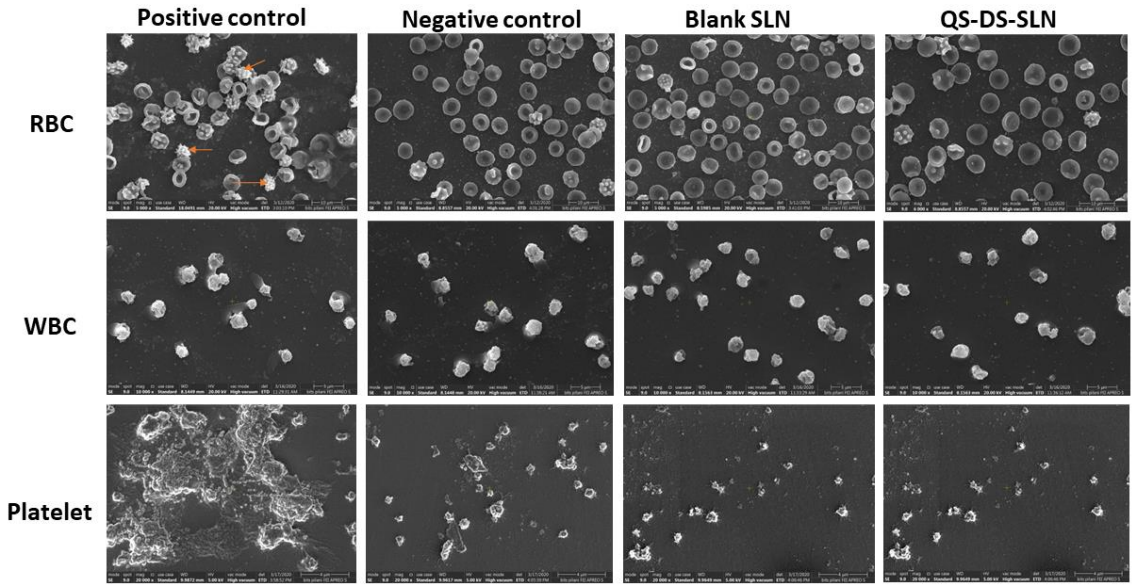

Fig. 3.6 Scanning electron micrographs showing morphological features of RBC, WBC and platelets after incubation with blank SLN and QS-DS-SLN

3.9 Cytotoxicity and cellular uptake studies

3.9.1 Cytotoxicity

Cytotoxicity of QS and QS-DS-SLN against THP-1 cells was studied by MTT assay. At the entire concentration range studied, the %cell viability was found to be significantly higher when THP-1 cells were incubated with QS-DS-SLN as compared to free quinapyramine sulphate ($p<0.0001$). However, a significant decrease in %cell viability was observed in both free QS and QS-DS-SLN treated groups with an increase in the QS concentration (Fig 3.7 (a)). After parenteral administration, nanoparticles are known to interact with the circulating macrophages (Rattan et al., 2017). The above observation suggests that QS-DS-SLN is safe for circulating macrophages after parenteral administration to the animals for the treatment of *trypanosomiasis*. Furthermore, QS-DS-SLN showed higher %cell viability as compared to free quinapyramine sulphate, indicating improvement in the safety of the drug after nanoencapsulation.

3.9.2 Cellular uptake

After parenteral administration, macrophage uptake of QS-DS-SLN could enable the creation of a drug reservoir within the macrophage which could lead to prolonged plasma concentration of the drug, reducing rapid elimination from the body (Surve and Jindal, 2020). We, therefore, studied time-dependent qualitative and quantitative uptake of Coumarin 6 loaded solid lipid

nanoparticles (C6 SLN) (a surrogate of QS-DS-SLN). Whereas, particle size, PDI, zeta potential, and %EE of C6 SLNs were found to be 263.14±21.17 nm, 0.24±0.02, -19.41±1.62 mV, and 62.31±4.74, respectively.

C6 SLNs showed enhanced cellular uptake as compared to free C6 at all the time points. Quantitative cellular uptake of C6 SLN was studied by the FACS which showed significantly higher uptake of C6 SLN ($p<0.0001$) as compared to free C6 at all time points [Fig 3.7 (b)]. Cellular uptake of C6 SLN was found to be increased with an increase in incubation time from 1 to 6 h as evidenced in [Fig 3.7]. Moreover, to understand the cellular uptake mechanism of C6 SLN, THP-1 cells were incubated with different endocytic pathway inhibitors including β-CD (lipid raft pathway inhibitor), NYS (caveolae-mediated pathway inhibitor), CPZ (clathin-mediated pathway inhibitor), and AMD (micropinocytosis inhibitor) for 1 h prior to C6 SLN treatment (Dutta and Donaldson, 2012; Kuhn et al., 2014; Lin et al., 2018). A significant decrease of 1.76-fold, 1.77-fold, and 1.83-fold in fluorescence intensity was observed when treated with CPZ, NYS, and β-CD respectively, indicating decreased cellular uptake of C6 SLN [Fig. 3.7 (c)].

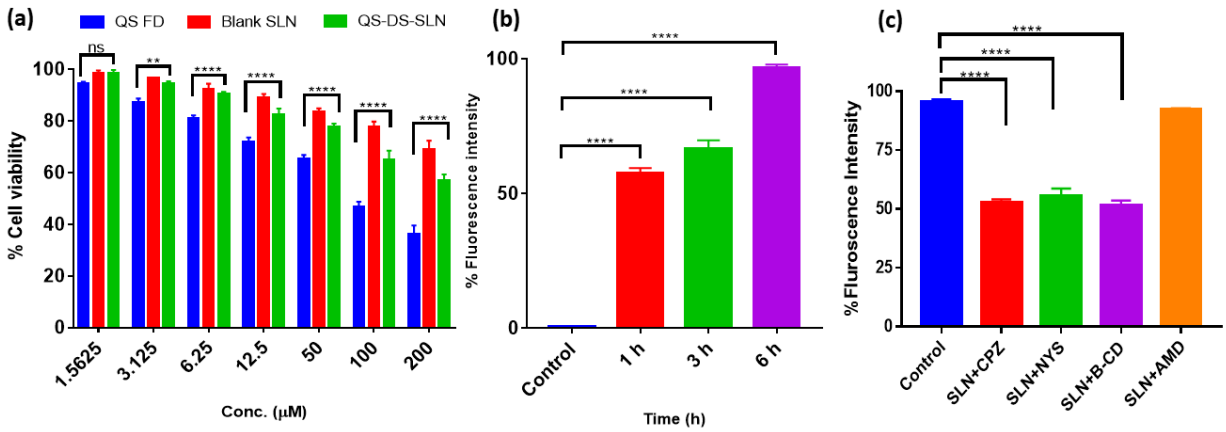

Fig. 3.7 Cytotoxicity and quantitative cellular uptake studies in THP-1 cells, a) cytotoxicity (statistical comparison was done using two-way ANOVA with Tukey's multiple comparison test **$p<0.01$, ****$p<0.0001$, b) time dependent quantitative cellular uptake C6 SLN as compared to free C6 (statistical comparison was done using one-way ANOVA with Sidak's multiple comparison test, ****$p<0.0001$), and c) cellular uptake of C6 SLN in presence of different endocytic inhibitors. (Statistical comparison was done using one-way ANOVA with Dunnett's multiple comparison test, ****$p<0.0001$)
[Data are represented as mean ± SD (n=3)]

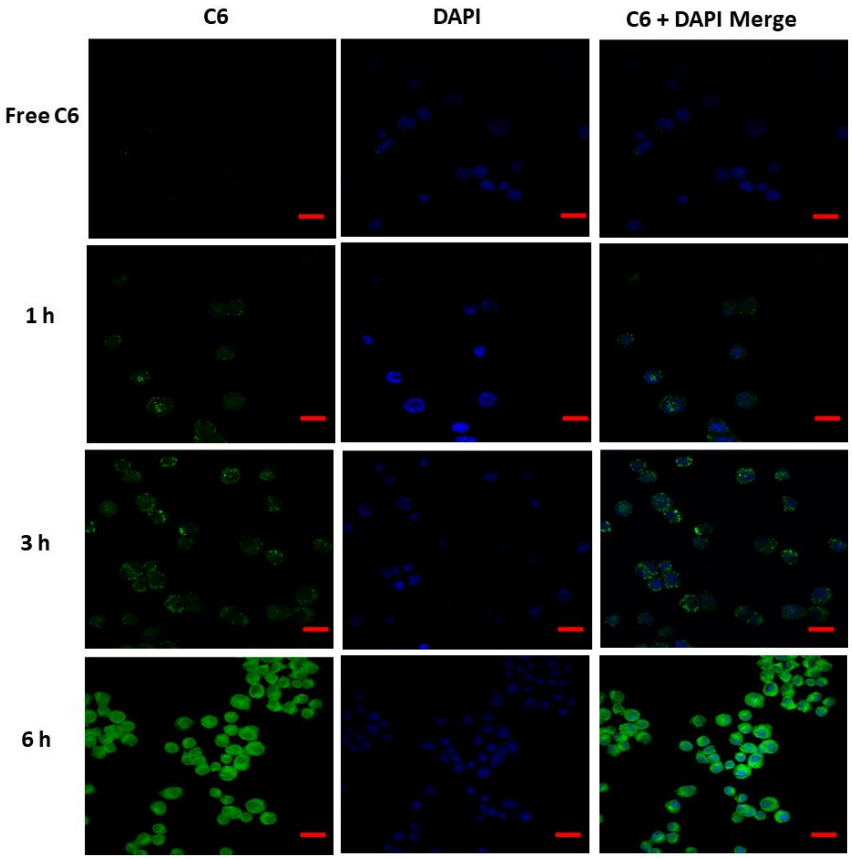

Fig. 3.8 Confocal images of THP-1 cells obtained after incubation with C6 SLN at different time points (magnification: 40X, scale: 20µm)

On the other hand, there was no change in fluorescence intensity observed when cells were incubated with AMD prior to C6 SLN treatment, indicating no change in cellular uptake of C6 SLN. The above observation suggests that C6 SLN could adopt multiple pathways including lipid raft, clathrin-mediated and caveolae-mediated pathways for the entry into the cells. However, it is independent of the micropinocytosis process of cellular uptake [Fig. 3.8 and Fig. 3.9].

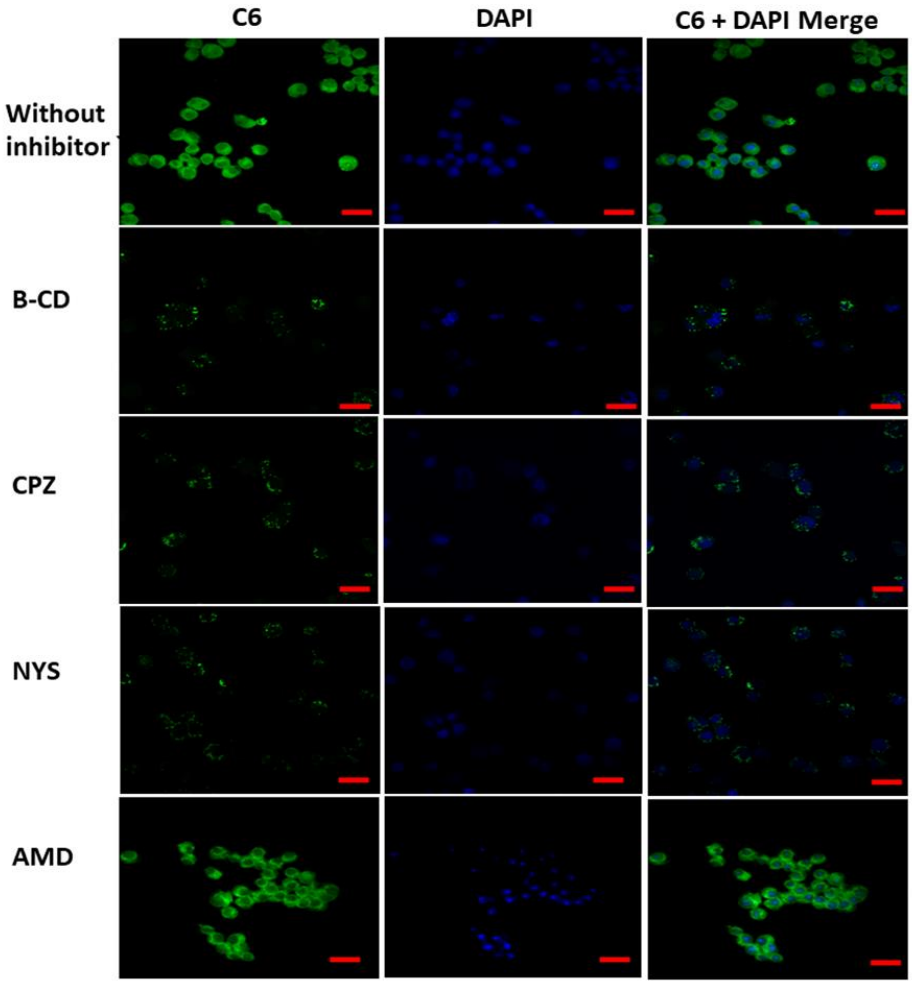

Fig. 3.9 Cellular uptake in THP-1 cells a) Confocal images of THP-1 cells obtained after treatment with various endocytic inhibitors prior to C6 SLN treatment (magnification: 40X, scale: 20µm)

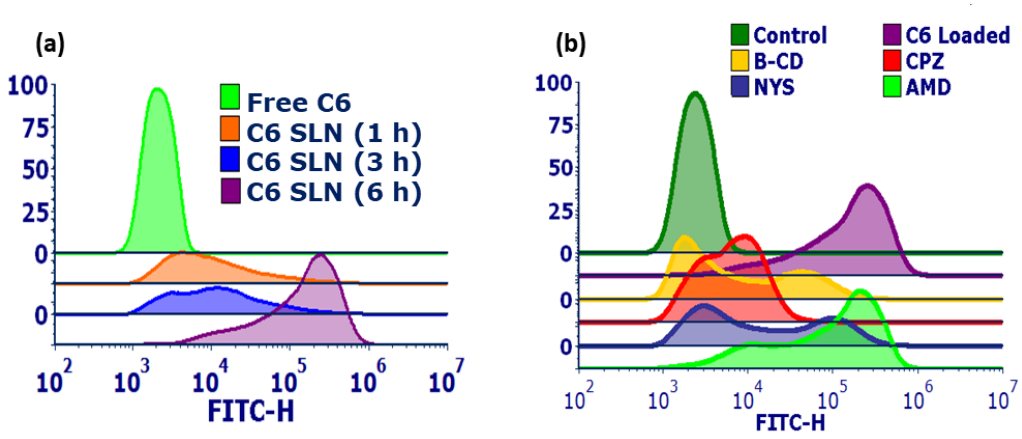

Fig. 3.10 Quantitative cellular uptake in THP-1 cells a) shift in fluorescence signals with time in when incubated with C6 SLN, and b) change in fluorescence signals after incubating cells with different endocytic inhibitors

3.10 Scale up of QS-DS-SLN

Rotational speed calculation in pilot scale batch basically depends upon the type of mixing i.e turbulent or laminar flow provided by impeller where, velocity and viscosity of blade and fluid plays a major role.

Rotational speed obtained from different approaches is presented in table 3.5. Particle size distribution of different batches obtained using different rotational speed as stated in Table 3.5 are presented in Fig. 3.11. It was observed that % particles obtained in the range of 150-350 nm was found to be decreased with increase in rotational speed. Furthermore, particle size distribution was found to be non-significant between lab scale and pilot scale batch having a rotational speed of 700 rpm obtained from the use of equal blending time approach.

While achieving similar particle size distribution profile for lab scale and pilot scale batch, interestingly we observed that lower agitation rates have profound effect on narrow particle size distribution and maximum particles were in the size range 150-350 nm when compared with higher agitation rates as shown in Table 3.5. For instance, rotational speed of 350 rpm for equal solid suspension approach and scale of agitation approach with 430 rpm had 66.23 ± 12.91% and 62.37 ± 6.08 % of particles in 150-350 nm size range respectively. Furthermore, it was observed that rotational speed of 350 rpm in pilot batch had least particles in the size range of 350-700 nm of 28.77 ± 8.76 when compared to other approaches of study boundaries. On the other hand, decrease in % EE was observed from 83.36 ± 5.78 to 56.97 ± 4.17% when rotational speed was increased from 350 rpm to 700 rpm. In all the approaches studied PDI was found to be less than 0.2.

Table 3.5: Particle size, PDI and % Entrapment Efficiency of pilot-scale batches

Scale-up Approach	**Calculated rotational Speed (rpm)**	**Particle size (nm)**	**PDI**	**% EE**
Scale of agitation	430	319.33 ± 28.16	0.14 ± 0.07	56.97 ± 4.17
Equal blending time (n=0)	700	347.82 ± 5.01	0.22 ± 0.03	59.24 ± 6.81
Equal surface motion (n=1/2)	440	319.27 ± 24.02	0.23 ± 0.10	83.36 ± 5.78
Equal percentage of solid (n=3/4)	350	297.97 ± 26.40	0.16 ± 0.06	75.41 ± 2.01
Froude Number	490	306.7 ± 16.59	0.18 ± 0.02	77.95 ± 2.39

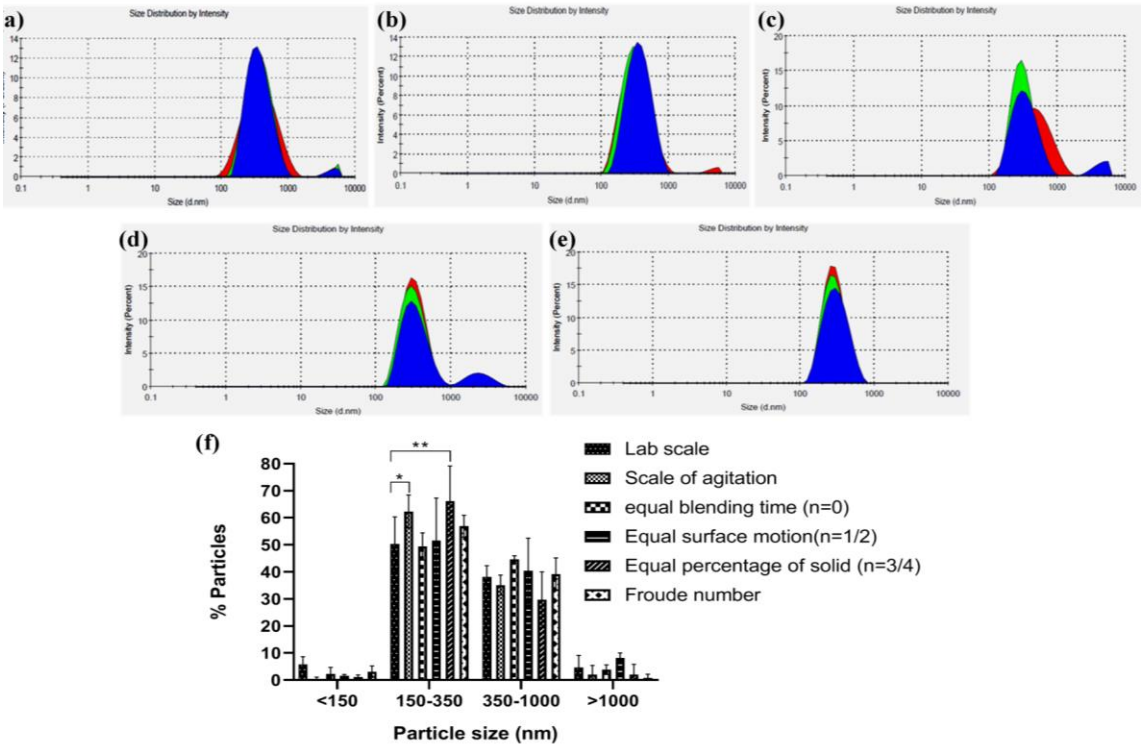

Fig. 3.11 Particle size distribution of pilot scale batches of pilot scale batches of QS-DS-SLN prepared with different approaches (a) Scale of agitation, (b) Equal blending time (n=0), (c) Equal surface motion(n=1/2), (d) Equal percentage of solid (n=3/4), (e) Froude number and (f) Particle size distribution of lab- and pilot- scale batches (data are represented as mean ± SD (n=3). Statistical comparison was done using two-way ANOVA with Dunnett's multiple comparison test*p<0.05, **p<0.01)

3.11 *In vitro* antitrypanosomal efficacy

[Fig. 3.12 (a)] presents concentration dependent trypanocidal activity of free QS and QS-DS-SLN against *T. evansi*, isolated from infected mice. %Viability of trypanosomes were found to be decreased with an increase in the QS concentration after treatment with the free QS or QS-DS-SLN. However, QS-DS-SLN showed higher trypanocidal effect against *T. evansi* parasite as compared to free quinapyramine sulphate at entire concentration range (0.05 – 100 µM) used in the study. There was significant difference in IC_{50} was observed between free quinapyramine sulphate (67.98µM) and QS-DS-SLN (44.13µM). An increase in trypanocidal activity of quinapyramine sulphate after encapsulation into lipidic nanocarrier may lead to decrease in the dose of the quinapyramine sulphate to produce the desired therapeutic effects and could result in decrease in dose dependent side effects of quinapyramine sulphate.

After incubation of quinapyramine sulphate or QS-DS-SLN with *T. evansi* parasite for 20h, CLSM images were acquired to observe morphological changes induced by the quinapyramine

sulphate or QS-DS-SLN to the *T. evansi* parasite. At lower quinapyramine sulphate concentration (0.25µM), there was no significant difference in the morphology of trypanosomes observed when compared with the control. When quinapyramine sulphate concentration was increased from 0.25µM to 0.5µM, QS-DS-SLN treatment showed aggregation of trypanosomes, which was higher than the free quinapyramine sulphate at the same concentration. When quinapyramine sulphate concentration was increased from 0.5µM to 5µM, detachment of flagella of the parasite was observed after treatment with QS-DS-SLN. While in case of quinapyramine sulphate (5µM), swelling of the parasite was observed [Fig. 3.12].

Trypanosomes are known to take up nutrients and other essential components such as fatty acids from the host through the transporters located at the flagella of the parasite. Detachment of the flagella after treatment with quinapyramine sulphate or QS-DS-SLN could lead to disruption of the parasite. The important findings of the study are that QS-DS-SLN showed significant morphological changes in the parasite at lower quinapyramine sulphate concentration as compared to the free quinapyramine sulphate. The difference in the ability to induce morphological changes could be due to the adaptation of different pathways by the QS-DS-SLN to enter inside the parasite.

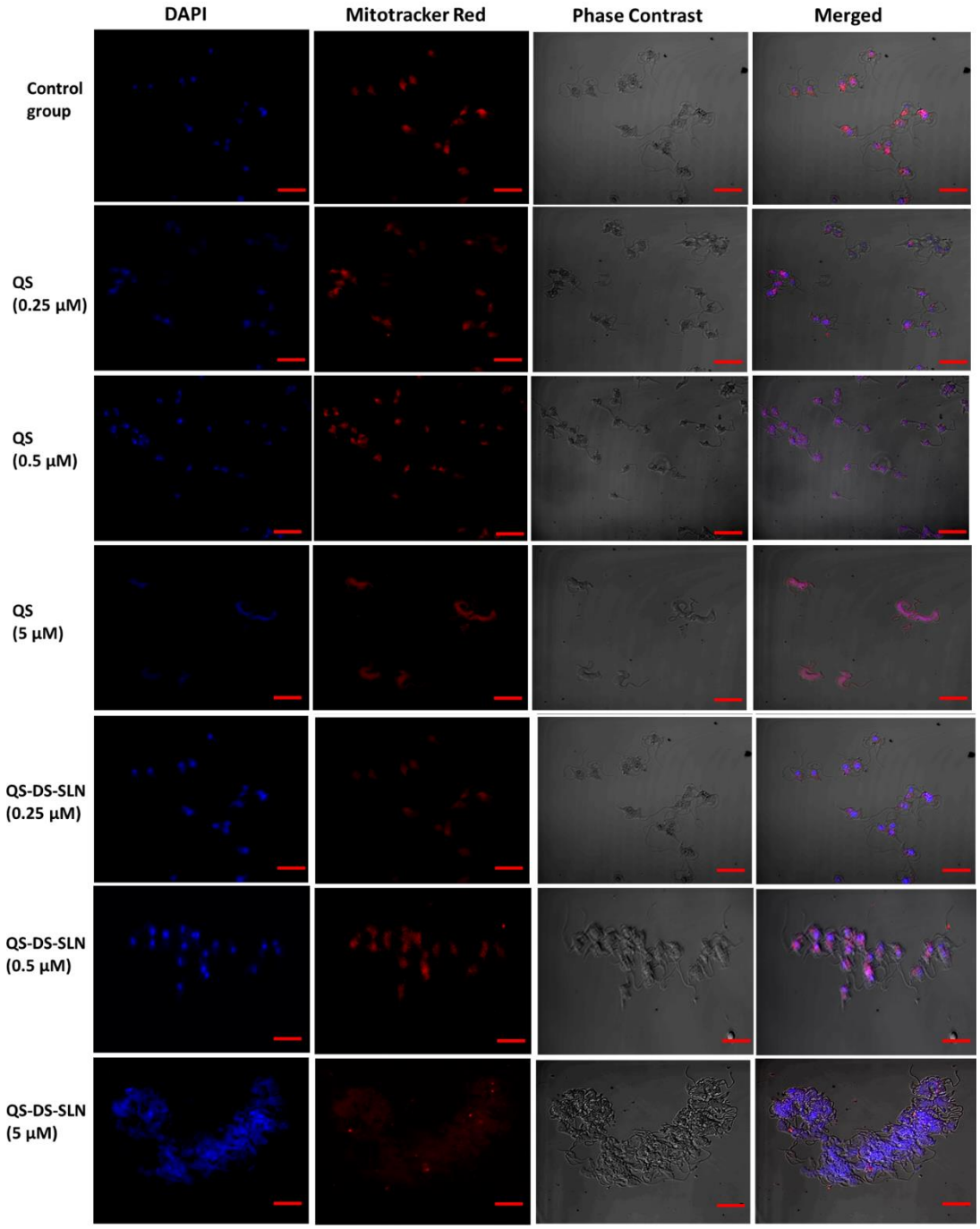

Fig. 3.12 Assessment of morphological changes in *T. evansi* parasite by confocal microscopy after incubation with free QS, and QS-DS-SLN with increasing concentration of QS, mitochondria stained with Mitotracker red and counterstained with DAPI, cell morphology accessed by phase contrast microscopy (magnification: 63X, scale: 5µm).

Furthermore, FESEM images of parasites were acquired after treatment with QS-DS-SLN to observe the presence of nanoparticles onto the parasite surface. It was observed that QS-DS-SLN were present all over the surface of the trypanosome including the body and the

kinetoplast of the parasite. Since endocytosis is a prerequisite for the trypanocidal action of the drug, interaction of administered QS-DS-SLN on the surface of trypanosome could induce uptake of particles and therefore elicit the necessary pharmacological effect of the quinapyramine sulphate. Moreover, although QS-DS-SLN and *T. evansi* exhibits negative charge on their surface, particle size and lipidic nanocarrier could affect the interaction with the parasite [Fig. 3.13 (b)].

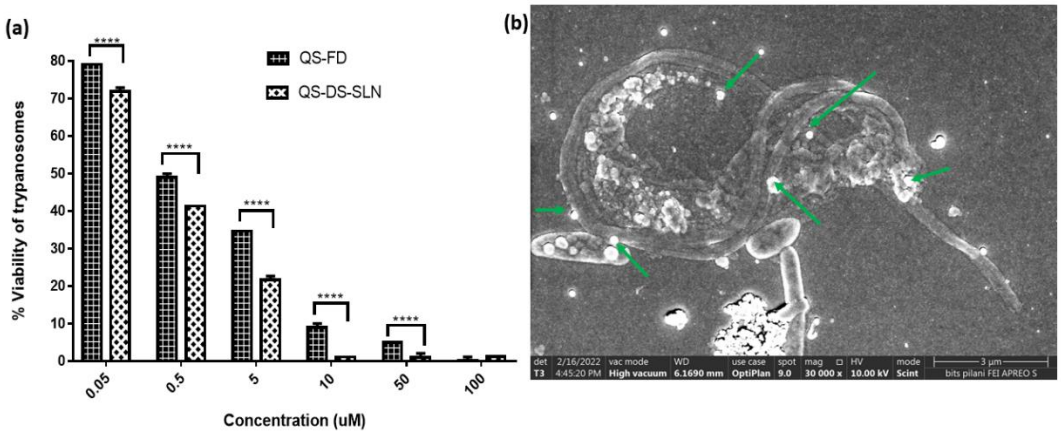

Fig. 3.13 *In vitro* antitrypanosomal efficacy against *T. evansi* parasite, a) *In vitro* trypanocidal assay of free QS and QS-DS-SLN (Data are represented as mean ± SD (n=3). Statistical comparison was done using two-way ANOVA with Sidak's multiple comparison test, ****p<0.0001), b) SEM image of *T. evansi* parasite incubated with QS-DS-SLN showing presence of nanoparticles over the surface of trypanosome.

3.12 Pharmacokinetic studies

Pharmacokinetic parameters obtained after non-compartmental analysis (NCA) of the data are presented in the Table 3.6 Whereas, fig. 3.14 represents plasma conc. Vs time profile of the various groups studied after SC administration.

After SC administration of free QS, C_{max} of QS was reached within 30 min and plasma concentration reached below detection limits after 18 h. As shown in the fig.3.14. QS when administered in a lipidic nanocarrier system showed increase in $AUC_{0-\infty}$, volume of distribution (Vz/F), and mean residence time ($MRT_{0-\infty}$) by 1.30-folds, 16.65-folds, and 3.35-folds, respectively as compared to the free QS. Whereas, $t_{1/2}$ was significantly increased by 1.30-folds suggesting the role of lipidic nanocarrier in protracted release *in vivo*.

Although we observed marked change in the PK parameters of the QS in QS-DS-SLN, the inherent higher water solubility could pose significant challenges in the drug delivery including quick removal of lipidic nanocarrier from the site of administration, leading to faster onset of action, and rapid elimination of the drug from the body.

Usually, hydrophilic APIs when injected by parenteral route shows quick elimination from the body by rapid distribution and elimination, whereas the lipid based nanocarriers could form a primary site injection depot, and subsequent engulfment by circulating macrophages as a secondary depot when injected by SC/IM route (Surve and Jindal, 2020). This primary mechanism could help in attaining protracted drug release. Furthermore, the study highlighted the role of hydrophobic ion-pairing along with lipidic encapsulation in protracted drug release of hydrophilic QS.

Table 3.6 Plasma non-compartmental PK parameters obtained after SC administration of QS and QS-DS-SLN in Wistar rats using Phoenix WiNonlin software (version 6.3)

Parameter	**Non-compartmental analysis**	
	Free QS	**QS-DS-SLN**
$t_{1/2}$ (h)	2.30 ± 11.25	8.84 ± 10.42
C_{max} (ng/mL)	3778.52 ± 32.61	517.47 ± 35.96
AUC $_{0-\infty}$	12389.51 ± 29.12	16218.54 ± 24.37
Vz/F (L/Kg)	2010.48 ± 11.26	33470.36 ± 19.91
Cl/F	605.35 ± 9.17	462.44 ± 15.24
$MRT_{0-\infty}$ (h)	3.28 ± 2.69	59.67 ± 15.80

Data represented as mean ± SE (n=4)

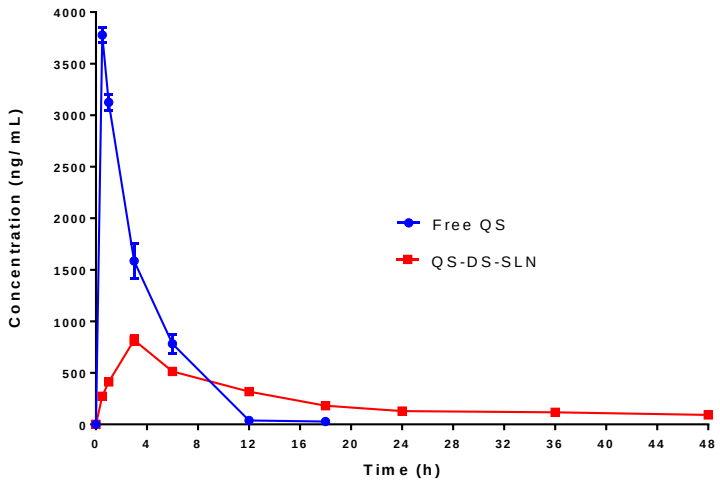

Fig. 3.14 Pharmacokinetic profile of free QS, and QS-DS-SLN in wistar rats, data represented as mean±SEM (n=4)

3.13 *In vivo* antitrypanosomal efficacy in *T. evansi* infected mice

Initially post-inoculation of *T. evansi*, all the infected mice showed different grades of infection as revealed by the matching method. A group was considered to be cured when ≥80% (a minimum of four out of five i.e.CD_{80} or CD_{100}) mice within one treatment group remained aparasitaemic during the observation period. The lowest dose of drugs which led to ≥80% treatment success was defined as the drug-sensitive dose. If fewer than four mice were cured, the drug dosage was ineffective, rather tolerant stock (Eisler et al., 2001). The test was considered valid if at least four out of five control mice became aparasitaemic.

In case of QS-DS-SLN (quinapyramine sulphate equivalent to 2.5 mg/kg body weight), all the five animals showed an initial response to the treatment and a decrease in the blood parasitaemia was observed on the 2nd day of the treatment. However, relapse in infection was observed in all animals and mice died within 11 days. In the parallel study, free QS was administered at 2.5 mg/kg body weight showed relapse and subsequent mortality by the end of the 15th day of the treatment suggesting neither QS nor QS-DS-SLN at the dose of 2.5mg/kg body weight achieved CD_{80} or CD_{100} resulting the failure of the therapy.

Furthermore, the effect of increasing the concentration of QS in free QS and QS-DS-SLN groups was evaluated by administering 5.0 mg/kg body weight dose. Initially, the treatment showed a steady-state decrease in parasitaemia, however, in progression relapse of infection and undulating parasitaemia were observed because all mice in the group died by the end of the 28th day. On the hand, mice treated with 5.0 mg/kg body weight of free QS showed variable degrees of response to the treatment.

Although three mice out of the five showed no relapse of infection, the curative rate of the administered dose was 60% only which failed to achieve either CD_{80} or CD_{100} which is indicative of successful chemotherapy.

Based on the results with an increasing concentration of QS, another group of *T. evansi-infected* mice was treated with a dose of QS equivalent to 7.5 mg/kg body weight with QS-DS-SLN. It was observed that a progressive decrease in parasitaemia was achieved wherein complete clearance of *T. evansi* was observed on 3rd day post-treatment which remained continued so far 60 days of treatment thereafter. All treated mice were found physically free of other visible parameters of growth in terms of weight and overall behaviour. The treatment with 7.5 mg/kg b.wt was repeated in a group animals having teeming parasitaemia and also showed survival in all the animals, revealing the therapeutic potentials of QS-DS-SLN in the treatment of *T. evansi* infection. On the other hand, the group treated with free QS at the dose of 7.5mg/kg body

weight showed that 4 mice out of 5 died within 24h of dosing indicating severe drug associated toxicity. The free drug achieved neither CD_{80} nor CD_{100} highlighting failure of therapy [Fig. 3.15 (a)]. Further, to confirm the efficacy of the treatment with 7.5mg/kg of QS-DS-SLN, a PCR assay was performed to amplify the presence of DNA if any belonging to the parasite. [Fig. 3.15 (b)] shows in the upper panel, that all the DNA samples from infected mice showed positive signals of standing infection and it is revealed by amplification of size ~500 bp. Well 1 indicates PBS only whereas, well 2 to 7 indicates spleen, heart, lungs, kidney, brain, and liver tissues, respectively, and well no 8 indicates *T. evansi* specific marker. It was observed that the intensity of the signals of amplification was found more in the case of spleen and lung tissues suggesting profound residence of the parasite in these tissues after the infection.

Moreover, well 2 to 7 from the lower panel indicate same tissues as that of the upper panel but after treatment with QS-DS-SLN. Whereas, well no 8 indicates the blood sample in an infected animal which showed positive amplicon as compared with the marker in well no 1. It was evident that there were no visible amplicons obtained in any of the isolated tissue samples suggesting QS-DS-SLN treatment has the potential of eliminating disease at the molecular level which could clear the established infection from the system.

Results suggest that with an increase in the concentration of quinapyramine sulphate from 2.5 mg to 7.5 mg/kg body weight there is a marked increase in the efficacy of the QS-DS-SLN showing long-term trypanocidal efficacy without relapse and reoccurrence of infection for the period of two months.

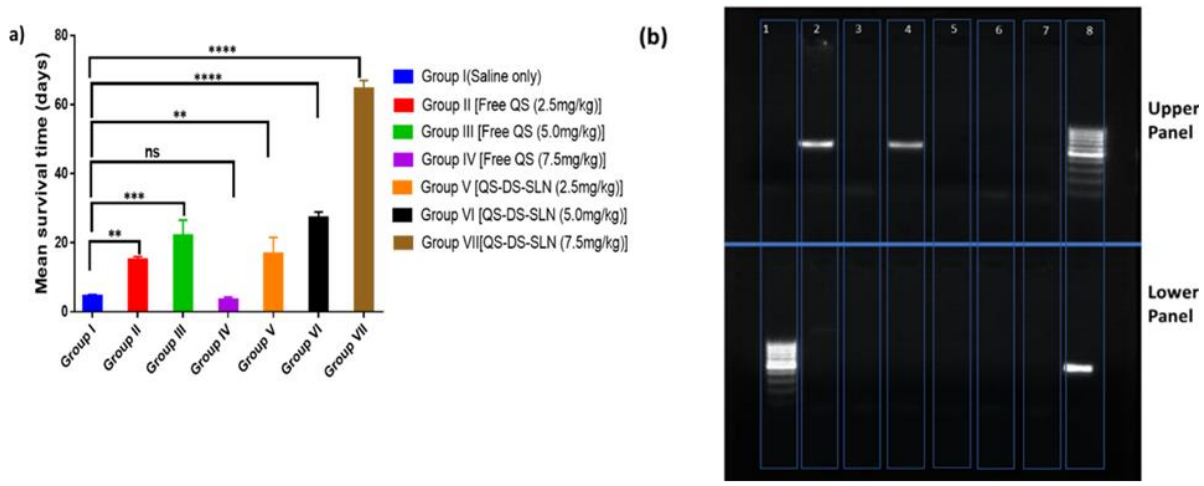

Fig. 3.15 *In vivo* antitrypanosomal efficacy against *T. evansi* in mouse model, a) mean survival time in different treated groups with QS or QS-DS-SLN, (Data are represented as mean ± SD (n=5). Statistical comparison was done using one-way ANOVA with Dunnett's multiple comparison test, *p<0.5, **p<0.01, ***p<0.001, ****p<0.0001), and b) PCR of DNA

extracted from various organs after treatment with QS-DS-SLN using mitochondrial DNA primer pair Kin1 and Kin 2 where, upper panel indicates infected mice organs and lower panel (excluding well 8) indicates DNA isolated from QS-DS-SLN (7.5mg/kg) treated group. Well no. 1 indicates PBS whereas, well 2 to 7 indicates spleen, heart, lungs, kidney, brain, and liver tissues, respectively, and well no 8 indicates *T. evansi* specific marker.

4. Conclusion:

A cationic charged QS was incorporated into solid lipid nanoparticles by preparing hydrophobic ionic complex of QS with docusate sodium. Ionic complexation of QS resulted in significant decrease in aqueous solubility and increase in % EE of the drug into solid lipid nanoparticles due to the enhanced partitioning of hydrophobic complex into lipid matrix. Moreover, QS-DS-SLN showed a sustained release of drug for up to 60 h, providing the possibility of creation of long-acting nanoformulations for the delivery of QS. Furthermore, nanocarriers were safe and biocompatible with different blood cells. Cellular uptake of surrogate C6 nanoformulation was also higher than free C6. In order to retain particle size, %EE during scale up of QS-DS-SLN, different approaches including equal blending time, equal surface motion, equal percentage of solids and dimensionless number approach were used to calculate optimum rotational speed by maintaining geometric similarity across the scaled nanoformulation. The study concludes the use of various scientific liquid mixing principles and their role in achieving the desired operational outcomes. Encapsulating QS in a lipidic nanocarrier resulted in a significant decrease in IC_{50} against *T. evansi* and induced significant morphological changes in the parasite. *In vivo* efficacy studies in a *T. evansi*-infected mouse model showed that QS-DS-SLN had an enhanced antitrypanosomal effect. These findings suggest that lipid based nanocarriers could be a promising advanced veterinary formulation for the treatment of *trypanosomiasis* in domestic animals. However, further clinical studies in naturally infected animals are needed to translate these results from the laboratory to the clinic.

References:

Arias, J.L., Unciti-broceta, J.D., Maceira, J., Castillo, T., Hernández-quero, J., Magez, S., Soriano, M., García-salcedo, J.A., 2015. Nanobody conjugated PLGA nanoparticles for active targeting of African Trypanosomiasis. J. Control. Release 197, 190–198. https://doi.org/10.1016/j.jconrel.2014.11.002

Battaglia L, Gallarte M, Peira E, Chrio D, Muntoni E, Biasibeti E, Capucchio M, Valazza A, Panciani P, Lanotte M, Schiffer D, Annovazzi L, Caldera V, Mellai M, R.C., 2014. Solid Lipid Nanoparticles for Potential Doxorubicin Delivery in Glioblastoma Treatment : Preliminary In Vitro Studies. Pharm. Nanotechnol. 103, 2157–2165.

Bellich, B., D'Agostino, I., Semeraro, S., Gamini, A., Cesàro, A., 2016. "The good, the bad and the ugly" of chitosans. Mar. Drugs 14.

Block, L.H., 2005. Scale Up of Liquid and Semisolid Manufacturing Processes. Pharm. Technol. s26–s33.

Bonferoni, M.C., Rossi, S., Ferrari, F., Caramella, C., 1999. A modified Franz diffusion cell for simultaneous assessment of drug release and washability of mucoadhesive gels. Pharm. Dev. Technol. 4, 45–53.

Colby, A.H., Liu, R., Doyle, R.P., Merting, A., Zhang, H., Savage, N., Chu, N.Q., Hollister, B.A., McCulloch, W., Burdette, J.E., Pearce, C.J., Liu, K., Oberlies, N.H., Colson, Y.L., Grinstaff, M.W., 2021. Pilot-scale production of expansile nanoparticles: Practical methods for clinical scale-up. J. Control. release 337, 144–154. https://doi.org/10.1016/J.JCONREL.2021.07.012

Desquesnes, M., Dargantes, A., Lai, D., Lun, Z., Holzmuller, P., Jittapalapong, S., 2013. Trypanosoma evansi and Surra : A Review and Perspectives on Transmission , Epidemiology and Control , Impact and Zoonotic Aspects. Biomed Res. Int. 1–20.

Desquesnes, M., McLaughlin, G., Zoungrana, A., Dávila, A.M.R., 2001. Detection and identification of Trypanosoma of African livestock through a single PCR based on internal transcribed spacer 1 of rDNA. Int. J. Parasitol. 31, 610–614. https://doi.org/10.1016/S0020-7519(01)00161-8

Dutta, D., Donaldson, J.G., 2012. Search for inhibitors of endocytosis. Cell. Logist. 2, 203–208. https://doi.org/10.4161/cl.23967

Eisler, M.C., Brandt, J., Bauer, B., Clausen, P.H., Delespaux, V., Holmes, P.H., Ilemobade, A., Machila, N., Mbwambo, H., McDermott, J., Mehlitz, D., Murilla, G., Ndung'u, J.M., Peregrine, A.S., Sidibé, I., Sinyangwe, L., Geerts, S., 2001. Standardised tests in mice and cattle for the detection of drug resistance in tsetse-transmitted trypanosomes of African domestic cattle. Vet. Parasitol. 97, 171–183. https://doi.org/10.1016/S0304-4017(01)00415-0

Emilia S, W.K., 2015. Stability of Chitosan—A Challenge for Pharmaceutical and Biomedical Applications. Mar. Drugs 13, 1819–1846.

Fu, S., Thacker, A., Sperger, D.M., Boni, R.L., Velankar S, Munson E, B.L., 2010. Rheological

Evaluation of Inter-grade and Inter-batch Variability of Sodium Alginate. AAPS PharmSciTech 11, 1662–1674.

Gohla, S., Ma, K., Muller, R.H., 2000. Solid lipid nanoparticles (SLN) for controlled drug delivery - a review of the state of the art 50.

Hansen, C.M., 2004. 50 Years with solubility parameters — past and future. Prog. Org. Coatings 51, 77–84.

Herbert, W.J., Lumsden, W.H.R., 1976. Trypanosoma brucei: A rapid "matching" method for estimating the host's parasitemia. Exp. Parasitol. 40, 427–431. https://doi.org/10.1016/0014-4894(76)90110-7

Hernández K, Rodríguez R, Gutiérrez C, Peñuñuri O, Zavala P, Guerrero P, L.A., 2020. PLGA nanoparticle preparations by emulsification and nanoprecipitation techniques: Effects of formulation parameters. RSC Adv. 10, 4218–4231.

How Human Body Fights Off African Parasite -- ScienceDaily [WWW Document], n.d. URL https://www.sciencedaily.com/releases/2007/09/070906214906.htm (accessed 6.6.22).

Ijaz M, Bonengel S, Zupančič O, Yaqoob M, Hartl M, Hussain S, Huck C, S.A., 2016. Development of oral self nano-emulsifying delivery system (s) of lanreotide with improved stability against presystemic thiol-disulfide exchange reactions. Expert Opin. Drug Deliv. 5247.

Jindal, A.B., Devarajan, P. V, 2015. Asymmetric lipid – polymer particles (LIPOMER) by modi fi ed nanoprecipitation : role of non-solvent composition. Int. J. Pharm. 1–6.

Juan, D.U.B., José MacEira, Sonia Morales, Angélica García-Pérez, Manuel, E.M.T., Garcia-Salcedo, J.A., 2013. Nicotinamide inhibits the lysosomal cathepsin b-like protease and kills African trypanosomes. J. Biol. Chem. 288, 10548–10557. https://doi.org/10.1074/jbc.M112.449207

K.S., J., Snigdha, S.S., Kalarikkal, N., Pothen, L.A., Thomas, S., 2017. Gelatin modified lipid nanoparticles for anti- viral drug delivery. Chem. Phys. Lipids 207, 24–37. https://doi.org/10.1016/J.CHEMPHYSLIP.2017.07.002

Kitak, T., Dumiˇ, A., 2015. Determination of Solubility Parameters of Ibuprofen and Ibuprofen Lysinate. Molecules 20, 21549–21568.

Krevelen, D.W. van, 2019. Properties of Polymers: Their Correlation with Chemical Structure, Their Numerical Estimation and Prediction from Additive Group Contributions. Elsevier, p. 1030.

Kuhn, D.A., Vanhecke, D., Michen, B., Blank, F., Gehr, P., Petri-Fink, A., Rothen-Rutishauser, B., 2014. Different endocytotic uptake mechanisms for nanoparticles in epithelial cells and macrophages. Beilstein J. Nanotechnol. 5, 1625–1636. https://doi.org/10.3762/bjnano.5.174

Kumar, R., Dkhar, D.S., Kumari, R., Divya, Mahapatra, S., Dubey, V.K., Chandra, P., 2022. Lipid based nanocarriers: Production techniques, concepts, and commercialization aspect.

J. Drug Deliv. Sci. Technol. 74, 103526. https://doi.org/https://doi.org/10.1016/j.jddst.2022.103526

Lin, H.P., Singla, B., Ghoshal, P., Faulkner, J.L., Cherian-Shaw, M., O'Connor, P.M., She, J.X., Belin de Chantemele, E.J., Csányi, G., 2018. Identification of novel macropinocytosis inhibitors using a rational screen of Food and Drug Administration-approved drugs. Br. J. Pharmacol. 175, 3640–3655. https://doi.org/10.1111/bph.14429

Manuja A, Dilbaghi N, Kaur H, Saini R, Barnela M, Chopra M, Manuja B, Kumar R, Kumar S, Riyesh T, Singh S, Y.S., 2018. Nano-Structures & Nano-Objects Chitosan quinapyramine sulfate nanoparticles exhibit increased trypanocidal activity in mice. Nano-Structures & Nano-Objects 16, 193–199.

Manuja A, Kumar B, Chopra M, Bajaj A, Kumar R, Dilbaghi N, Kumar S, Singh S, Riyesh T, Y.S., 2016. Cytotoxicity and genotoxicity of a trypanocidal drug quinapyramine sulfate loaded-sodium alginate nanoparticles in mammalian cells. Int. J. Biol. Macromol. 88, 146–155.

Manuja A, Kumar S, Dilbaghi N, Bhanjana G, Chopra M, Kaur H, Kumar R, Manuja B, Singh S, Y.S., 2014. Quinapyramine sulfate-loaded sodium alginate nanoparticles show enhanced trypanocidal activity. Nanomedicine 9, 1625–1634.

Mehnert, W., Mäder, K., 2012. Solid lipid nanoparticles : Production , characterization and applications. Adv. Drug Deliv. Rev. 64, 83–101.

Muthu, M.S., Wilson, B., 2012. Challenges posed by the scale-up of nanomedicines. Nanomedicine 7, 307–309. https://doi.org/10.2217/nnm.12.3

Peres L, Peres La, Henrique P, S.C., 2016. Solid lipid nanoparticles for encapsulation of hydrophilic drugs by an organic solvent free double emulsion technique. Colloids Surfaces B Biointerfaces 140, 317–323.

Poudel B, Gupta B, Ramasamy T, Thapa R, Youn Y, Choi H, Yong C, K.J., 2016. Development of polymeric irinotecan nanoparticles using a novel lactone preservation strategy. Int. J. Pharm. 512, 75–86.

Prayag, K., Surve, D.H., Paul, A.T., Kumar, S., Jindal, A.B., 2020. Nanotechnological interventions for treatment of trypanosomiasis in humans and animals. Drug Deliv. Transl. Res. 10, 945–961.

Raina, H., Kaur, S., Jindal, A.B., 2017. Development of efavirenz loaded solid lipid nanoparticles: Risk assessment, quality-by-design (QbD) based optimisation and physicochemical characterisation. J. Drug Deliv. Sci. Technol. 39, 180–191.

Rattan, R., Bhattacharjee, S., Zong, H., Swain, C., Siddiqui, M.A., Visovatti, S.H., Kanthi, Y., Desai, S., Pinsky, D.J., Goonewardena, S.N., 2017. Nanoparticle-macrophage interactions: A balance between clearance and cell-specific targeting. Bioorg. Med. Chem. 25, 4487. https://doi.org/10.1016/J.BMC.2017.06.040

Räz, B., Iten, M., Grether-Bühler, Y., Kaminsky, R., Brun, R., 1997. The Alamar Blue® assay

to determine drug sensitivity of African trypanosomes (T.b. rhodesiense and T.b. gambiense) in vitro. Acta Trop. 68, 139–147. https://doi.org/10.1016/S0001-706X(97)00079-X

Ristroph, K.D., Prud, R.K., 2019. Hydrophobic ion pairing : encapsulating small molecules , peptides , and proteins into nanocarriers. Nanoscale Adv. 4207–4237.

Schouenborg, N.J., 2016. Hydrophobic ion pairing of a minocycline/Ca2+/AOT complex for preparation of drug-loaded PLGA nanoparticles with improved sustained release. Int. J. Pharm. 499, 351–357.

Seeligmüller, N., 2016. Faster Isolation of PBMC Using Ficoll-Paque ® Plus in the Eppendorf ® Centrifuge 5920 R 3–8.

Sidney H Wiling, n.d. Good manufacturing practices for pharmaceuticals: A plan for Total Quality product from manufacturer to consumer, in: Gorsky, I. (Ed.), . Marcel Dekker, INC.

Sidney H Wiling, Levin, M., 2003. Good manufacturing practices for pharmaceuticals: A plan for Total Quality product from manufacturer to consumer, Fifth. ed.

Silva E, Lima F, Carneiro G, Ramos J, Gomes D, Maria E, F.L., 2016. Improved In Vitro Antileukemic Activity of All-Trans Retinoic Acid Loaded in Cholesteryl Butyrate Solid Lipid Nanoparticles. J. Nanosci. Nanotechnol. 16, 1291–1300.

Sivajothi, S., Rayulu, V.C., Sudhakara Reddy, • B, n.d. Haematological and biochemical changes in experimental Trypanosoma evansi infection in rabbits. J. Parasit. Dis. https://doi.org/10.1007/s12639-013-0321-6

Surve, D.H., Jindal, A.B., 2021. Development of cationic Isometamidium chloride loaded long-acting lipid nanoformulation: optimization, cellular uptake, pharmacokinetics, biodistribution, and immunohistochemical evaluation. Eur. J. Pharm. Sci. 167, 106024. https://doi.org/10.1016/J.EJPS.2021.106024

Surve, D.H., Jindal, A.B., 2020. Recent advances in long-acting nanoformulations for delivery of antiretroviral drugs. J. Control. Release 324, 379–404.

Tang, C., Zhang, E., Li, Y., Yang, L., 2017. An innovative method for preparation of hydrophobic ion-pairing colistin entrapped poly (lactic acid) nanoparticles : Loading and release mechanism study. Eur. J. Pharm. Sci. 102, 63–70.

Taylor, P., Srivastava, G.P., Weaire, D., 1987. The theory of the cohesive energies of solids. Adv. Phys. 36, 463–517.

Wong, H.L., Bendayan, R., Rauth, A.M., Wu, X.Y.U., 2004. Development of Solid Lipid Nanoparticles Containing Ionically Complexed Chemotherapeutic Drugs and Chemosensitizers. J. Pharm. Sci. 93, 1993–2008.

Yashica Pharmaceuticals Pvt. Ltd., n.d. Product Information- Quinapyramine Chloride/Sulphate BP [WWW Document]. URL https://www.pharmarawmaterials.com/quinapyramine-chloride-sulphate.html

Chapter 4: Development and Evaluation of Long-Acting Oil-Based Nanosuspension for Efficient Delivery of Quinapyramine Sulphate

1. Introduction

Quinapyramine sulphate (QS) is an antitrypanosomal drug commonly used to treat *trypanosomiasis* in domestic and wild animals, including pigs, cats, dogs, donkeys, equines, cattle, and camelids (Health, 2009; Manual, n.d.; Murray and Gray, 1984; Prayag et al., 2020). It is a highly hydrophilic drug, with a pKa of 14.16 and a log P of -2.80. In the market, QS is dispensed as a ready-to-use powder for reconstitution for subcutaneous administration. (Vollner, 2018; Yashica Pharmaceuticals Pvt. Ltd., n.d.). The anti-trypanosomal activity of QS has been shown to be enhanced through lipidic/polymeric nanoencapsulation. For example, Manuja et al. demonstrated that when QS was encapsulated in a sodium alginate nanocarrier, it had similar activity and a 100% survival rate at a dose of 0.73 mg/kg in a *T. evansi* infected mouse model, compared to 5 mg/kg of free QS (Manuja A, et.al., 2014). The same research group also showed similar activity of the formulation with a 5.88 to 25-fold reduction in the dose of QS-chitosan nanoparticles compared to free QS in a *T. evansi*-infected rabbit model (Manuja A, et.al., 2018).

The total dose of QS is typically administered in divided doses at 12-hour intervals, and repeat dosing every 2-3 months is often recommended in areas where the disease is prevalent. However, repeated administration can result in poor compliance with therapy in treating animal trypanosomiasis. Frequent dosing can be challenging for animal owners and negatively impact treatment adherence (Barrett et al., 2011). Moreover, high dosing frequency increases the number of visits to the veterinarian, which escalates the economic implication for the animal caretakers. As a result, there is a need to develop drug delivery systems that can provide sustained release of QS and reduce the frequency of dosing required for effective treatment. To this end, a long-acting (LA) formulation of QS could be a promising strategy (Edagwa et al., 2014; Surve and Jindal, 2021).

Two primary strategies have been employed to develop long-acting (LA) formulations for water-soluble drugs. The first strategy involves synthesizing a prodrug or salt form of the drug with a lower solubility in the water (Rautio et al., 2008). This approach allows for the slow release of the active drug over an extended period. The second strategy involves encapsulating the drug within polymeric microparticles that serve as a reservoir, steadily releasing the

contents over an extended period (Cattaneo and Gervasoni, 2019; Hirota et al., 2016; Vilos et al., 2015; Wu et al., 2016). Development of the LA formulations for water-soluble drugs can present challenges, and the two primary strategies of prodrug or insoluble salt formation and encapsulation within polymeric microparticles have limitations. Prodrug or salt formation can require complex chemical reactions and toxic chemicals, which may pose challenges for scaling up production (Jornada et al., 2015; Markovic et al., 2020). Meanwhile, polymeric microparticles may have limitations with drug loading for hydrophilic drugs and can involve complex manufacturing processes, including the removal of organic solvents and sterilization. In the present study, we report a simple yet innovative approach for the preparation of LA QS nanoformulation. The approach involved the transformation of QS to a non-ionic, hydrophobic complex by induced electrostatic interaction with an anionic agent (Devrim and Bozkır, 2015; Kalhapure et al., 2014; Ristroph and Prud, 2019; Wibel et al., 2020). The hydrophobic complex was then dispersed in oil and subjected to probe sonication to obtain a nanosuspension. The resulting formulation was then evaluated for pharmacokinetics and efficacy in animal studies. This approach offers a simpler method for preparing a LA formulation without the need for complex chemical reactions or the use of toxic chemicals.

2. Materials and methods

2.1 Materials

Quinapyramine sulphate was procured from ProVentus Life Sciences Pvt. Ltd. (Chennai, India). Olive oil was received as a gift from Loba Chemie (Mumbai, India). 1-octanol was procured from CDH chemicals (New Delhi, India). Sodium tripolyphosphate, docusate sodium, sodium alginate and sodium carboxymethylcellulose were procured from SD Fine-Chem Ltd. (Mumbai. India). Aluminium monostearate was obtained from the Sigma-Aldrich Chemicals Company (Missouri, United States). Sodium cholate was procured from Sisco Research Laboratories Pvt. Ltd. (Mumbai, India). Acetonitrile and methanol of HPLC-grade were purchased from Merck (Darmstadt, Germany). Milli-Q system (Millipore GmbH, Germany) was used to get pure HPLC-grade water. The prepared buffers and solvents were filtered and degassed through a 0.22m Millipore™ membrane filter (Merck, Darmstadt, Germany) and ultrasonic bath, respectively. All the other reagents, solvents, and chemicals utilised during experimentation were either of HPLC or analytical grade.

2.2 Methods

2.2.1 Preparation of QS-Na.C hydrophobic ionic complex

1.0 g of QS and 1.617 g of sodium cholate were dissolved separately in 10.0 mL of purified water. Sodium cholate solution was added to the QS solution to obtain QS- sodium cholate ion-pair complex. The ion-pair complex was separated by centrifugation at 8,000 rpm for 15 min at 20°C. After centrifugation, the pellet was separated and freeze-dried by utilization of FreeZone® Triad Benchtop Freeze Dryer (Labconco, USA). Freeze-dried QS-Na.C complex was mechanically pulverised using a glass mortar pestle, passed through a 100# mesh screen, and stored at room temperature until further use.

2.2.2 Characterisation of QS-Na.C complex

2.2.2.1 % Yield and % complexation efficiency

The % yield and % complexation efficiency of the QS-Na.C complex were determined by equations (4.1) and (4.2), respectively. To determine the amount of QS in the QS-Na.C complex, 10.0 mg of the complex was dissolved in 1.0 mL of dichloromethane: propylene glycol (4:1) solution. Thereafter, the solution was diluted appropriately, using acetonitrile: water (1:1), and analysed using an RP-HPLC-based analytical method.

$$\%\, Yield = \frac{Practical\ weight\ of\ QS{-}Na.C\ complex}{Therotical\ weight\ of\ (QS{+}Na.C)} \quad (4.1)$$

$$\%\, Complexation\ efficiency = \frac{Actual\ amount\ of\ QS\ present\ in\ QS{-}Na.C\ complex}{Therotical\ amount\ of\ QS\ used\ for\ complexation} \quad (4.2)$$

2.2.2.2 Fourier Transform Infrared Spectroscopy

The Fourier Transform Infrared Spectroscopy (FTIR) spectra of QS, NC, and QS-Na.C ionic complex were obtained using a Bruker alpha-one FTIR spectrophotometer (Bruker Optik, Germany). A sample weighing 10.0 mg was placed on a ZnSe sample crystal, and the spectra were recorded by scanning from 3800-600 cm-1.

2.2.2.3 Differential Scanning Calorimetry (DSC)

DSC thermograms of QS, Na.C, QS-Na.C physical mixture, and QS-Na.C complex were obtained using a DSC-60 Plus instrument (Shimadzu, Japan) under a nitrogen gas purge to

maintain an inert atmosphere. Approximately 5.0 mg of each sample was placed in an aluminium pan and hermetically sealed using a crimper. The samples, as well as an empty aluminium pan used as a reference, were heated at a constant rate of 10°C/min between 30 and 300°C under a continuous nitrogen purge.

2.2.2.4 X-Ray Diffraction (XRD)

XRD spectra were recorded by utilization of an X-ray diffractometer (Rigaku Miniflex II, Tokyo, Japn), for the pure drug QS, Na.C and QS-Na.C complex. The diffractometer was equipped with nickel-filtered Cu K radiation, which was operated at a voltage of 3 kV, 5 mA current, 4°/min scanning speed, and scanned between 5-40° 2Θ range.

2.2.2.5 *Equilibrium solubility of QS-Na.C complex in different oils*

The equilibrium solubility of the QS-Na.C hydrophobic complex was determined in different oils, including castor oil, oleic acid, peceol, olive oil, maisine, isopropyl myristate, ethyl oleate and cod liver oil by the saturated solubility method as reported previously with some modifications (Shah et al., 2007). Briefly, an excess quantity of complex (in increments of 5.0 mg) was added to each test tube consisting of different oils (5.0 mL) warmed in a water bath at 45-50°C until visible signs of precipitation were observed. Samples were gently shaken for 24 h at room temperature using SPINIX™ Orbital Shaker (Tarsons, India). Thereafter, the samples were centrifuged, and 200 µL aliquot of the supernatant was appropriately diluted with a warm mixture of methanol:0.3M $CaCl_2$ solution (80:20) (Wong et al., 2004). The above solution was analysed using a UV-visible spectrophotometer at λ_{max} of 297 nm to determine the amount of QS.

2.2.3 Preparation of QS-Na.C complex-loaded oily nanosuspension

Based on the equilibrium saturation solubility studies, olive oil was selected to prepare QS-Na.C loaded oily nanosuspension. Olive oil (10.0 mL) was heated up to 150°C, and aluminium monostearate (150.0 mg) was added under continuous stirring to obtain 1.5% w/v oily solution. Thereafter, the oil was cooled at room temperature. To the above oily solution, QS-Na.C complex (140.0 mg) was added under continuous stirring for about 30 min to get uniform dispersion. Further, the above oily dispersion was subjected to size reduction using probe sonicator (Sonics & Materials, Inc., US), and amplitude of 28% for 6 min (20 sec: ON and 10 sec: OFF).

2.2.4 Evaluation of QS-Na.C loaded oily nanosuspension

2.2.4.1 Viscosity

The viscoelastic behaviour of QS-Na.C complex loaded oily injection was evaluated using Rheometer (MCR 92, P-PTD 200, Anton Paar, Germany). Briefly, samples including olive oil, thixotropically thickened olive oil, and QS-Na.C complex loaded nanosuspension, were placed in small amounts on the plate with a gap of 0.5 mm between the plate and cone. A spindle of suitable size was attached, and shear rate, time and rpm were kept constant during the experiment to study the effect of varying shear rates on shear stress (Donthi et al., 2023).

2.2.4.2 Cytotoxicity

To evaluate the cytotoxicity of QS, QS-Na.C complex, and QS-Na.C complex loaded oily nanosuspension, an MTT assay was performed using THP-1 cell lines (monocyte-macrophage-like cells). A 96-well plate was seeded with $5x10^4$ THP-1 cells per well in 100 µL of RPMI 1640 cell culture medium fortified with 10%v/v FBS and Phorbol 12-myristate 13-acetate (PMA) at a concentration of 0.1 ng/mL. The cells were incubated for 48 hours at 37°C and 5% CO_2 [25,26]. After removal of the media, cells were treated with free QS, QS-Na.C complex, and QS-Na.C complex loaded oily nanosuspension at various concentrations of QS, including 2, 4, 8, 16, 32, 64, and 128 µM for 24 hours. Following treatment, the media was removed, and cells were washed with phosphate-buffered saline (PBS). MTT reagent was then added to the cells at a concentration of 500 µg/mL and incubated for another 4 hours in an incubator at 37°C and 5% CO2. After incubation, the treatment was discarded, and 100 µL of DMSO was added to dissolve formazan crystals formed. The plate was placed on a horizontal shaker for about 2 hours, and the absorbance of the plate was measured at 570 nm using an Epoch Elisa plate reader (BioTek U.S., Winooski). The % cell viability was estimated using equation 4.3.

$$\%\ \text{Cell viability} = \frac{\text{Sample absorbance} - \text{Blank absorbance}}{\text{Conntrol absorbance} - \text{Blank absorbance}} \text{x}100 \qquad (4.3)$$

2.2.4.3 Trypanotoxicity assay

Alamar Blue assay method was used in order to evaluate the impact of hydrophobic ion pairing of the QS on its trypanocidal activity against *T. evansi* parasite as described previously with some modifications (Juan et al., 2013; Räz et al., 1997). Briefly, *T. evansi* infected mice was

used to collect parasite by cardiac puncture, the isolated parasites from the blood o were suitably diluted with phosphate buffered saline with 10mM glucose (PSG) to get the initial density of 10^4 parasites/ 50µL. Further, a 96-well plate was seeded with 50 µL of parasite suspension, and treated with different concentrations (0.05, 0.25, 2, 10, 25, 50 µM) of QS, QS-Na.C complex, and QS-Na.C complex-loaded oily nanosuspension. Further, plate was incubated for 20 h in an incubator at 37ºC and 5% CO_2 and, 20µl of 0.5mM sodium resarzurin dye was added to the above plate and incubated again for 4h. In order to seize the reaction in the mixture, 50µl of 3%w/v sodium lauryl sulphate was added in the above plate (Amisigo et al., 2019; Baldissera et al., 2014). The plate was placed on Epoch Elisa plate reader and the excitation and emission wavelengths were set at 535 nm and 590 nm, respectively. %Viability of trypanosomes were calculated using equation 4.4.

$$\%\ \text{viability of trypanosome} = \frac{\text{Absorbance of the sample} - \text{Absorbance of the blank}}{\text{Absorbance of the control} - \text{Absorbance of the blank}} \text{x} 100 \qquad (4.4)$$

2.2.4.4 In vitro drug release

To determine the in vitro drug release profile of QS from the formulation, we used the sample and separate method as previously described with some modifications [31,32]. Briefly, either free QS or QS-Na.C loaded oily nanosuspension (equivalent to 10.0 mg of drug) was added to an Eppendorf centrifuge tube containing 1.0 mL of 0.2%v/v tween-80 and 0.05%w/v sodium azide in phosphate-buffered saline pH 7.4. The samples were maintained at 37°C in a water bath shaker assembly and kept under constant agitation of 100 rpm. At predetermined time points, the samples were centrifuged at 10,000 rpm for 5 minutes, and 200 µL was withdrawn from the supernatant. Fresh media was added to the Eppendorf tube after sample collection at each time point to replenish and maintain sink conditions. To determine the QS concentration, the samples were suitably diluted with acetonitrile: water (1:1), centrifuged and analysed by an RP-HPLC-based analytical method.

2.2.4.5 Pharmacokinetic studies in Wistar rats

The study protocol was approved by the Institutional Animal Ethics Committee of Birla Institute of Technology and Science, Pilani campus, Pilani, with Protocol no.: IAEC/RES/31/16. Male or female Wistar rats weighing 290.0±40.0g were habituated for 12 h

light-dark cycle for about week on a regular basis, housed in a sufficiently-ventilated cages along with proper exposure to food and water *ad libitum*. The animals were categorised into four different groups (n=4) such as free QS in water (I), QS in thixotropically thickened oil (II), QS-Na.C complex in olive oil (III), and QS-Na.C complex loaded oily nanosuspension at a dose of 7.5 mg/kg body weight.

Briefly, 300 µl of blood was collected by puncturing retro-orbital plexus of the rat at pre-determined time points (0, 1, 3, 6, 12, 24, 36, 48, 72, 120, 168, and 240 h) in an Eppendorf® centrifuge tube containing 10% w/v EDTA solution. Plasma from the blood was separated by the centrifugation at 7000 rpm for 10 minutes using REMI cooling centrifuge and further stored at -80ºC until analysis (Krishna et al., 2019, 2018). QS was analysed by developed and validated RP-HPLC method of analysis. Briefly, the plasma (100 µL) was spiked with 5 µL of internal standard (1 µg/mL 4,7-dichoromethane), QS was extracted from the plasma by protein precipitation method using 400µL of methanol: acetonitrile (1:1) as an extracting solvent. The samples were vortexed, and organic solvent was evaporated under a continuous N_2 stream and then were reconstituted with 100µL of ACN: water (1:1). QS was analysed using HPLC chromatography with Waters Sunfire® C18 3.5 um ODS (4.6 x 50 mm) column and sample injection volume of 50 µL. The binary mobile phase system consisted of acetonitrile (40%) and 2.5 mM sodium lauryl sulphate in 0.1% formic acid in water (60%) at a flow rate of 1 ml/min in isocratic mode with a total run time of 22 min and detection wavelength of 297 nm where HPLC column was maintained at 30°C throughout the study. Further, WiNonlin software version 6.3. was utilised to evaluate the pharmacokinetic parameters by non-compartmental analysis.

2.2.4.6 Pharmacokinetic studies in camels

Healthy camels weighing 550±30.0 kg with average age of 4-5 years were selected randomly from the farm of NRCC, Bikaner. Camels were observed periodically and given with proper exposure to food and water *ad libitum* during complete study period. One camel in each group was dosed by subcutaneous route with free QS or QS-Na.C complex loaded oily nanosuspension at a dose of 7.5 mg/kg body weight.

Briefly, 2-4 mL of the blood was collected from camel at pre-determined time points (0, 1, 3, 6, 12, 24, 36, 48, 72, 120, 168, 240, and 360 h) in a heparinised blood collection tube. Plasma was separated from the blood by the centrifugation at 5000 rpm for 8 minutes using REMI cooling centrifuge and further stored at -80ºC until analysis. The plasma samples were

extracted for the drug content by protein precipitation technique as described earlier for rat plasma with some modifications.

QS was analysed by developed and validated RP-HPLC method of analysis. Briefly, the plasma (200 µL) was spiked with 10 µL of internal standard (1 µg/mL 4,7-dichoromethane), QS was extracted from the plasma by protein precipitation method using 1 mL of methanol: acetonitrile (1:1) as an extracting solvent. The samples were vortexed, and organic solvent was evaporated and reconstituted with 200µL of ACN: water (1:1). QS in camel plasma was analysed using HPLC chromatography with Waters Sunfire® C18 3.5 um ODS (4.6 x 50 mm) column and sample injection volume of 50 µL. The binary mobile phase system consisted of acetonitrile (40%) and 2.5 mM sodium lauryl sulphate in 0.1% formic acid in water (60%) at a flow rate of 1 ml/min in isocratic mode with a total run time of 22 min and detection wavelength of 297 nm where HPLC column was maintained at 30°C throughout the study. Further, WiNonlin software version 6.3. was utilised to evaluate the pharmacokinetic parameters by non-compartmental analysis.

2.2.4.7 Antitrypanososmal efficacy in T. evansi infected mice model

Either male or female mice in each group of five, weighing 25 to 30 g each, were used for the study. Groups of 5 mice of almost uniform body weight were infected by intraperitoneal inoculation with 0.2ml of 1×10^3 viable trypanosomes. Mice diagnosed with parasitemia after 2-3 days of parasite inoculation were categorized as infected, and divided in different groups for subsequent treatments. Animal study protocol was approved by the Institute Animal Ethics Committee vide No. NRCC/PSME/6/(141)2000-Tech. The animals were provided with laboratory food and water *ad libitum* and maintained at ICAR-NRCC facility.

The mice showing consistent parasitemia for 3-5 days post inoculation of the parasites were labeled as infected and divided into 5 different groups of 5 animals, and the treatment was given by subcutaneous route. Group I [vehicle control (0.2mL normal saline solution)], group II [free QS (3.75mg/kg)], group III [free QS (7.5mg/kg)] and group IV [QS-Na.C complex loaded oily nanosuspension (3.75 mg/kg)], and group V [QS-Na.C complex loaded oily nanosuspension (7.5 mg/kg)]. The treatment was given subcutaneously near post scapular region, wherein each treatment group received the desired dosage according to the body weight. Two days post-treatment and subsequently once a week until day 75 each mouse was examined with the Matching Method for the presence of parasites by collecting about 2µL blood from the tail vein. Whereas to avoid errors in data recording and ensure accurate and comprehensive

analysis, body markings and codes were made on different anatomical areas of mice. The effectiveness of the therapy was determined by screening for the parasite presence and comparing the survival rate of animals to that of control group. Blood and organs from the group V were taken 75 days after the start of the therapy and were processed by polymerase chain reaction (PCR) assay method to determine whether parasite residues present if any after treatment. More detailed procedure about the infection in mice, extraction of the DNA from blood and various organs to determine efficacy of the treatment was adopted from (Prayag et al., 2023).

3. Results and discussion

3.1 Preparation of QS-Na.C complex

A hydrophobic ion-pairing approach was adopted to convert cationic hydrophilic quinapyramine sulphate into a hydrophobic complex. The number of anionic agents were screened as a counter-ion to QS as described in our previous publication (Prayag et al., 2021). It was evident from the study that sodium cholate showed maximum complexation at 1:2 molar ratio of drug: complexing agent. Owing to the bivalent nature of quinapyramine sulphate 2 moles of sodium cholate having unit negative charge were able to effectively form the complexation between the two. Hence, further studies were carried out using sodium cholate as a hydrophobic ion-pairing agent.

3.2 Characterization of QS-Na.C complex

3.2.1 % Yield and % complexation efficiency

% Yield of the QS-Na.C complex at optimised ratio of QS:Na.C of 1:2 was found to be 93.21 ± 4.23%. Whereas, % complexation was found to be 18.54 ± 3.89 and 81.35 ± 7.14 % at QS:Na.C ratio of 1:0.5 and 1:2, respectively.

3.2.2 FTIR

Fig. 4.1 a) showed FTIR spectra of QS, Na.C and QS-Na.C complex (descending order). FTIR spectra (blue coloured) of QS showed characteristic C=N stretch at 1729 cm^{-1}, N-H stretch representing amine salt at 2915 cm^{-1} and 2854 cm^{-1}, and S=O stretch corresponding to sulphoxide at 1184 cm^{-1}. Spectra in red corresponding to NC showed characteristic strong peak at 1052 cm^{-1} corresponding to C-O stretch of primary alcohol, and at 3741 cm^{-1} due to free -OH present in the structure. Further, FTIR spectra of QS-Na.C complex (black colour) showed

absence of characteristic amine salt peaks (2915 cm^{-1}, 2854 cm^{-1}), and S=O stretch at 1184 cm^{-1}, respectively which can be attributed to the loss of disodium sulphate after ionic exchange of sodium from Na.C and sulphate from QS.

3.2.3 XRD

Fig. 4.1 c) indicates XRD peaks of QS which shows sharp peaks at a diffraction angle (2Θ) of 7.50º, 14.45º, 15.95º, 20.44 º, 21.69 º, 26.43º and 27.43º representing crystalline nature of the drug. On the other hand, QS-Na.C complex showed absence of any sharp peaks indicating amorphous nature of QS in the complex.

3.2.4 DSC

Differential scanning calorimetric analysis of QS, Na.C, QS-Na.C physical mixture and QS-Na.C complex was performed as shown in fig. 4.1 b) Thermogram of QS showed two endothermic peaks at 252º and 260º C indicating the melting point of the QS and the degradation of the QS started beyond 282º C. Thermogram of Na.C showed three endothermic peaks corresponding to presence of water, glass transition (T_g) and melting at 107º, 192º and 270º C, respectively. Further, the physical mixture of QS-Na.C showed characteristic endothermic peaks as that of pure compounds. Whereas the QS-Na.C complex showed an exothermic peak at 244ºC probably due to the melt crystallization process occurred due to heating of the sample above glass transition temperatures (Corporation, n.d.). Moreover, endothermic peaks of both QS and Na.C were diminished as seen in the thermogram of QS-Na.C complex indicating physical interaction has occurred.

3.2.5 Solubility of QS-Na.C complex in different oils

Since the hydrophobic compounds rapidly dissolves in the oily phase, a solubility of the QS-Na.C complex in various oils was determined and presented in the fig. 4.1 d). It was observed that QS-Na.C complex showed high solubility glyceryl monolinoleate (Maisine), oleic acid, and castor oil. Whereas, cod liver oil and olive oil showed poor solubility of the complex. Olive oil showed minimal solubility of QS-Na.C complex and hence selected for the development of oil based nanosuspension.

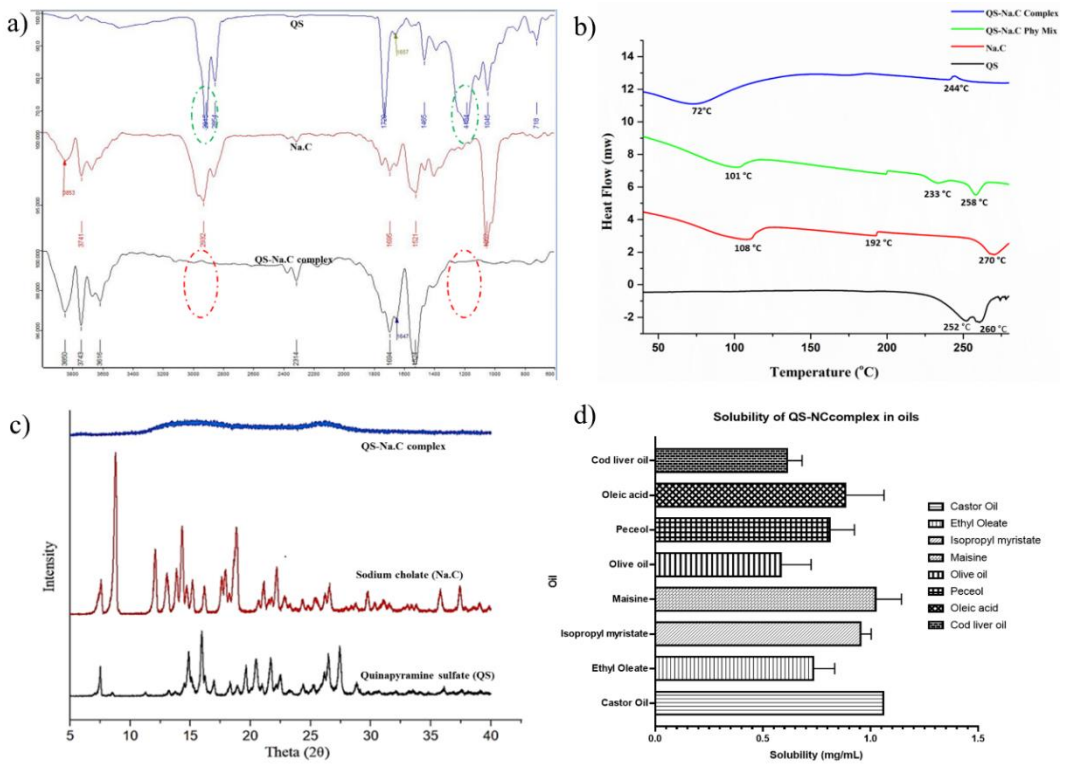

Fig. 4.1 Physicochemical characterization of QS-Na.C complex a) FTIR spectra, b) DSC thermograms of QS, Na.C, QS-Na.C physical mix and QS-Na.C complex, c) XRD spectra of QS, Na.C and QS-Na.C complex, and d) saturation solubility of QS-Na.C complex in different oils

3.3 Formulation and characterisation of QS-Na.C loaded oily nanosuspension

3.3.1 Formulation optimization of QS-Na.C complex loaded oily nanosuspension

Particle size, PDI, viscosity, and drug loading of the QS-Na.C loaded oily nanosuspension are presented in the table 4.1. Various critical process parameters (CPP) including, homogenization speed, homogenization time, sonication time and frequency as well as combined effect of homogenization and sonication was studied to obtain the desired particle size range as shown in the table 4.1.

Table 4.1. Optimization trials of QS-Na.C loaded oily nanosuspension

Process description	**Processing parameters**	**Particle size (nm) ± SD**
Complex dispersed in oil as is	None	9503 ± 58.93
High shear homogenizer	10,000 RPM, 5 min	7654 ± 19.27
	20,000 RPM, 5 min	6013 ± 26.74
	20,000 RPM, 15 min	5846 ± 39.65
High shear homogenizer Followed by probe sonication	20,000 RPM, 5 min 1 min (20 sec: ON, 10 sec: OFF)	2865 ± 47.65
Probe sonication	2 min (20 sec: ON, 10 sec: OFF)	3775 ± 22.13

Probe sonication	5 min 30 sec (20 sec: ON, 10 sec: OFF)	823 ± 21.14

It was found that there was significant impact of sonication process on the particle size of the formulation whereas, foam formation was evident in the batches where utilization of high shear homogenization was done. Furthermore, impact of drug loading on particle size as well as viscosity was also accessed in order to evaluate the injectability of the finished product (Fig. 4.2).

Table 4.2 represents the optimized formulation of QS-Na.C complex loaded oily nanosuspension which exhibits significantly high drug loading of about 38% w/v in the system. Although there are no specific claims for the limit viscosity of the optimized formulation, the syringability of the contents directly depends on the viscosity of the formulation. Here we evaluated the impact of % drug loading and % of Al-MS on the viscosity.

Table 4.2. The optimized formulation of the QS-Na.C complex-loaded nanosuspension

Sr no.	**Ingredient**	**Quantity**	**Role of ingredient**
1.	Quinapyramine sulphate	50.00 mg	Active
2.	Sodium cholate	80.85 mg	Hydrophobic-ion pairing agent
3.	Aluminium monostearate	150.00 mg	Thickening agent
4.	Olive oil	10.00 mL	Vehicle

3.3.2 Characterization of QS-Na.C complex loaded oily nanosuspension

3.3.2.1 Particle size determination by dynamic light scattering

Since particle size, and PDI has a significant role in the drug release from the formulation, it becomes essential to study the particle size of the finished product. Fig. 4.2 depicts particle size, and PDI of the QS-Na.C loaded oily nanosuspension.

3.3.2.2 Viscosity determination

As discussed earlier, syringability, transportation of the fluids during formulation development, and *in vivo* performance of the developed formulation is directly dependent on the viscosity of the formulation. Since oil-based formulations exhibit inherent viscosity, it becomes essential to study this parameter as a quality control parameter. The present study utilizes the incorporation of aluminium monostearate (AL-MS) in the olive oil, which imparts thixotropic

behaviour to the oil, hereby enhancing the viscosity. Fig. 4.2 b) depicts the viscosity of olive oil, 1.5% w/v Al-MS in olive oil, and QS-Na.C complex loaded oily nanosuspension as determined by Anton Paar Rheometer. It is evident from the experiment that a 3.42-fold increase in viscosity was observed after the such incorporating Al-MS in the olive oil. Further, the viscosity of olive oil containing 1.5% Al-MS and QS-Na.C complex enhanced the viscosity to significantly higher levels (8.61-folds) than the olive oil, describing the role of % solids and concentration of Al-MS in the impartation of resistance to flow in the system.

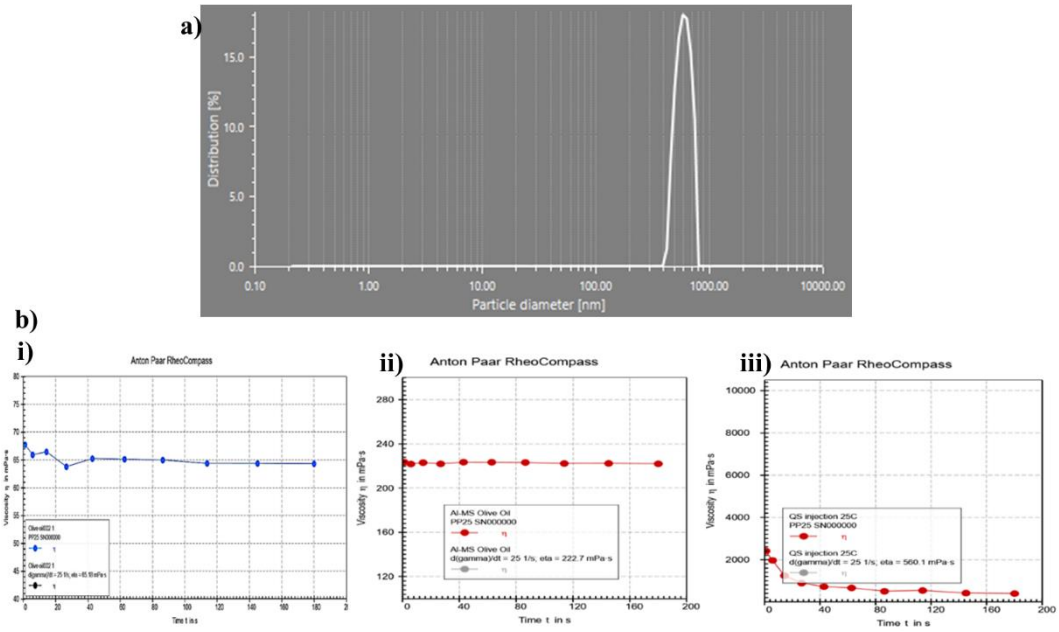

Fig. 4.2 Physicochemical characterisation of QS-Na.C complex loaded oily nanosuspension, a) Particle size histogram of QS-Na.C complex loaded oily nanosuspension, b) rheogram of i) olive oil, ii) 1.5% Al-MS in olive oil, and iii) QS-Na.C complex loaded oily nanosuspension.

3.3.2.3 Trypanocidal assay

Different concentrations of the free QS, QS-Na.C complex, and QS-Na.C complex loaded oily nanosuspension were assessed for the *in vitro* trypanocidal activity against the *T. evansi* parasite. It was observed that at higher concentrations of complex, (more than 5.0 µM), the enhanced trypanocidal effect can be seen as compared to free drug.

Fig. 4.3 a) presents the concentration-dependent trypanocidal activity of free QS, QS-Na.C complex and QS-Na.C complex loaded oily nanosuspension against *T. evansi*. It was evident that there was linear corelation between increase in concentration of QS and decrease in viability of the *trypanosome* after the treatment with free QS or QS-Na.C complex loaded oily nanosuspension. A significant difference in IC_{50} of 51.12 µM and 38.15 µM was observed for free QS and QS-Na.C complex-loaded oily nanosuspension, respectively. An increase in

trypanocidal activity of the QS-Na.C complex could be attributed to the hydrophobic nature exhibited after the complexation of parent QS with sodium cholate, which enables the molecule to enter the cellular component of the *trypanosome*.

3.3.2.4 Cytotoxicity assay

Cytotoxic potential of the QS, QS-Na.C complex and QS-Na.C complex loaded oily nanosuspension was evaluated in THP-1 cells using the MTT assay method. It was evident from the study that free QS showed higher cytotoxicity at all concentration ranges studied due to cytotoxic potential exhibited by the molecule itself. Whereas, it was observed that impartation of the hydrophobicity in the QS-Na.C complex group had a similar cytotoxic effect as that of free QS on the THP-1 cells at lower concentration but, eventually at higher concentrations there was significant difference ($p<0.0001$) in the cytotoxicity between two (fig. 4.3 b). Further, % cell viability of THP-1 cells was found to be 73.87 ± 2.56%, and 83.91 ± 3.19% for free QS and QS-Na.C complex loaded oily injection, respectively at minimum effective concentration (MEC) of QS (30.04 µM) (Zhang et al., 1992). Moreover, QS-Na.C complex incorporated in oily vehicle showed minimal cytotoxicity at all the concentrations studied, suggesting the role of the hydrophobic oily vehicle in the release of QS from the system. It can be postulated from the study that the oily vehicle forms an intermediate barrier layer between the hydrophilic cell culture medium used during study.

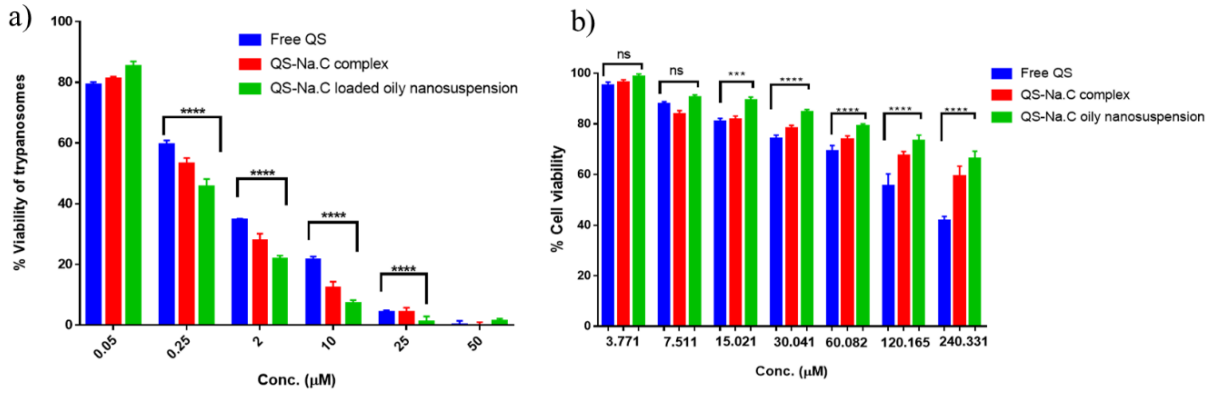

Fig. 4.3 *In vitro* studies a) *In vitro* trypanocidal assay of free QS and QS-Na.C complex loaded oily nanosuspension in *T. evansi* parasite (Data are represented as mean ± SD (n = 3). Statistical comparison was made using two-way ANOVA with Tukey's multiple comparison tests, where ****p < 0.0001) and, b) cytotoxicity assay of free QS, QS-Na.C complex, and QS-Na.C complex loaded oily nanosuspension in THP-1 cell lines (statistical comparison was made using two-way ANOVA with Tukey's multiple comparison test ****p < 0.0001).

3.3.2.5 In vitro drug release

Sample and separate method with small volumes of release media, and the other experimental conditions were adopted during the release studies usually mimics the presence of small volumes of tissue fluids at the S.C. site of administration. Fig. 4.4 depicts various drug release profiles of free QS in water, free QS in olive oil consisting of 1.5% AL-MS w/v, QS-Na.C complex in olive oil and QS-Na.C complex in olive oil with 1.5% w/v AL-MS. It was observed that almost 80% of the drug was present in release media at the end of 4 h in free QS group whereas, it took almost 40 h to reach 80% drug release from free QS in structured olive oil group. Further, the ability of hydrophobic QS-Na.C complex to retard the release rate also showed positive results wherein, QS-Na.C complex dispersed in olive oil showed 81.42 ± 4.78% of QS released after 72 h. Further, QS-Na.C complex loaded oily nanosuspension showed more than 80% drug release at the end of 7th day of the study. It was evident from the study that significant decrease in water solubility of the parent molecule QS as well as hydrophobic microenvironment created by the oily component has enabled the sustained drug release of the drug over period of time. Moreover, experimentally it was observed that there was marked gelling behaviour exhibited by the study groups consisting Al-MS in olive oil which necessarily could have contributed to the slowing of drug release (Gray and Alexander, 2002; Wang and Rackaitis, 2008).

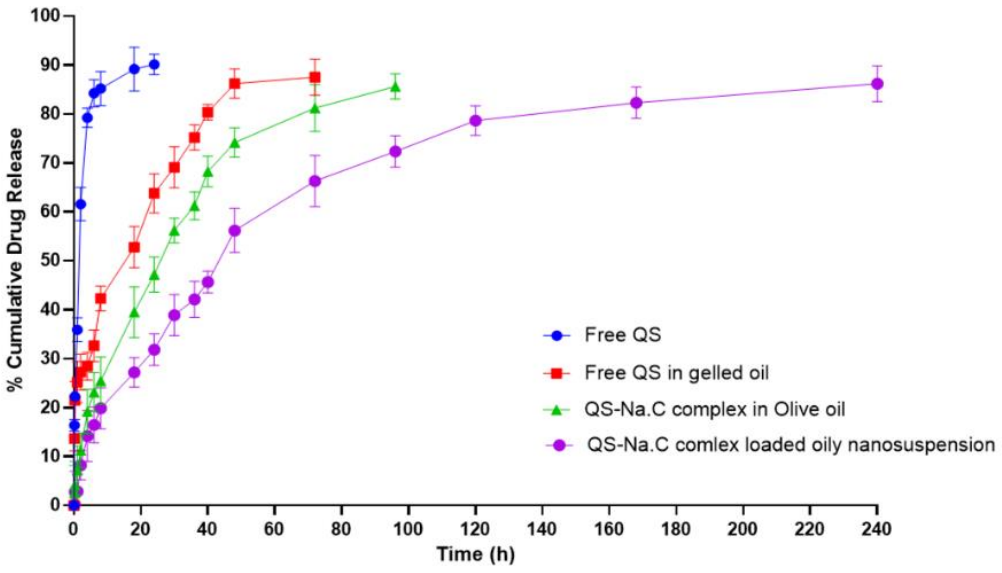

Fig. 4.4 *In vitro* drug release profile of free QS, free QS in gelled oil, QS-NC complex dispersed in olive oil and QS-NC complex loaded oily nanosuspension (n=5)

3.3.2.6 Pharmacokinetic study in rats

Pharmacokinetic parameters obtained after non-compartmental analysis (NCA) of the data are presented in the Table 4.3. Whereas, fig. 4.5 represents plasma conc. Vs time profile of the various groups studied after SC administration.

After SC administration of free QS, C_{max} of QS was found to be 30 min and plasma concentration reached below detection limits after 12 h. As shown in the fig. 4.5, free QS when administered in a structured vehicle showed increase in $AUC_{0-\infty,}$ volume of distribution (Vz/F), and mean residence time ($MRT_{0-\infty}$) by 1.14-folds, 4.01-folds, and 3.35-folds, respectively as compared to the free QS. Whereas, $t_{1/2}$ was significantly increased by 3.49-folds suggesting the role of oily vehicle in protracted release *in vivo*. Although we observed marked change in the PK parameters of the free QS, the inherent higher water solubility could pose significant challenges in the drug delivery including quick removal of oily vehicle from the site of administration, leading to faster onset of action, and rapid elimination of the drug from the body. In order to overcome above cited limitations, we studied the impact of hydrophobization of the parent molecule QS on the PK parameters wherein, QS-Na.C complex was dispersed in olive oil and PK parameters were determined after subcutaneous administration. It was observed that $t_{1/2}$, $AUC_{0-\infty}$, Vz/F, and $MRT_{0-\infty}$ were 5.37-folds, 1.75-folds, 2.75-folds and 17.35-folds, respectively higher than the observed PK parameters of the free QS in water. Further, 1.98-folds reduction in the plasma clearance (Cl/F) of the drug highlighted impact of reduced water solubility of the QS on the protracted drug plasma concentrations. Although the QS-Na.C complex dispersed in olive oil showed significant improvement in the PK parameters than free QS, the drug plasma concentrations reached below detection limits after 3rd day post administration. The above studies highlighted the role of oily vehicle and hydrophobicity of the drug in prolongation of *in vivo* performance of the drug. Hence, the dual impact of vehicle and hydrophobization was studied by administering QS-Na.C complex loaded oily nanosuspension group in rats which showed 13.54-folds, 7.09-folds, 1.78-folds, and 17.35-folds increase in $t_{1/2}$, $AUC_{0-\infty}$, Vz/F, and $MRT_{0-\infty}$, respectively as compared to free QS. Further, 7.08-folds reduction in plasma clearance was also prominent indicator of protracted drug plasma concentrations than the free QS. Moreover, C_{max} ranged from 5778.27 ± 5.61 ng/mL to 1075.07 ± 6.67 ng/mL for free QS and QS-Na.C complex in olive oil was well within the reported MEC of 1-16µg/mL (Zhang et al., 1992). The PK profile showed following the initial rise in plasma concentration of QS, drug concentrations were reduced significantly from 280.9

± 119.2 ng/mL at the 5th day of dosing and reached to 22.12 ± 9.51 ng/mL at the end of 10th day of treatment reaching below quantification limits beyond it.

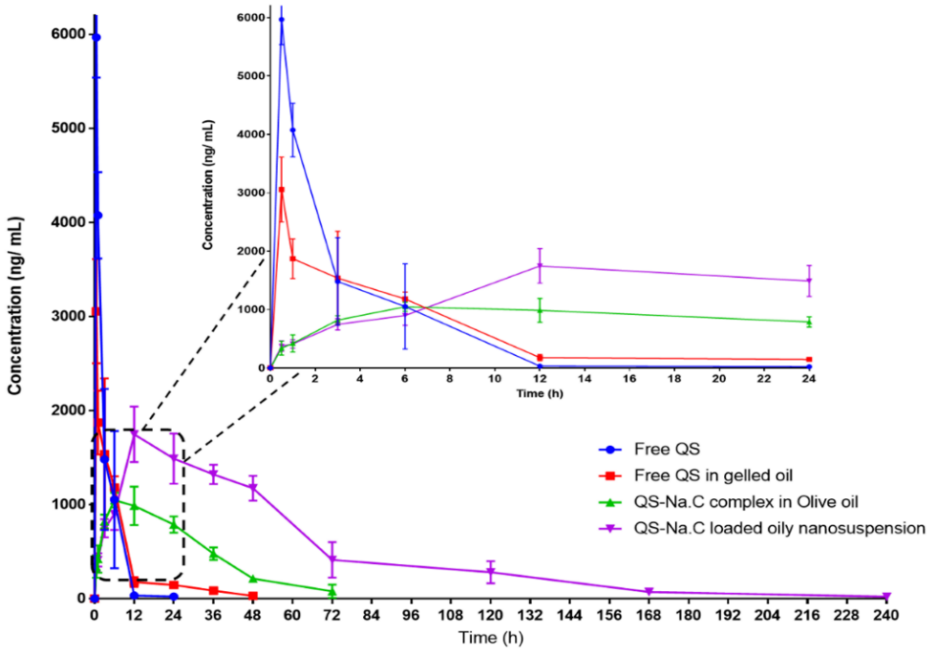

Fig 4.5 Pharmacokinetic profile of free QS, free QS in gelled oil, QS-NC complex in olive oil, and QS-Na.C complex loaded oily nanosuspension

Usually, APIs soluble or dispersed in oily vehicles when injected subcutaneously (SC) or intramuscularly (IM) creates a depot which can retard the drug release from days to months depending on the characteristic of API and the oily vehicle used (Surve and Jindal, 2020). It has been observed that drug partitioning from oily solution to tissue fluids, spreading of oil from administered site and lymphatic and secondary depot formation are the major determinants of the drug release. When compared with most of the other LAI depot, oil-based formulations relish various advantages including ease of formulation development, large scale production, and most importantly least number of excipients making it cost effective product. We hereby, assume the protracted drug plasma concentrations of the QS in oily nanosuspension could be attributed to dual retard mechanism exhibited by the formulation. For instance, it is well known that rapid depot formation takes place after S.C administration of the treatment. Here, the formulation once injected into SC region forms a primary depot which is primary cause of protracted drug release by forming a barrier which restricts the spreading into the nearby tissue fluids. Further, the ability of Al-MS to form a gel on contact with tissue fluids causes slow diffusion of tissue fluids, and further reduced solubilization of the hydrophobic QS-Na.C complex molecules in tissue fluids serves the purpose of protracted drug release.

Table 4.3. Plasma non-compartmental PK parameters obtained after SC administration of QS and QS-Na.C complex loaded oily nanosuspension in Wistar rats using Phoenix WiNonlin software (version 6.3)

Parameter	**Results**			
	Free QS	**Free QS in structured oil**	**QS-Na.C complex in olive oil**	**QS-Na.C complex loaded oily nanosuspension**
$t_{1/2}$ (h)	2.53 ± 14.37	8.84 ± 10.42	13.59 ± 15.97	34.27 ± 12.10
C_{max} (ng/mL)	5778.27 ± 5.61	3055.62 ± 18.13	1075.07 ± 6.67	1803.46 ± 10.87
AUC $_{0-\infty}$	15891.76 ± 3.12	18255.12 ± 12.37	27934.91 ± 20.16	112820.52 ± 2.76
Vz/F (L/Kg)	1232.83 ± 7.26	4949.68 ± 29.93	3395.78 ± 22.78	2193.39 ± 12.62
Cl/F	314.09 ± 3.01	275.77 ± 11.51	157.81 ± 14.85	44.34 ± 2.77
$MRT_{0-\infty}$ (h)	3.25 ± 9.61	10.89 ± 15.80	24.21 ± 24.37	56.4 ± 8.81

Data represented as mean ± SE (n=4)

3.3.2.7 Pharmacokinetic study in camels

As evidenced during PK studies in Wistar rats, PK studies in camels too showed protracted drug plasma concentrations of the QS after SC administration of QS-Na.C complex loaded oily nanosuspension. Based on the body physiology of the camels, free QS was detectable up to 3rd day whereas, QS-Na.C complex loaded oily nanosuspension showed detectable drug plasma concentration by the end of 15th day post dosing.

Non-compartmental PK analysis evaluated using Phoenix WiNonlin 6.3 showed substantial enhancement in the PK parameters in formulation treated group than free QS. For instance, there was 42.6-folds, 10-folds, 5.01-folds, and 15.98-folds increase in $t_{1/2}$, $AUC_{0-\infty}$, Vz/F, and $MRT_{0-\infty}$ respectively, in QS-Na.C complex loaded nanosuspension group than the free QS treatment group. Further 10-fold reduction in plasma clearance showed the enhanced exposure of the QS from the formulation which could serve for betterment of antitrypanosomal efficacy in target population i.e. camels. The results suggest that the protracted drug release *in vivo* could serve as a pathbreaking in the treatment of *trypanosomiasis* in animals.

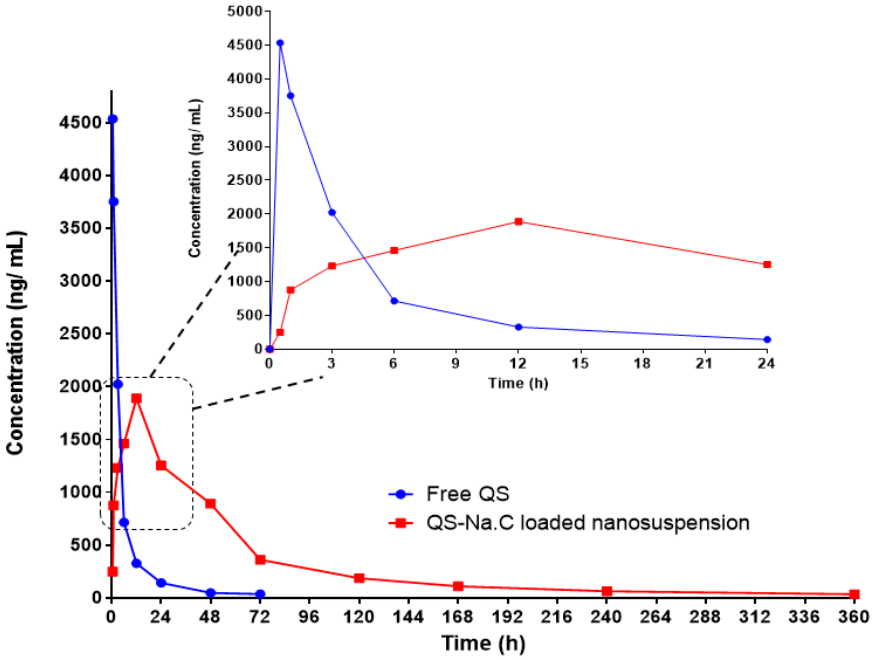

Fig.4.6. Pharmacokinetic profile of QS in camels

Table 4.4 Plasma non-compartmental PK parameters obtained after SC administration of QS and Q1S-Na.C complex loaded oily nanosuspension in Camels using Phoenix WiNonlin software (version 6.3)

Parameter	**Non-compartmental analysis**	
	Free QS	**QS-Na.C loaded oil-based nanosuspension**
$t_{1/2}$ (h)	2.23	95.45
C_{max} (ng/mL)	3671.89	2388.03
AUC $_{0-\infty}$	12389.43	123931.32
Vz/F (L/Kg)	2010.40	10080.086
Cl/F	605.35	60.51
$MRT_{0-\infty}$ (h)	3.94	63.04

3.3.2.8 In vivo antitrypanosomal efficacy in T. evansi infected mice

Post inoculation of the treatments, mice showed varying grades of responses towards treatment which was confirmed by the presence of parasitaemia and confirmed by matching method described earlier (Herbert and Lumsden, 1976). A group of mice treated with QS-Na.C complex loaded oily nanosuspension (equivalent to 3.75 mg/kg of QS) showed initial response to the treatment with a steady decrease of blood parasitaemia by the 2nd day of dosing. However, 3 out of 5 mice got relapsed on 7th day leading to death by the 11th day of treatment. The rest 2 mice survived in the group showed relapse after 9th day of treatment. Further, the 2

mice survived in the group were repeated with dose of 3.75 mg/kg and were examined further on alternate days for the presence of parasitaemia. Finally, by the end of 55th day of 1st dose, both animals died due to relapse of infection and undulating parasitaemia. In the parallel study, mice treated with free QS (3.75 mg/kg) showed relapse of parasitaemia by the 11th day post treatment, all of which died by the end of 15th day.

In order to evaluate the impact of increasing concentrations of drug on parasite clearance in infected mice, the dose was doubled to 7.5 mg/kg and evaluated for presence of parasitaemia post treatment. The group treated with QS-Na.C complex loaded oily nanosuspension revealed progressive decrease in parasite numbers in microscopic fields. All the mice in this group showed steady decrease in level of parasitaemia on 3rd day post therapy and became aparasitaemic by 7th or 8th day onwards and remained so for next 60 days and beyond highlighting CD_{100} was achieved in the treatment group. During the treatment period no further parasite relapse or parasitaemic wave was observed. Usually, *trypanosomiasis* is characterised by the frequent relapse of infection followed by parasitaemic wave due to the ability of *trypanosome* to evade immune evasion and conceal in the interstitial spaces of different tissues or organs, which leads to failure of the therapy (Matthews, 2005; Smith et al., 2017). To address this issue and confirm the parasite clearance and loss of infectivity in the treated animals, blood from the treated mice was injected into healthy mice, which failed to elicit any passage of subsequent infection.

Besides the treatment in this particular group, the QS-Na.C complex loaded oily nanosuspension was also inoculated in the mice exhibiting teeming parasitaemia, different age and weight animals which showed parasite clearance in these animals too.

On the other hand, *T. evansi-infected* mice treated with 7.5 mg/kg of free QS showed pronounced acute toxicity where 4 out of 5 animals died within 16 h of treatment. The single surviving mice in the group showed parasite clearance by the 4th-day post-treatment and remained aparasitaemic till 75 days. These observations showed that neither CD_{80} nor CD_{100} was achieved in the free drug-treated group.

Amplification of DNA was done by PCR assay to study presence of DNA of the parasite if any to confirm the efficacy of the QS-Na.C complex loaded oily nanosuspension treatment [fig. 4.7 b) and 4.7 c)]. It was observed that all the DNA samples from the infected mice showed positive signals of standing infection revealed by amplification of size ~500 bp.

Fig. 4.7 b) indicated PCR amplicon from infected mice where well no 1 indicates *T. evansi* specific marker, well 2 to 7 indicate liver, lungs, kidney spleen, heart, and brain tissues,

respectively, and well no 8 indicates PBS alone. Further, Fig. 4.7 c) represents organs from the mice treated with QS-Na.C complex loaded oily nanosuspension treatment group where well no. 1 represents *T. evansi* specific marker and well 2 to 6 indicate liver lungs, kidney spleen, and heart, respectively, and well 7 represents blood from an infected animal. Well, 8 has no specific marker in it. It is evident from the intensity of signals that the treated group showed an absence of amplicons as compared to its infected tissue counterpart, indicating that treatment led to the complete clearance of parasites from the system. (Brain tissues were omitted due to minimal brain involvement as suggested by weak bands in infected tissue samples [fig. 4.7 b)]. Hence, it can be concluded that the single dose of the designed QS-Na.C complex-loaded oily nanosuspension could effectively clear the infection at the molecular level from the system.

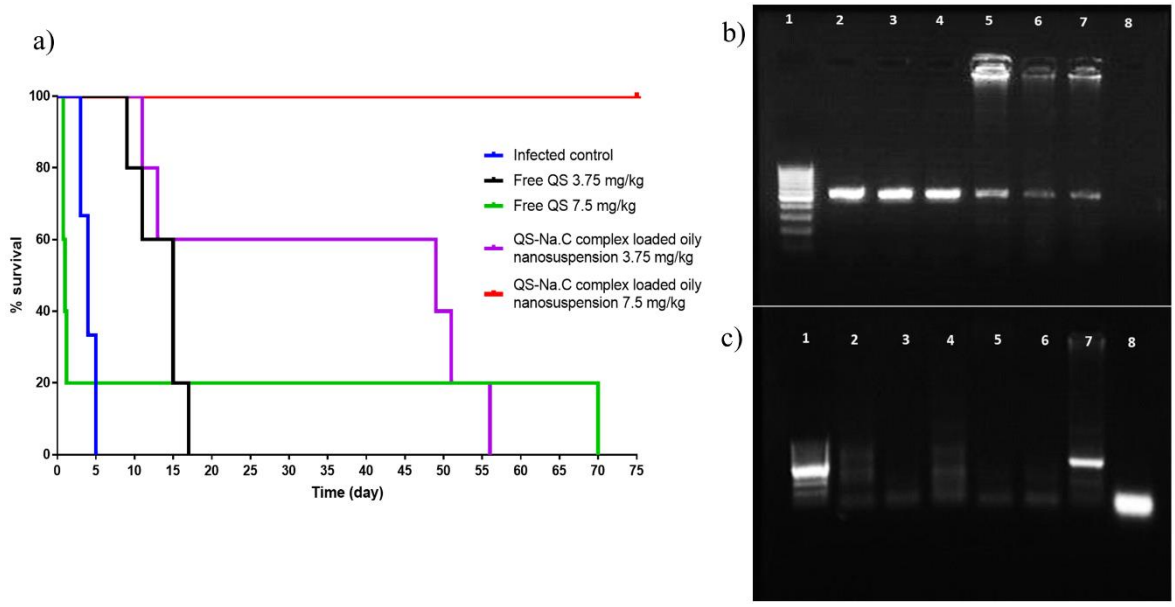

Fig. 4.7 *In vivo* pre-clinical efficacy of QS-Na.C oily nanosuspension a) % survival plot of the *T. evansi* infected mice after treatment, b), and c) PCR of DNA extracted from various organs after treatment with QS-Na.C complex loaded oily nanosuspension using mitochondrial DNA primer pair Kin1 and Kin 2 where upper panel indicates infected mice organs and lower panel (excluding well 1 and 8) indicates DNA isolated from 7.5 mg/ kg treated group.
Fig 4.7 b)- Well no. 1 indicates *T. evansi* specific marker, well no. 2 to 7 indicates liver, lungs, kidney spleen, heart, and brain, respectively. Lane 8 represents PBS alone.
Fig 4.7 c)- Well no. 1 indicates *T. evansi* specific marker, well no 7 indicates blood from infected animal, and well no. 8 indicated no target specific marker. Whereas well 2 to 6 indicate, liver, lungs, kidney spleen, and heart, respectively.

4. Conclusion

Hydrophilic quinapyramine sulphate (QS) can be ionically reacted with a hydrophobic counter-ion to reduce its hydrophilicity, resulting in an approach known as hydrophobic-ion pairing. In our study, we employed this method to impart hydrophobicity to QS and disperse it in thixotropically thickened oily vehicles. The resulting hydrophobized QS exhibited a significant increase in trypanocidal activity, as well as protracted drug plasma concentrations observed through in vivo pharmacokinetic studies. Moreover, *in vivo* efficacy studies showed enhanced antitrypanosomal activity in an infected mouse model of *T. evansi*. Our findings suggest about simple, cost-effective formulation with high drug loading which has the potential to serve as an advanced veterinary treatment for *trypanosomiasis* in domestic animals.

References:

Amisigo, C.M., Antwi, C.A., Adjimani, J.P., Gwira, T.M., 2019. In vitro anti-trypanosomal effects of selected phenolic acids on Trypanosoma brucei. PLoS One 14, 1–17. https://doi.org/10.1371/journal.pone.0216078

Baldissera, M.D., Da, A.S., Oliveira, C.B., Santos, R.C. V, Vaucher, R.A., Raffin, R.P., Gomes, P., Dambros, M.G.C., Miletti, L.C., Boligon, A.A., Athayde, M.L., Monteiro, S.G., 2014. Experimental Parasitology Trypanocidal action of tea tree oil (Melaleuca alternifolia) against Trypanosoma evansi in vitro and in vivo used mice as experimental model. Exp. Parasitol. 141, 21–27. https://doi.org/10.1016/j.exppara.2014.03.007

Barrett, M.P., Vincent, I.M., Burchmore, R.J., Kazibwe, A.J., Matovu, E., 2011. Drug resistance in human African trypanosomiasis. Future Microbiol. 6, 1037–1047. https://doi.org/10.2217/FMB.11.88

Cattaneo, D., Gervasoni, C., 2019. Pharmacokinetics and Pharmacodynamics of Cabotegravir, a Long-Acting HIV Integrase Strand Transfer Inhibitor. Eur. J. Drug Metab. Pharmacokinet. 44, 319–327.

Corporation, S., n.d. Chapter 2: What is a DSC? : SHIMADZU [WWW Document]. URL https://www.shimadzu.com/an/service-support/technical-support/analysis-basics/fundament_thermal/2/index.html (accessed 2.2.23).

Devrim, B., Bozkır, A., 2015. Design and Evaluation of Hydrophobic Ion-Pairing Complexation of Lysozyme with Sodium Dodecyl Sulfate for Improved Encapsulation of Hydrophilic Peptides / Proteins by Lipid-Polymer Hybrid Nanoparticles Nanomedicine & Nanotechnology. J. Nanomed. Nanotechnol. 6, 1–5. https://doi.org/10.4172/2157-7439.1000259

Donthi, M.R., Saha, R.N., Singhvi, G., Dubey, S.K., 2023. Dasatinib-Loaded Topical Nano-Emulgel for Rheumatoid Arthritis: Formulation Design and Optimization by QbD, In Vitro, Ex Vivo, and In Vivo Evaluation. Pharm. 2023, Vol. 15, Page 736 15, 736. https://doi.org/10.3390/PHARMACEUTICS15030736

Edagwa, B.J., Guo, D., Puligujja, P., Chen, H., Mcmillan, J., Liu, X., Gendelman, H.E., Narayanasamy, P., 2014. Long-acting antituberculous therapeutic nanoparticles target macrophage endosomes. https://doi.org/10.1096/fj.14-255786

Gray, V.R., Alexander, A.E., 2002. Studies on Aluminum Soaps. II. The Composition, Structure, and Gelling Properties of Aluminum Soaps. J. Phys. Colloid Chem. 53, 23–38. https://doi.org/10.1021/J150466A003

Health, T. center for food security and public H., 2009. African Animal Trypanosomiasis.

Herbert, W.J., Lumsden, W.H.R., 1976. Trypanosoma brucei: A rapid “matching” method for estimating the host’s parasitemia. Exp. Parasitol. 40, 427–431. https://doi.org/10.1016/0014-4894(76)90110-7

Hirota, K., Doty, A.C., Ackermann, R., Zhou, J., Olsen, K.F., Feng, M.R., Wang, Y., Choi, S., Qu, W., Schwendeman, A.S., Schwendeman, S.P., 2016. Characterizing release mechanisms of leuprolide acetate-loaded PLGA microspheres for IVIVC development

I: In vitro evaluation. J. Control. Release 244, 302–313. https://doi.org/10.1016/J.JCONREL.2016.08.023

Jornada, D.H., Dos Santos Fernandes, G.F., Chiba, D.E., De Melo, T.R.F., Dos Santos, J.L., Chung, M.C., 2015. The Prodrug Approach: A Successful Tool for Improving Drug Solubility. Mol. 2016, Vol. 21, Page 42 21, 42. https://doi.org/10.3390/MOLECULES21010042

Juan, D.U.B., José MacEira, Sonia Morales, Angélica García-Pérez, Manuel, E.M.T., Garcia-Salcedo, J.A., 2013. Nicotinamide inhibits the lysosomal cathepsin b-like protease and kills African trypanosomes. J. Biol. Chem. 288, 10548–10557. https://doi.org/10.1074/jbc.M112.449207

Kalhapure, R.S., Mocktar, C., Sikwal, D.R., Sonawane, S.J., Kathiravan, M.K., Skelton, A., Govender, T., 2014. Ion pairing with linoleic acid simultaneously enhances encapsulation efficiency and antibacterial activity of vancomycin in solid lipid nanoparticles. Colloids Surfaces B Biointerfaces 117, 303–311. https://doi.org/10.1016/j.colsurfb.2014.02.045

Krishna, K.V., Saha, R.N., Puri, A., Viard, M., Shapiro, B.A., Dubey, S.K., 2019. Pre-clinical compartmental pharmacokinetic modeling of 2-[1-hexyloxyethyl]-2-devinyl pyropheophorbide-a (HPPH) as a photosensitizer in rat plasma by validated HPLC method. Photochem. Photobiol. Sci. 18, 1056–1063. https://doi.org/10.1039/C8PP00339D/METRICS

Krishna, K.V., Saha, R.N., Singhvi, G., Dubey, S.K., 2018. Pre-clinical pharmacokinetic-pharmacodynamic modelling and biodistribution studies of donepezil hydrochloride by a validated HPLC method. RSC Adv. 8, 24740–24749. https://doi.org/10.1039/C8RA03379J

Manual, M.V., n.d. Drugs Commonly Used for Trypanosomiasis in Domestic Animals [WWW Document]. URL https://www.msdvetmanual.com/multimedia/table/drugs-commonly-used-for-trypanosomiasis-in-domestic-animals (accessed 1.4.23).

Manuja A, Dilbaghi N, Kaur H, Saini R, Barnela M, Chopra M, Manuja B, Kumar R, Kumar S, Riyesh T, Singh S, Y.S., 2018. Nano-Structures & Nano-Objects Chitosan quinapyramine sulfate nanoparticles exhibit increased trypanocidal activity in mice. Nano-Structures & Nano-Objects 16, 193–199.

Manuja A, Kumar S, Dilbaghi N, Bhanjana G, Chopra M, Kaur H, Kumar R, Manuja B, Singh S, Y.S., 2014. Quinapyramine sulfate-loaded sodium alginate nanoparticles show enhanced trypanocidal activity. Nanomedicine 9, 1625–1634.

Markovic, M., Ben-Shabat, S., Dahan, A., 2020. Prodrugs for Improved Drug Delivery: Lessons Learned from Recently Developed and Marketed Products. Pharmaceutics 12, 1–12. https://doi.org/10.3390/PHARMACEUTICS12111031

Matthews, K.R., 2005. The developmental cell biology of Trypanosoma brucei. J. Cell Sci. 283–290. https://doi.org/10.1242/jcs.01649

Murray, M., Gray, A.R., 1984. The current situation on animal trypanosomiasis in Africa. Prev. Vet. Med. 2, 23–30. https://doi.org/10.1016/0167-5877(84)90045-X

Prayag, K., Surve, D.H., Paul, A.T., Kumar, S., Jindal, A.B., 2020. Nanotechnological interventions for treatment of trypanosomiasis in humans and animals. Drug Deliv. Transl. Res. 10, 945–961.

Prayag, K.S., Paul, A.T., Ghorui, S.K., Jindal, A.B., 2023. Preclinical evaluation of quinapyramine sulphate-loaded lipidic nanocarriers for trypanocidal effect against Trypanosoma evansi. J. Drug Deliv. Sci. Technol. 81, 104215. https://doi.org/10.1016/j.jddst.2023.104215

Prayag, K.S., Paul, A.T., Ghorui, S.K., Jindal, A.B., 2021. Preparation and Evaluation of Quinapyramine Sulphate-Docusate Sodium Ionic Complex Loaded Lipidic Nanoparticles and Its Scale Up Using Geometric Similarity Principle. J. Pharm. Sci. 110, 2241–2249.

Rautio, J., Kumpulainen, H., Heimbach, T., Oliyai, R., Oh, D., Järvinen, T., Savolainen, J., 2008. Prodrugs: design and clinical applications. Nat. Rev. Drug Discov. 7, 255–270. https://doi.org/10.1038/nrd2468

Räz, B., Iten, M., Grether-Bühler, Y., Kaminsky, R., Brun, R., 1997. The Alamar Blue® assay to determine drug sensitivity of African trypanosomes (T.b. rhodesiense and T.b. gambiense) in vitro. Acta Trop. 68, 139–147. https://doi.org/10.1016/S0001-706X(97)00079-X

Ristroph, K.D., Prud, R.K., 2019. Hydrophobic ion pairing : encapsulating small molecules , peptides , and proteins into nanocarriers. Nanoscale Adv. 4207–4237.

Shah, K.A., Date, A.A., Joshi, M.D., Patravale, V.B., 2007. Solid lipid nanoparticles (SLN) of tretinoin: Potential in topical delivery. Int. J. Pharm. 345, 163–171. https://doi.org/10.1016/J.IJPHARM.2007.05.061

Smith, T.K., Bringaud, F., Nolan, D.P., Figueiredo, L.M., 2017. Metabolic reprogramming during the Trypanosoma brucei life cycle. F1000 Res. 6, 1–12. https://doi.org/10.12688/f1000research.10342.1

Surve, D.H., Jindal, A.B., 2021. Development of cationic Isometamidium chloride loaded long-acting lipid nanoformulation: optimization, cellular uptake, pharmacokinetics, biodistribution, and immunohistochemical evaluation. Eur. J. Pharm. Sci. 167, 106024. https://doi.org/10.1016/J.EJPS.2021.106024

Surve, D.H., Jindal, A.B., 2020. Recent advances in long-acting nanoformulations for delivery of antiretroviral drugs. J. Control. Release 324, 379–404.

Vilos, C., Velasquez, L.A., Rodas, P.I., Zepeda, K., Bong, S.-J., Herrera, N., Cantin, M., Simon, F., Constandil, L., 2015. Preclinical Development and In Vivo Efficacy of Ceftiofur-PLGA Microparticles. https://doi.org/10.1371/journal.pone.0123335

Vollner, H., 2018. Determination of the trypanocidal drugs Homidium , Isometamidium and Quinapyramine in bovine serum or plasma using HPLC Isometamidium and Quinapyramine in bovine serum or plasma Vollner.

Wang, X., Rackaitis, M., 2008. Gelling nature of aluminum soaps in oils. J. Colloid Interface Sci. 331, 335–342. https://doi.org/10.1016/J.JCIS.2008.11.032

Wibel, R., Friedl, J.D., Zaichik, S., Bernkop-Schnürch, A., 2020. Hydrophobic ion pairing (HIP) of (poly)peptide drugs: Benefits and drawbacks of different preparation methods. Eur. J. Pharm. Biopharm. 151, 73–80. https://doi.org/10.1016/J.EJPB.2020.04.004

Wong, H.L., Bendayan, R., Rauth, A.M., Wu, X.Y., 2004. Development of solid lipid nanoparticles containing ionically complexed chemotherapeutic drugs and chemosensitizers. J. Pharm. Sci. 93, 1993–2008.

Wu, J., Williams, G.R., Branford-White, C., Li, H., Li, Y., Zhu, L.M., 2016. Liraglutide-loaded poly(lactic-co-glycolic acid) microspheres: Preparation and in vivo evaluation. Eur. J. Pharm. Sci. 92, 28–38. https://doi.org/10.1016/J.EJPS.2016.06.018

Yashica Pharmaceuticals Pvt. Ltd., n.d. Product Information- Quinapyramine Chloride/Sulphate BP [WWW Document]. URL https://www.pharmarawmaterials.com/quinapyramine-chloride-sulphate.html (accessed 7.6.22).

Zhang, Z.Q., Giroud, C., Baltz, T., 1992. In vivo and in vitro sensitivity of Trypanosoma evansi and T . equiperdum to diminazene, suramin, MelCy, quinapyramine and isometamidium. Acta Trop. 50, 101–110.

Chapter 5: *In Vitro-In Vivo* Correlation of Quinapyramine Sulphate-Loaded Oil-Based Nanosuspension

1. Introduction

Establishing reliable and predictive relationships between *in vitro* drug release and *in vivo* pharmacokinetics is essential for modified dosage forms. The USFDA introduced a Guidance document for *in vitro-in vivo* correlation (IVIVC) in September 1997 for extended-release (ER) oral dosage forms. This document sets specifications for *in vitro* dissolution and *in vivo* predictability and serves as an additional tool for bioequivalence studies (Malinowski et al., 1997).

Since extended-release formulations offer advantages such as reduced dosing frequency, increased patient compliance, and decreased therapy cost, it's crucial to understand the in vivo fate of the drug and predict its behaviour (Gangurde et al., 2011; Owen and Rannard, 2016; Surve and Jindal, 2020; Williams et al., 2015). Once established, IVIVC can predict the absorption pattern of a drug or dosage form by examining its *in vitro* drug release profile. Furthermore, it can guide the formulation and process changes due to scale-up.

Despite the significant development of long-acting injectables, there is a lack of literature on IVIVC with these dosage forms. The primary challenge in establishing IVIVC for non-oral dosage forms is the need for a standard compendial method to determine the *in vitro* drug release rate. In chapter 4, we discussed the role of hydrophobization of QS and thixotropically thickened oily vehicles in prolonging drug release both *in vitro* and *in vivo*. We found that after administering QS-loaded oil-based nanosuspension subcutaneously (at a dose of 7.5mg/kg) to Wistar rats, drug plasma concentration was detectable up to 10 days post-dosing, owing to significant differences in the physicochemical properties of QS in the formulation compared to its free drug counterpart. In this study, our objective was to establish a correlation between in vitro drug release and in vivo pharmacokinetic behaviour. We report a reliable, standard mathematical correlation based on the data obtained from *in vitro* drug release and pharmacokinetic studies of QS-loaded oil-based nanosuspension. To establish the correlation function, we used GastroPlus™ simulation software to develop IVIVC as a surrogate to evaluate the in vivo behaviour of the formulation based on *in vitro* drug release. We used various deconvolution models to mathematically correlate *in vitro* drug release and in vivo pharmacokinetic plasma concentrations to understand the drug's fate after administration.

2. Methods

2.1 ADMET Prediction of quinapyramine

The structural characteristics of quinapyramine were utilized to predict its absorption, distribution, metabolism, elimination, and toxicological profile. To achieve this, GastroPlus™ offers a predictive tool that assesses the *in vivo* behaviour of a molecule based on its physicochemical properties, such as solubility and permeability (Sohlenius-Sternbeck and Terelius, 2022) . Input data was provided in the form of a simplified molecular-input line-entry system. Additionally, other parameters including Log D, water solubility (at pH 7.4), metabolic stability, effective jejunal permeability, and potential models following the administration of QS.

2.2 *In vitro* drug release

The drug release profile of QS was evaluated using a modified sample and separate method as previously described (Wang et al., 2016). Briefly, either free QS or QS-loaded oil-based nanosuspension (equivalent to 10.0 mg of drug) was added to an Eppendorf centrifuge tube containing 1.0 mL of 0.2% v/v tween-80 and 0.05% w/v sodium azide in phosphate-buffered saline pH 7.4. The samples were kept at 37°C in a water bath shaker assembly with constant agitation at 100 rpm. At predetermined intervals including 0.25, 0.5, 1, 3, 6, 12, 24, 30, 36, 48, 60, 72, 108, and 120 h, the samples were centrifuged at 10,000 rpm for 5 minutes, and 200 µL was collected from the supernatant. Sink conditions were maintained by adding fresh media to the Eppendorf tube after each sample collection. QS concentration was determined by suitably diluting the samples with acetonitrile: water (1:1), centrifuging and analysing them by an RP-HPLC-based analytical method described earlier.

2.3 Pharmacokinetic studies

The study protocol for conducting pharmacokinetic (PK) studies in rats was approved by the Institutional Animal Ethics Committee of Birla Institute of Technology and Science, Pilani campus, Pilani, with the reference Protocol no.: IAEC/RES/31/16. Male Wistar rats weighing between 270-290 g were acclimatized for a few days under a regular 12-hour light-dark cycle and housed in well-ventilated cages with free access to food and water. The animals were divided into two groups, namely free QS (Group I) and QS-NC complex-loaded oily nanosuspension (Group II), each consisting of four rats. The free QS or QS

nanoformulationwas administered via subcutaneous route at a dose of 7.5 mg/kg body weight equivalent to QS.

After treatment, blood samples were collected from the retroorbital plexus at predetermined time intervals (0, 0.5, 1, 3, 6, 12, 24, 36, 48, 72, 120, 168, and 240 hours) and immediately transferred to Eppendorf centrifuge tubes containing 10% w/v EDTA solution. The collected blood samples were then subjected to plasma separation by centrifugation at 7000 rpm for 10 minutes using a REMI cooling centrifuge and subsequently stored at -80ºC until further analysis.

The PK analysis parameters were assessed using the PKPlus™ module of Gastroplus™ (version 10.0, Simulations Plus Inc., Lancaster, CA, USA), with all the necessary experimental or literature-based physicochemical input parameters added to the system prior to program execution. Non-compartmental analysis was conducted to determine various pharmacokinetic parameters, including peak plasma drug concentration (C_{max}), half-life of the drug ($t_{1/2}$), area under the plasma drug concentration-time curve from time zero to time t (AUC_{0-t}), area under the plasma drug concentration-time curve from time zero to infinity ($AUC_{0-\infty}$), area under the moment curve (AUMC), clearance (CL), mean residence time (MRT), absorption rate constant (K_a), elimination rate constant (K_{el}), volume of distribution (V_d), and other relevant constants. The PK profile obtained from the sample analysis was fitted into various pharmacokinetic compartment models, which included one, two, and three compartments. The most suitable model was determined based on several statistical parameters, such as the correlation coefficient (R^2), Schwartz Criterion (SC), and Akaike Information Criterion (AIC) to obtain the best-fit model (Ali et al., 2017; Krishna et al., 2019, 2018).

2.4 Development of *IVIVC* correlation

The correlation between *in vitro* release data and *in vivo* drug concentration was established using the *IVIVC* module of GastroPlus™ software. This module involves deconvolution followed by convolution of the data to generate predictions and construct the drug plasma concentration profile curve. Additionally, a correlation between *vitro* drug release and the fraction absorbed was determined by mechanistic model fitting.

PK parameters obtained from pharmacokinetic modelling to fit one, two, or three compartment models were exported prior to deconvolution. The *in vitro* release data was then deconvoluted against the *in vivo* plasma concentration data using various deconvolution methods, including Wager- Nelson-one-compartment, Loo-Riegelman-two-compartment, Loo-Riegelman-three-

compartment, Numerical deconvolution-single-Weibull, and numerical deconvolution double Weibull. During the deconvolution process, the best-fit correlation function was established by evaluating various linear, power function, second and third order polynomial equations. The most suitable correlation function was selected based on the values of R^2, standard error of prediction (SEP), and mean absolute error (MAE). Additionally, two important PK parameters, C_{max} and AUC, were evaluated based on the percent prediction error (%PE) between observed and predicted values (Balant and Gex-Fabry, 1990; Rajoli et al., 2018, 2015).

3. Results and discussion

3.1 ADMET Prediction

Table 5.1 enlists various characteristics of the quinapyramine on the basis of structure. It can be seen that the drug exhibits significantly high hydrophilicity (log P of -1.79) with multiple basic pKa values whereas, pH of 9.38 further confirmed the basic nature of QS. Further, distribution and clearance predictor indicated the drug could follow two-compartment model after administration (McCarthy et al., 2017).

Table 5.1 ADMET Predictions of quinapyramine from GastroPlus™ (ADMET Predictor v10.4.0.0)

Physicochemical Properties	
Molecular weight (g/mol)	309.4
pKa (basic)	Multiple 7.22, 1.73, -0.22, -1.41
Octanol/water partition coefficient (log P)	-1.79
Biopharmaceutical Properties	
Diffusion coefficient (cm2/ sec × 10^{-5})	0.71
Jejunal Effective Permeability (P.eff) (X 10^{-4} cm/s)	0.044
pH at reference solubility	9.38
Solubility at reference pH (mg/mL)	1.06
Distribution and Clearance	
Pharmacokinetic model	2-compartment
Blood/plasma conc. Ratio	1.47
Unbound Percent in Human Plasma (Fup %)	78.24
Clearance (Cl) (L/hr/ kg)	0.847
Volume of distribution (L/kg)	1.77
Distribution constant k_{12} (1/h)	0.745
Distribution constant k_{21} (1/h)	0.638

3.2 *In vitro* drug release

Sample and separate method with small volumes of release media, and the other experimental conditions were adopted during the release studies usually mimics the presence of small volumes of tissue fluids at the S.C. site of administration. Fig. 5.1 depicts drug release profiles of free QS in water, and QS-loaded oil-based nanosuspension. It was observed that almost 80% of the drug was present in release media at the end of 4 h in free QS group whereas, QS-loaded oil-based nanosuspension showed more than 80% drug release at the end of 7th day of the study. It was evident from the study that significant decrease in water solubility of the parent molecule QS as well as hydrophobic microenvironment created by the oily component has enabled the sustained drug release of the drug over period of time. Moreover, experimentally it was observed that there was marked gelling behaviour exhibited by the study groups consisting Al-MS in olive oil which necessarily could have contributed to the slowing of drug release (Gray and Alexander, 2002; Wang and Rackaitis, 2008).

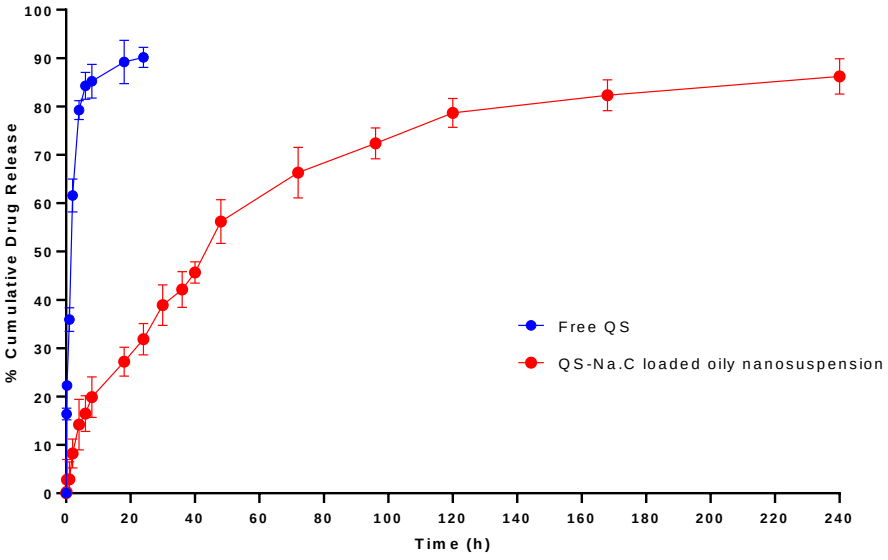

Fig. 5.1 *In vitro* drug release profile of free QS and QS-loaded oil-based nanosuspension (n=5)

3.3 Pharmacokinetic study

Generally, physiochemical properties, route of drug/ dosage administration, clinical state of the individual, and various other biological factors governs the *in vivo* fate of particular drug. In order to modify the PK profile of the drug, there are numerous carrier-based systems have been developed which essentially govern the different path than their free drug counterparts. Hence, it becomes essential to study the mechanism of drug absorption (which will govern its effect) by applying non-compartmental and compartmental PK modelling. The comparative PK

parameters evaluated by non-compartment and compartmental analysis has been presented in table 5.1. Whereas the plasma drug conc. Vs time profile curve has been presented in figure 5.2. After subcutaneous administration of free QS, the C_{max} of QS was observed at 30 min, and plasma concentration dropped below the detection limit after 18 hours of administration. The results of the *in vitro* drug release study were confirmed *in vivo*, indicating the dual impact of the vehicle and hydrophobization of QS on the prolongation of drug release. The group treated with QS-loaded oil-based nanosuspension showed a 13.54-fold, 7.09-fold, 1.78-fold, and 17.35-fold increase in $t_{1/2}$, $AUC_{0-\infty}$, Vz/F, and $MRT_{0-\infty}$, respectively, compared to free QS. Moreover, there was a prominent 7.08-fold reduction in plasma clearance, indicating protracted drug plasma concentrations compared to free QS. The pharmacokinetic profile of the nanosuspension treated group showed an initial rise in QS plasma concentration, followed by a significant reduction from 280.9 ± 119.2 ng/mL on the 5th day of dosing, reaching 22.12 ± 9.51 ng/mL by the end of the 10th day of treatment and dropping below quantification limits thereafter.

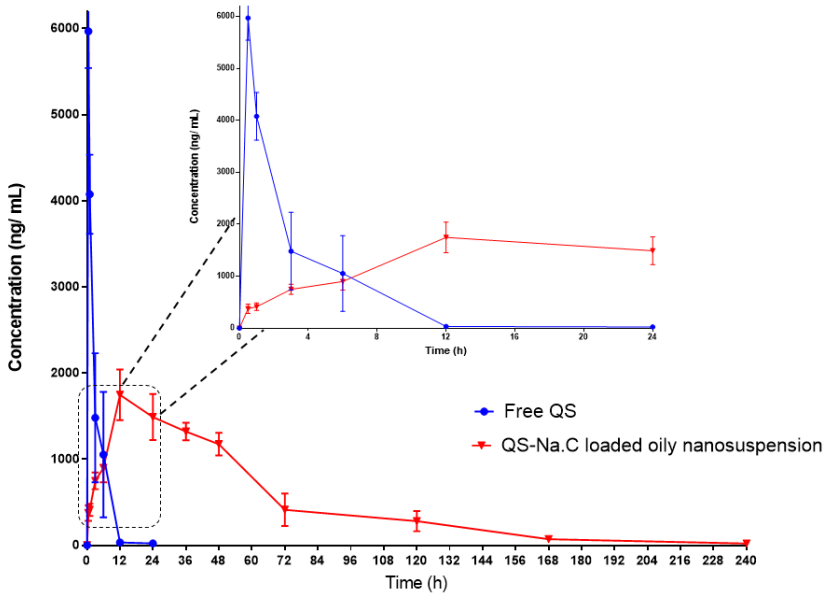

Fig. 5.2 The comparative plasma concentration time profile of free QS and QS-loaded oil-based nanosuspension

3.4 Compartment modelling

Figure 5.3 compares observed and predicted plasma drug concentrations using one-, two-, and three-compartment models for both free QS [Fig. 5.3 (I)] and QS-loaded oil-based nanosuspension [Fig. 5.3 (II)]. The boxes within each image indicate the corresponding compartment model, while the arrows show the blood flow direction in each compartment. The

transfer rate constants depicted on the arrows indicate the rate at which blood moves between compartments, and determine the fate of drug transport throughout the body.

Compartment modelling is a useful concept for studying the pharmacokinetic behaviour of drugs/formulations, which assumes that the body can be simplified as a single compartment or represented as a more complex multi-compartment model that governs absorption, distribution, metabolism, and elimination (ADME) (Gray and Alexander, 2002; McCarthy et al., 2017; Wang and Rackaitis, 2008). For example, the one-compartment model assumes the entire body is a single, homogeneous unit, where the drug enters through the central compartment from outside the body. The absorption rate constant (K_a) represents the rate of drug entry, while the elimination rate constant (K_{el}) denotes drug elimination from the body without recirculation (Savic et al., 2007). These models assume body as a single, kinetically homogeneous unit without physical restrictions on drug movement, and a first-order disposition mechanism, which can be used to predict plasma drug concentration over time. However, as shown in Fig. 5.3 (I) A and (II) A, the observed and predicted drug plasma concentrations have poor correlation. In addition, Table 5.2 indicates that the regression coefficient values (R^2) of 0.887 and 0.708 for free QS and QS-loaded oil-based nanosuspension, respectively, indicating neither free QS nor QS-loaded oil-based nanosuspension follow the one-compartment model.

The two- and three-compartment models assume that drug concentration can be estimated as a function of time, depending on whether the body is composed of highly vascular organs/tissues (central compartment) or less vascular organs (peripheral compartment) post treatment. In case of two-compartment model, the drug can recirculate between the peripheral and central compartments, which is indicated by the micro constant K_{21}. The model assumes the body is made up of two compartments, with drugs leaving the body through the central compartment. Fig. 5.3 (I) B and (II) B show a good correlation between observed and predicted drug plasma concentration values, with regression coefficient values (R^2) of 0.9939 and 0.9581 for free QS and QS-loaded oil-based nanosuspension, respectively (Table 5.2) which suggests, both QS and QS-loaded oil-based nanosuspension follows two-compartment model of disposition. Further, the predicted values obtained during ADMET predictor closely resembles the observed values of distribution constants such as K_{12} and K_{21} (Table 5.1 and Table 5.2) for QS.

The three-compartment model assumes the presence of two peripheral compartments and one central compartment. In this model, the drug is constantly distributed and redistributed between the peripheral compartments and the central compartment, while elimination occurs solely from the central compartment. Fig. 5.3 (I) C and (II) C demonstrate a moderate correlation

between the observed and simulated drug plasma concentrations over time. However, the statistical significance indicated by the R^2 and AIC values was lower than that of the two-compartment model (Table 5.2), indicating poor model fitness.

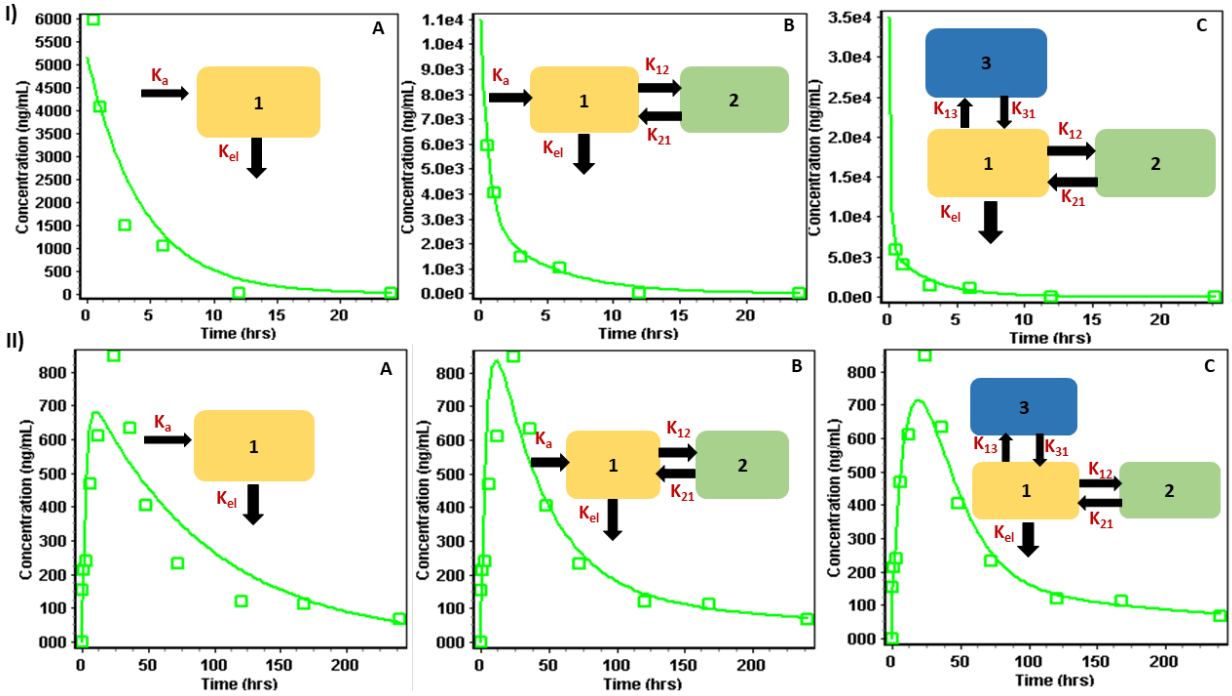

Fig. 5.3 Different plots of true (green square) and simulated (green curve) plasma concentration time profile of I) QS, and II) QS-loaded oil-based nanosuspension using (A) one compartment, (B) two compartment and (C) three compartment models. Blocks in the image are representation of the corresponding pharmacokinetics models.

3.5 *In vitro-in vivo* corelation (IVIVC)

IVIVC provides predictive mathematical tool to understand the relationships between *in vitro* drug release from the dosage form to that of *in vivo* drug concentrations (Hirota et al., 2016; Li et al., 2015). *In vitro* drug release and *in vivo* drug plasma concentrations were quantified before conducting correlation analysis. The *in vitro* drug release profile is subsequently transformed into the percentage of drug absorbed *in vivo* using the convolution/deconvolution method. Various deconvolution approaches were evaluated to identify the optimal method for establishing a correlation between *in vitro* drug release and *in vivo* drug concentration. Figure 5.4 depicts the extent of concordance between the experimentally observed values and convoluted values of the plasma drug concentration-time, and area under the curve (AUC). Table 5.3 provides the statistical correlation function for each deconvolution approach along with the percent prediction error (%PE) between observed and predicted values of C_{max} and AUC.

Table 5.2. Pharmacokinetic parameters of QS and QS-loaded oil-based nanosuspension obtained after non-compartmental and compartmental analysis by the PKPlus™ module of GastroPlus™ software (n=4)

PK Parameters		Free QS				QS-loaded oil-based nanosuspension			
	Unit	NCA	1-comp.	2-comp.	3-comp.	NCA	1-comp.	2-comp.	3-comp.
C_{max}	ng/mL/mgdose	5409	1031	2199	6996	847	1360	1680	1436
AUC_{0-t}	ng-h/mL	18920	-	-	-	57100	-	-	-
$AUC_{0-\infty}$	ng-h/mL	19670	19670	-	-	66520	66520	-	-
AUMC	µg-h^2/mL	94980	97880	-	-	7553800	6468700	-	-
$t_{1/2}$	h	2.72	3.021	3.375	85.24	96.2	63.95	220.7	181.8
MRT	h	4.828	-	-	-	113.6	92.26	-	-
K_{el}	1/h	0.031	-	-	-	0.00721	-	-	-
CL	L/h	0.254	0.223	0.254	0.202	0.075	0.071	0.061	0.066
V_d	L	-	0.97	-	-	-	6.58	-	-
V_c	L	-	-	0.455	0.143	-	-	0.527	0.263
V_{ss}	L	1.227	-	-	-	8.536	-	-	-
K_a	h^{-1}	0.031	-	-	-	0.0072	0.362	0.027	0.054
K_{10}	h^{-1}	-	0.229	0.559	1.415	-	0.011	0.116	0.252
K_{12}	h^{-1}	-	-	0.745	4.401	-	-	0.116	7.071
K_{21}	h^{-1}	-	-	0.638	1.548	-	-	0.00635	0.8
K_{13}	h^{-1}	-	-	-	0.194	-	-	-	0.269
K_{31}	h^{-1}	-	-	-	0.00927	-	-	-	0.00859
R^2	-	-	0.8873	0.9939	0.9774	-	0.7083	0.9581	0.939
AIC	-	-	-6.035	-7.9917	-0.5502	-	-27.726	-46.987	-39.522
SC	-	-	-6.451	-8.8247	-1.7997	-	-26.082	-44.162	-35.567

Here, both *in vitro* drug release and *in vivo* drug plasma concentrations are determined prior to mathematical treatment for studying their corelation. Firstly, the *vitro* drug release profile data was transformed to the % fraction absorbed *in vivo* linearly by employing convolution/ deconvolution method. For instance, input data of *in vitro* release was given to the software to estimate the plasma drug concentration as an output function process called as convolution of data. Whereas, the *in vivo* fraction absorbed was calculated on the basis of plasma drug concentration called as deconvolution. After convoluting the *in vitro* drug release data, various deconvolution approaches were screened to plot best-fit corelation between *in vitro* release and *in vivo* drug concentration. Fig. 5.4 depicts extent of match between experimentally observed value and convoluted values of plasma drug concentration-time profile. Further, relation between AUC and time is also significant from the figure. Moreover, statistical corelation function associated with each deconvolution approach with percent prediction error (%PE) between observed and predicted values of C_{max} and AUC has also been tabulated in table 5.3. The statistics involved in plasma drug concentration-time profiles from the experimentally convoluted data is mainly given by various constants including regression coefficient (R^2), SEP, and MAE as depicted in table 5.3. Fraction absorbed *in vivo* as per Wagner-Nelson one compartment pharmacokinetic model is given by the equation (5.1)

$$Fa\ (T) = \frac{Xa\ (T)}{Xa\ (\infty)} = \frac{C + k\int_0^T Ctdt}{k\int_0^\infty Ctdt} \qquad (5.1)$$

Where, Fa(T) is the fraction of drug available in the body at time (T), Xa(T) and Xa(∞) are the cumulative concentrations of the drug absorbed at time T, and infinity, respectively. C is the drug present in the central compartment at time 'T', and 'k' is the first order elimination rate constant. The difference in observed vs predicted values is given by %PE and expressed as

$$\%\ PE = \left(\frac{observed - predicted}{observed}\right) x\ 100 \qquad (5.2)$$

From the figure 5.4 B it is evident that experimental values (denoted by inverted triangle) and the convoluted/ estimated data (denoted by continuous line) had maximum number points matching which represents plot of Loo-Riegelman two compartment model. Further, model fitting was confirmed by the least % PE values from the Table 5.3. For instance, experimentally observed C_{max} was 848 ng/mL, whereas it was predicted to be 844 ng/mL with % PE of 0.472 only. Whereas, observed AUC of 56500 ng h/mL is in good agreements with 55100 ng h/mL as per prediction with %PE of 2.479. Moreover, statistical significance with R^2 of 0.702 shows that the adopted model is suitable for model fitting.

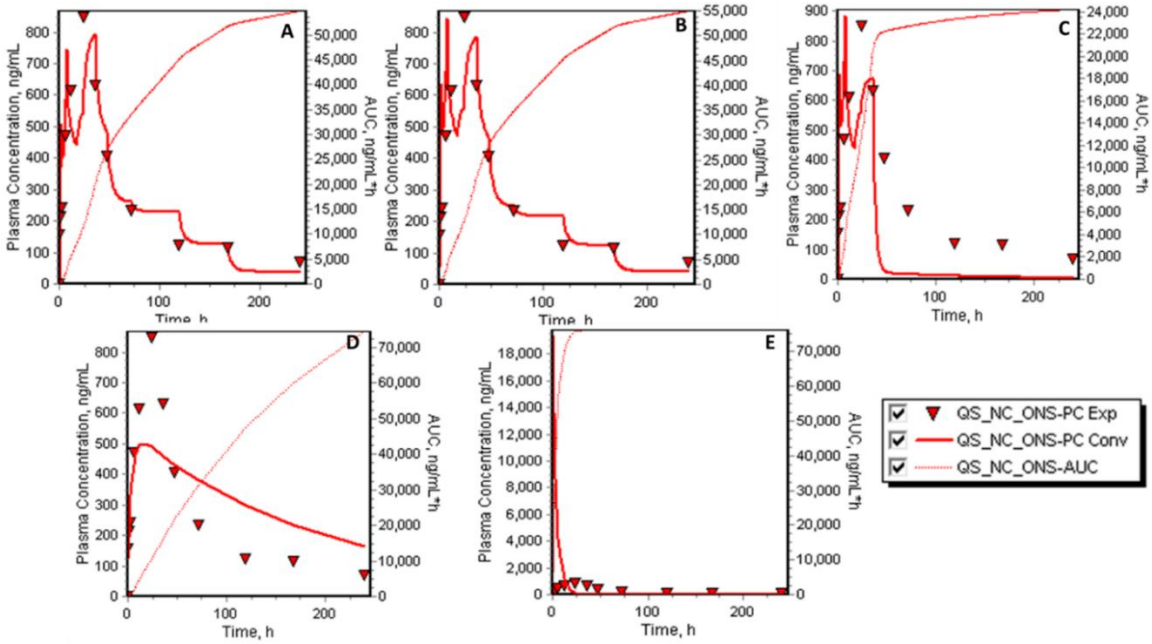

Fig. 5.4 IVIVC plots indicating the correlation of the observed and convoluted plasma drug concentration time profile (A) Wagner-Nelson one compartment method; (B) Loo-Riegelman two compartment method, (C) Loo-Riegelman three compartment method, (D) numerical deconvolution single Weibull, and (E) numerical deconvolution double Weibull. (▼represents experimentally obtained values, ▬represents convoluted data from various models, -------- represents AUC)

Table 5.3 Correlation function and statistical analysis of the *in vitro–in vivo* correlation of QS-loaded oil-based nanosuspension using various methods and models

IVIVC methods	Pharmacokinetic parameter						Statistical analysis			
	C_{max} (ng/mL)			AUC_{0-t} (ng h/mL)						
	Obs.	Pred.	%PE	Obs.	Pred.	%PE	R^2	SEP	MAE	AIC
Wagner-Nelson method (one compartment)	848	795	6.25	56500	54800	2.904	0.698	135.5	105.8	163
Loo-Riegelman method (two compartment)		844	0.472		55100	2.479	0.702	134.6	102.7	162.8
Loo-Riegelman method (three compartment)		883	-4.127		24200	57.09	0.423	187.4	156.7	171.4
Numerical deconvolution single Weibull		500	41.04		74400	-31.77	0.671	141.6	107.5	164.1
Numerical deconvolution double Weibull		19300	-2180.7		76200	-34.97	-762.7	6818.5	3578.6	264.9

4. Conclusion:

Pharmacokinetic parameters of QS and QS-loaded oil-based nanosuspension were reported with compartmental and non-compartmental modelling approach using the GastroPlus™ software. It was observed that QS when hydrophobically complexed with sodium cholate showed significant increase in C_{max}, AUC, $t_{1/2}$, and MRT. IVIVC was established with the help of IVIVCPlus™, toolkit of GastroPlus™. Amongst various IVIVC approaches studied statistical analysis of Loo-Riegelman was found to be the best fit. The study showed that oil-based nanosuspension could be a game-changing strategy to deliver highly hydrophilic drug like QS. To best of our knowledge no significant study has yet predicted theoretically or experimentally about the quinapyramine sulphate in depth.

References:

Ali, H., Prasad Verma, P.R., Dubey, S.K., Venkatesan, J., Seo, Y., Kim, S.K., Singh, S.K., 2017. In vitro - In vivo and pharmacokinetic evaluation of solid lipid nanoparticles of furosemide using Gastroplus™. RSC Adv. 7, 33314–33326. https://doi.org/10.1039/c7ra04038e

Balant, L.P., Gex-Fabry, M., 1990. Physiological pharmacokinetic modelling. Xenobiotica 20, 1241–1257. https://doi.org/10.3109/00498259009046841

Gangurde, H.H., Chordiya, M.A., Tamizharasi, S., Senthilkumaran, K., Sivakumar, T., 2011. Formulation and evaluation of sustained release bioadhesive tablets of ofloxacin using 32 factorial design. Int. J. Pharm. Investig. 1, 148. https://doi.org/10.4103/2230-973X.85964

Gray, V.R., Alexander, A.E., 2002. Studies on Aluminum Soaps. II. The Composition, Structure, and Gelling Properties of Aluminum Soaps. J. Phys. Colloid Chem. 53, 23–38. https://doi.org/10.1021/J150466A003

Hirota, K., Doty, A.C., Ackermann, R., Zhou, J., Olsen, K.F., Feng, M.R., Wang, Y., Choi, S., Qu, W., Schwendeman, A.S., Schwendeman, S.P., 2016. Characterizing release mechanisms of leuprolide acetate-loaded PLGA microspheres for IVIVC development I: In vitro evaluation. J. Control. Release 244, 302–313. https://doi.org/10.1016/J.JCONREL.2016.08.023

Krishna, K.V., Saha, R.N., Puri, A., Viard, M., Shapiro, B.A., Dubey, S.K., 2019. Pre-clinical compartmental pharmacokinetic modeling of 2-[1-hexyloxyethyl]-2-devinyl pyropheophorbide-a (HPPH) as a photosensitizer in rat plasma by validated HPLC method. Photochem. Photobiol. Sci. 18, 1056–1063. https://doi.org/10.1039/C8PP00339D/METRICS

Krishna, K.V., Saha, R.N., Singhvi, G., Dubey, S.K., 2018. Pre-clinical pharmacokinetic-pharmacodynamic modelling and biodistribution studies of donepezil hydrochloride by a validated HPLC method. RSC Adv. 8, 24740–24749. https://doi.org/10.1039/C8RA03379J

Li, X., Zhao, Z., Li, L., Zhou, T., Lu, W., 2015. Pharmacokinetics, in vitro and in vivo correlation, and efficacy of exenatide microspheres in diabetic rats. Drug Deliv. 22, 86–93. https://doi.org/10.3109/10717544.2013.871760

Malinowski, H., Marroum, P., Uppoor, V.R., Gillespie, W., Ahn, H.Y., Lockwood, P., Henderson, J., Baweja, R., Hossain, M., Fleischer, N., Tillman, L., Hussain, A., Shah, V., Dorantes, A., Zhu, R., Sun, H., Kumi, K., Machado, S., Tammara, V., Ong-Chen, T.E., Mahayni, H., Lesko, L., Williams, R., 1997. FDA guidance for industry extended release solid oral dosage forms: Development, evaluation, and application of in vitro/in vivo correlations, USFDA. https://doi.org/10.14227/DT040497P23

McCarthy, C.A., Faisal, W., O'Shea, J.P., Murphy, C., Ahern, R.J., Ryan, K.B., Griffin, B.T., Crean, A.M., 2017. In vitro dissolution models for the prediction of in vivo performance of an oral mesoporous silica formulation. J. Control. release 250, 86–95. https://doi.org/10.1016/J.JCONREL.2016.12.043

Owen, A., Rannard, S., 2016. Strengths, weaknesses, opportunities and challenges for long acting injectable therapies: Insights for applications in HIV therapy. Adv. Drug Deliv. Rev. 103, 144–156. https://doi.org/10.1016/j.addr.2016.02.003

Rajoli, R.K.R., Back, D.J., Rannard, S., Freel Meyers, C.L., Flexner, C., Owen, A., Siccardi, M., 2015. Physiologically Based Pharmacokinetic Modelling to Inform Development of Intramuscular Long-Acting Nanoformulations for HIV. Clin. Pharmacokinet. 54, 639–650. https://doi.org/10.1007/s40262-014-0227-1

Rajoli, R.K.R., Back, D.J., Rannard, S., Meyers, C.F., Flexner, C., Owen, A., Siccardi, M., 2018. In Silico Dose Prediction for Long-Acting Rilpivirine and Cabotegravir Administration to Children and Adolescents. Clin. Pharmacokinet. 57, 255–266. https://doi.org/10.1007/s40262-017-0557-x

Savic, R.M., Jonker, D.M., Kerbusch, T., Karlsson, M.O., 2007. Implementation of a transit compartment model for describing drug absorption in pharmacokinetic studies. J. Pharmacokinet. Pharmacodyn. 34, 711–726. https://doi.org/10.1007/S10928-007-9066-0

Sohlenius-Sternbeck, A.K., Terelius, Y., 2022. Evaluation of ADMET Predictor in Early Discovery Drug Metabolism and Pharmacokinetics Project Work. Drug Metab. Dispos. 50, 95–104. https://doi.org/10.1124/DMD.121.000552/-/DC1

Surve, D.H., Jindal, A.B., 2020. Recent advances in long-acting nanoformulations for delivery of antiretroviral drugs. J. Control. Release 324, 379–404.

Wang, X., Rackaitis, M., 2008. Gelling nature of aluminum soaps in oils. J. Colloid Interface Sci. 331, 335–342. https://doi.org/10.1016/J.JCIS.2008.11.032

Wang, Y., Sun, T., Zhang, Y., Chaurasiya, B., Huang, L., Liu, X., Tu, J., Xiong, Y., Sun, C., 2016. Exenatide loaded PLGA microspheres for long-acting antidiabetic therapy: Preparation, characterization, pharmacokinetics and pharmacodynamics. RSC Adv. 6, 37452–37462. https://doi.org/10.1039/c6ra02994a

Williams, P.E., Crauwels, H.M., Basstanie, E.D., 2015. Formulation and pharmacology of long-acting rilpivirine. Curr. Opin. HIV AIDS 10, 233–238.

Chapter 6: Summary and conclusions

Trypanosomiasis is a neglected tropical parasitic disease which needs special attention of both the Government and the pharmaceutical industry for the discovery and development of new antitrypanosomal drugs. Although nanotechnological interventions in antitrypanosomal therapy have shown a significant reduction in the toxicity and dose of FDA-approved drugs in preclinical research, clinical translation of these technologies has not yet been possible. Another important area which requires special focus is overcoming drug resistance. Furthermore, very limited efforts have been made in the direction of developing a vaccine against *trypanosomiasis*. Most of the reported studies focused on improvement in efficacy of anti-trypanosomal drug–loaded nanocarriers after intravenous or intraperitoneal administration. However, long-acting injectable nanoformulations of antitrypanosomal drugs administered by either intramuscular or subcutaneous route could be next-generation nanocarriers for the treatment of trypanosomiasis. Moreover, ligand-anchored nanocarriers for targeting specifically to trypanosomes in order to overcome the drug resistance or increase the drug concentration within the parasite are yet to be studied comprehensively both *in vitro* and *in vivo.*

To address limitations in the current treatment regimen, we have investigated novel nanoformulations of QS that are lipid-based, biocompatible, cost-effective, and feasible for industrial-scale production. In order to modify the physicochemical properties of the hydrophilic QS, we utilized hydrophobic-ion pairing to render it hydrophobic. We evaluated SLNs and oil-based nanosuspensions for their in vitro and in vivo pharmacokinetics and pre-clinical efficacy. Moreover, we utilized the sophisticated GastroPlus™ software to assess the *in vitro* and *in vivo* correlation of QS oily nanosuspension. Finally, we conducted a pharmacokinetic study in larger animals (camels) as a target population to evaluate the fate of *in vivo* drug release.

The hydrophilic nature of QS posed significant challenges when developing an RP-HPLC-based analytical technique. To address this, we explored the use of an ion-pair reagent in the mobile phase to improve retention of QS on a hydrophobic C18 column. For routine assay determination in formulation trials, drug content during drug release, and plasma sample analysis in rats and camels, we employed a Waters Sunfire® C18 3.5 um ODS (4.6 x 50 mm) column. Our binary mobile phase system consisted of acetonitrile and 2.5 mM sodium lauryl sulphate in 0.1% formic acid in water, with a flow rate of 1 ml/min in isocratic mode, and

detection at a wavelength of 297 nm. The developed method effectively determined QS content without interference from formulation, release media, or plasma components during analysis.

Further, we developed a lipid-based QS-DS-SLN by an in-situ ionic complexation method using the solvent evaporation process, which provides efficient delivery of QS with improved physicochemical and biopharmaceutical properties. Lipid screening was rationally carried out using theoretical solubility parameters, and the developed nanoformulation was scientifically scaled up by using geometrical scaling principle based on the rotational speed during manufacturing of lab-scale and pilot-scale preparation. In drug release studies, our formulation demonstrated sustained drug release for 60 hours, while PK studies in Wistar rats showed detectable levels for approximately two days. The developed lipidic nanoformulation also exhibited significantly higher cytocompatibility and hemocompatibility as compared to free QS. Cellular uptake studies showed enhanced uptake of nanoparticles in macrophage cell lines leading to an increase in intracellular concentration. Moreover, in a *T. evansi* infected mice model of *trypanosomiasis*, our formulation showed enhanced efficacy at a single dose of QS-DS-SLN without relapse of infection and increased survival in treated mice as compared to free QS which was confirmed by blood smear and PCR assay.

In another approach, our hydrophobic ion-pair complex of QS with Na.C, when it was loaded into a thixotropically-thickened vegetable oil vehicle, demonstrated extensive and prolonged drug plasma concentrations during in vitro release studies which were reflected in vivo during PK studies in rats and camels. Moreover, the developed oil-based nanosuspension of QS showed enhanced efficacy in *T. evansi* infected mice at a single dose of nanoformulation and showed absence of parasitaemia without relapse of infection for more than 75 days which was again confirmed by blood smear analysis and PCR assay.

Since the QS-Na.C loaded oil-based nanosuspension showed significant improvement in PK parameters of parent compound QS, it was crucial to determine the impact of formulation variables on the in vivo drug performance of drug. To accomplish this, we utilized the USFDA-approved GastroPlus™ software to establish *an in vitro-in vivo* correlation between drug release and PK profile. We employed compartment modelling along with the mathematical convolution-deconvolution approaches. Based on the input data of in vitro drug release and in vivo PK profile, it was revealed that QS follows two-compartment model. This served as a mathematical tool in establishing the impact of formulation variables and other parameters which determines the fate of drug release.

The focus of research has primarily been on overcoming the critical barriers presented by current antitrypanosomal therapy. Lipid-based nanoformulations, for example, have shown an increase in drug concentrations for a prolonged period, potentially reducing the frequency of dosing required for complete parasite removal and decreasing dose-dependent side effects. However, reports in the literature regarding increasing the therapeutic efficacy of quinapyramine sulphate are limited, and they often lack FDA-approved excipients for developing dosage forms. In the current research, the solvents, excipients, and other materials used in the development of lipid-based nanoformulation are well within the acceptable range listed by the FDA's GRAS list, highlighting the safety of the developed formulation.

APPENDICES

Publications from thesis work

Kedar Prayag, Dhanashree Surve, Atish Paul, Sanjay Kumar, Anil Jindal, "Nanotechnological Interventions for Treatment of Trypanosomiasis in Humans and Animals", 2020, published in ***Drug Delivery and Translational Research,*** DOI: 10.1007/s13346-020-00764-x, **(IF-5.671)**

Kedar Prayag, Atish Paul, Samar Ghorui, Anil Jindal, "Preparation and Evaluation of Quinapyramine Sulphate-Docusate Sodium Ionic Complex Loaded Lipidic Nanoparticles and Its Scale Up Using Geometric Similarity Principle", 2021, ***Journal of Pharmaceutical Sciences***, DOI: 10.1016/j.xphs.2021.01.033 **(IF-3.534)**

Kedar Prayag, Atish Paul, Samar Ghorui, Anil Jindal, Preclinical evaluation of quinapyramine sulphate loaded in lipidic nanocarriers for trypanocidal effect against *Trypanosoma evansi*, 2023, published in ***Journal of Drug Delivery Science and Technology,*** DOI**:** 10.1016/j.jddst.2023.104215 **(IF-5.061)**

Kedar Prayag, Atish Paul, Samar Ghorui, Anil Jindal, **Long-term antitrypanosomal effect of quinapyramine sulphate-loaded oil-based nanosuspension in *T. evansi* infected mouse model** (under review).

Patent

Jindal Anil B., **Prayag Kedar S.**, Formulation for delivery of a hydrophilic drug and method of preparation thereof **(Application no - 202211059070)**

Other Publications

Sagar Salave, **Kedar Prayag**, Dhwani Rana, Prakash Amate, Rupali Pardhe, Ajinkya Jadhav, Anil B Jindal and Derajram Benival, Recent Progress in Hot Melt Extrusion Technology in Pharmaceutical Dosage Form Design, ***Recent Advances in Drug Delivery & Formulation, Bentham Sciences,*** DOI: 10.2174/2667387816666220819124605 **(IF-1.73)**

Sagar Salave, Dhwani Rana, **Kedar Prayag**, Srushti Shah, Garima Rawat, Nitish Sharma, Anil Jindal, Rikin Patel, Derajram Benival, **Recent Advances in Teriparatide Delivery by-virtue-of Novel Drug Delivery Approaches for the Management of Osteoporosis**, 2023 published in ***Critical Reviews™ in Therapeutic Drug Carrier Systems*** **(IF-4.889),** DOI: 10.1615/CritRevTherDrugCarrierSyst.2023045014

Book chapters

Kedar Prayag, Anil Jindal, Nanomedicines for the treatment of trypanosomiasis in ***Nanomedicines for the prevention and treatment of infectious diseases***, 2023, edited by Vandana Patravale, Abhijit Date, and Anil B. Jindal**, Springer Nature.**

Kedar Prayag, Anil Jindal**,** Scale-up of liquid mixing process, ***Pharmaceutical process engineering and scale up principles,*** 2023, edited by Anil B. Jindal, **Springer Nature** (131-148).

Conference presentations

Kedar S. Prayag, Anil B. Jindal, Cellular uptake, pharmacokinetic and biodistribution of isometamidium chloride loaded long-acting lipid based nanoformulation in 19th **International e-symposium on Advances in Technology and Business Potential of New Drug Delivery Systems** dated 25-27th Feb. 2021. (CRS India Local Chapter)

Kedar S. Prayag, Anil B. Jindal, scale-up of quinapyramine sulphate-loaded lipidic nanoparticles using geometric similarity principle **"One-Day National Webinar on "Nanotechnology in Healthcare: Opportunities and Challenges"** dated 28th Oct. 2021. (CRS India Local Chapter, Nirma University).

Kedar S. Prayag, Anil B. Jindal, Preclinical evaluation of quinapyramine sulphate-docusate sodium-loaded solid lipid nanoparticles for enhanced trypanocidal effect against *T. Evansi* in **21st International Symposium on Advances in Technology and Business Potential of New Drug Delivery Systems** dated 24-25th Feb. 2023. (CRS India Local Chapter, NMIMS, Mumbai)

Supervisor's Biography

Dr. Anil Jindal is an Associate Professor at the Department of Pharmacy at the Birla Institute of Technology and Science Pilani Pilani Campus. His research is focused on developing innovative drug delivery systems to treat infectious diseases in both humans and animals. Dr. Jindal holds a PhD from the Institute of Chemical Technology Mumbai and worked with leading pharmaceutical companies such as Pfizer and IPCA Laboratories before joining BITS Pilani. He is the author of numerous publications and book chapters and the inventor of three patent applications, including one PCT application in nano-drug delivery systems. He is also an editor of the book "Pharmaceutical Process Engineering and Scale-up Principles", published by Springer as a part of AAPS Introduction in the Pharmaceutical Sciences Series. Dr. Jindal's contributions to the field of pharmacy earned him several prestigious academic awards, including the Prof. M.L. Khorona Memorial Award in 2010, the Eudragit Award in 2018, and the Early Career Research Award in 2019, presented by SERB, Government of India, for his significant contribution to research. Dr. Jindal's interview was recently featured in Voices Editorial of Molecular Pharmaceutics, demonstrating his recognition as a thought leader in his field. Additionally, he has been appointed as a managing theme editor for Advanced Drug Delivery Reviews, a highly respected journal with an impact factor of 17.87.

Candidates Biography

Kedar Shridhar Prayag is currently a Ph.D. research scholar in Department of Pharmacy, BITS-Pilani. He has obtained his Bachelor of Pharmacy degree from Government college of Pharmacy, Aurangabad, and Master of Pharmacy in Pharmaceutics from L.M. College of Pharmacy, Ahmedabad. He has received Sir Ratan Tata Trust Fellowship for 3 consecutive years during his Bachelor of Pharmacy course. He secured AIR-38 in GPAT-2013, and NIPER rank 157 in the year 2013. During his Master's degree he completed his Industrial training for 9 months in Sun Pharma Advanced Research Center (SPARC), Vadodara. He worked for almost 4 years in Formulation development department in Torrent Research Centre, Ahmedabad, and Zyduc Cadila, Ahmedabad before joining his PhD course. Since his admission in BITS-Pilani, he has been working on the development and characterization of lipid-based nanoformulations against infectious disease *Trypanosomiasis*. He has also

worked on developing industrially feasible development of nanoformulations. His proficiency in the field of research is evident by her publications in Scopus indexed journals and books (2-review publications, 2-book chapters, 3-research publication, and 1-paent filled).